Mechanisms of PINK1-Associated Parkinson's Disease: From Genetic Mutations to Human Dopaminergic Neuron Models

Dissertation

der Mathematisch-Naturwissenschaftlichen Fakultät

der Eberhard Karls Universität Tübingen

zur Erlangung des Grades eines

Doktors der Naturwissenschaften

(Dr. rer. nat.)

vorgelegt von

M.Sc. Karan Sharma

aus Cuttack, Indien

Tübingen

2025

Gedruckt mit Genehmigung der Mathematisch-Naturwissenschaftlichen Fakultät der Eberhard Karls Universität Tübingen.

Tag der mündlichen Qualifikation:	19.12.2025
Dekan:	Prof. Dr. Thilo Stehle
1. Berichterstatterin:	PD Dr. Julia Fitzgerald
2. Berichterstatter:	Prof. Dr. Boris Macek
3. Berichterstetterin:	Prof. Dr. Anne Grünewald
4. Berichterstatter:	Prof. Dr. Axel Methner

Preface

This thesis includes three papers where we study the functional role of PINK1 and explore the protein dynamics of human midbrain dopaminergic neurons to gain deeper insights into the biology of PINK1-associated Parkinsons disease.

The study was conducted from October 2021 until September 2025 under the supervision of:

- PD Dr. Julia Fitzgerald, Department of Neurodegenerative Diseases, Hertie Institute for Clinical Brain Research, University of Tübingen.
- Prof. Dr. Boris Macek, Institute for Cell Biology, University of Tübingen.
- Prof. Dr. Eran Hornstein, Department of Molecular Neuroscience, Weizmann Institute of Science, Israel.

The work was funded by the Deutsche Forschungsgemeinschaft (DFG) Research Training Group 2364 'MOMbrane: The multifaceted functions and dynamics of the mitochondrial outer membrane (MOM)‘.

Contents

1. Abbreviations.

ALP – Autophagy lysosomal pathway
ATP - Adenosine triphosphate
BBB – Blood brain barrier
βCD – β-cyclodextrin
CCCP - Carbonyl cyanide m-chlorophenyl hydrazone
CHX – Cycloheximide
CSF – Cerebrospinal fluid
DAT - Dopamine transporter
DFG motif – Aspartate Phenylalanine Glycine motif in kinases
DIA – Data independent acquisition
ER - Endoplasmic reticulum
ETC - Electron transport chain
FLOT1 - Flotillin-1
GBA/GBA1 - Glucocerebrosidase gene/protein
GFAP - Glial fibrillary acidic protein
GWAS - Genome-wide association study
HMGCR - 3-hydroxy-3-methylglutaryl-CoA reductase
IFN-γ - Interferon gamma
IL-6 – Interleukin-6
IL-1β – Interleukin-1 beta
INSIG2 - Insulin-induced gene 2
KO - Knockout
LAMP1 – Lysosome associated membrane glycoprotein 1
LOF - Loss of function
LRRK2 – Leucine rich repeat kinase 2
MAP1B – Microtubule associated protein 1B
MDV – Mitochondria derived vesicle
MFN2 - Mitofusin 2
MOM - Mitochondrial outer membrane
MPP+ - 1-Methyl-4-phenylpyridinium
MPTP - 1-Methyl-4-phenyl-1,2,3,6-tetrahydropyridine

NAC - Non-amyloid component

NLRP3 - NOD, LRR and pyrin domain containing protein 3

NF-κB - Nuclear factor kappa light chain enhancer of activated B cells

OPC - Oligodendroglial progenitor cells

OPTN - Optineurin

PAK2 - p21 activated kinase 2

PARL – Presenilin associated rhomboid-like protease

PD - Parkinson's disease

PFO - Perfringolysin O (cholesterol binding protein)

PINK1 - PTEN induced putative kinase 1

PRKN - E3 ubiquitin ligase parkin

PTEN - Phosphatase and tensin homolog

ROS - Reactive oxygen species

SCAP - SREBP cleavage activating protein

SNpc – Substantia nigra pars compacta

SREBP - Sterol regulatory element binding protein

SQLE - Squalene monooxygenase

TLR2 - Toll like receptor 2

TNF-α - Tumor necrosis factor alpha

UB - Ubiquitin

UPS – Ubiquitin proteasomal system

WT - Wild-type

2. Abstract.

Parkinson's disease (PD) is a progressive neurodegenerative disorder characterized by the loss of dopaminergic neurons in the substantia nigra. While environmental and genetic factors both contribute to disease risk, pathogenic mutations in *PINK1* are among the most well-established causes of autosomal recessive early-onset PD. Despite two decades of research, the precise physiological cellular mechanisms through which PINK1 regulates neuronal health remain incompletely understood.

This thesis explores the biology of PINK1 in human dopaminergic neurons using stem cell derived neuronal models, proteomics, and functional assays. First, a novel pathogenic mutation, PINK1 p.F385S, was characterized in an Indian family with early-onset PD. Functional studies revealed that this mutation destabilizes the kinase domain, abolishes phosphorylation of ubiquitin at Ser65, prevents Parkin recruitment, and thereby disrupts PINK1/Parkin mitophagy.

Second, spatio-temporal proteomics using microfluidic chambers was applied to investigate protein turnover, axonal enriched and synthesized proteins and protein trafficking between the soma and axonal part of human dopaminergic neurons. These studies provide a quantitative resource of proteome dynamics and highlight neuronal compartment specific regulation of proteostasis.

Third, a previously unrecognized role of PINK1 in regulating cholesterol metabolism was identified in human dopaminergic neurons. Using phosphoproteomics, we showed altered phosphorylation of a sterol regulatory protein, SCAP. Loss of PINK1 stabilizes SCAP, increases cholesterol biosynthesis and leads to cholesterol accumulation in plasma membranes and lipid rafts. This dysregulation disrupts dopamine transporter localization and impairs neurotransmitter uptake, identifying cholesterol imbalance as an early phenotype in the pathogenesis of PINK1 associated PD.

Collectively, this work expands the mechanistic repertoire of PINK1 biology beyond mitochondrial quality control and identifies a previously unreported mechanism on how PINK1 dysfunction contributes to PD. Additionally, we also provide a proteomic framework using human dopaminergic neurons for future studies into the cellular pathways driving PD pathogenesis.

3. Zusammenfassung.

Die Parkinson-Krankheit (PD) ist eine fortschreitende neurodegenerative Erkrankung, die durch den Verlust dopaminerger Neuronen in der Substantia nigra gekennzeichnet ist. Zwar tragen sowohl Umwelt- als auch genetische Faktoren zum Krankheitsrisiko bei, dennoch gehören pathogene Mutationen in PINK1 zu den bekanntesten Ursachen der autosomal rezessiv vererbten, früh auftretenden Parkinson-Krankheit. Trotz zwei Jahrzehnten Forschung sind die genauen physiologischen molekularen und zellulären Mechanismen, durch die PINK1 die neuronale Gesundheit reguliert, noch immer nicht vollständig verstanden.

In dieser Thesis wird die Biologie von PINK1 in menschlichen dopaminergen Neuronen mit Hilfe von aus Stammzellen gewonnenen neuronalen Modellen, Proteomik und funktionellen Assays untersucht. Zunächst haben wir eine neue pathogene Mutation, PINK1 p.F385S, in einer indischen Familie mit früh einsetzender Parkinson-Krankheit charakterisiert. Funktionelle Studien zeigten, dass diese Mutation die Kinasedomäne destabilisiert, die Phosphorylierung von Ubiquitin an Ser65 aufhebt, die Parkin-Rekrutierung verhindert und dadurch die Mitophagie stört.

Zweitens haben wir die räumlich-zeitliche Proteomik mit Hilfe von Mikrofluidikkammern angewandt, um den Proteinumsatz, axonal angereicherte und synthetisierte Proteine und die Proteintranslokation zwischen dem somatischen und axonalen Teil menschlicher dopaminerger Neuronen zu untersuchen. Diese Studien stellen eine quantitative Ressource für die Proteomdynamik dar und zeigen die kompartimentspezifische Regulierung der Proteostase in den Neuronen auf.

Drittens entdeckten wir eine bisher unbekannte Rolle von PINK1 bei der Regulierung des Cholesterinstoffwechsels. Mithilfe der Phosphoproteomik konnten wir eine veränderte Phosphorylierung eines Sterol-regulierenden Proteins, SCAP, nachweisen. Der Verlust von PINK1 stabilisiert SCAP, erhöht die Cholesterinbiosynthese und führt zu einer Anhäufung von Cholesterin in Plasmamembranen und Lipid Rafts. Diese Dysregulation stört die Lokalisierung von Dopamintransportern und beeinträchtigt die Aufnahme von Neurotransmittern, was ein Cholesterin-Ungleichgewicht als frühen Phänotyp in der Pathogenese der PINK1-assoziierten Parkinson-Erkrankung identifiziert.

Insgesamt erweitert diese Arbeit das mechanistische Repertoire der PINK1-Biologie über die mitochondriale Qualitätskontrolle hinaus und bietet neue Perspektiven für die

Frage, wie eine PINK1-Dysfunktion zu Parkinson beiträgt. Darüber hinaus bieten wir einen proteomischen Rahmen mit menschlichen dopaminergen Neuronen für zukünftige Studien über die zellulären Wege der PD-Pathogenese.

4. List of Publications.

Published:

1. **Sharma, K.**, Kishore, A., Lechado-Terradas, A., Passannanti, R., Raimondi, F., Sturm, M., ... & Sharma, M. (2024). A Novel PINK1 p. F385S Loss-of-Function Mutation in an Indian Family with Parkinson's Disease. Movement Disorders, 39(7), 1217-1225.
2. Cavarischia-Rega, C., **Sharma, K.**, Fitzgerald, J. C., & Macek, B. (2024). Proteome dynamics in iPSC-derived human dopaminergic neurons. Molecular & Cellular Proteomics, 23(10).

Submitted to journal:

3. **Sharma, K.**, Cavarischia-Rega, C., Ivaniuk, D., Bus, C., Brouwers, J. F... & Fitzgerald, J. C. (2025). PINK1 regulates cholesterol homeostasis via SCAP phosphorylation in human dopaminergic neurons. (BioRxiv preprint)

Other publications not included in the thesis:

1. Arena, G., **Sharma, K.**, Agyeah, G., Krüger, R., Grünewald, A., & Fitzgerald, J. C. (2022). Neurodegeneration and Neuroinflammation in Parkinson's Disease: a Self-Sustained Loop. Current neurology and neuroscience reports, 22(8), 427-440. (review)
2. Schwarz, L., **Sharma, K.**, Dodi, L. D., Rieder, L. S., Fallier-Becker, P., Casadei, N., & Fitzgerald, J. C. (2022). Miro1 R272Q disrupts mitochondrial calcium handling and neurotransmitter uptake in dopaminergic neurons. Frontiers in Molecular Neuroscience, 15, 966209.
3. Lechado-Terradas, A., Schepers, S., Zittlau, K. I., **Sharma, K.**, Ok, O., Fitzgerald, J. C., ... & Kahle, P. J. (2022). Parkin-dependent mitophagy occurs via proteasome-dependent steps sequentially targeting separate mitochondrial sub-compartments for autophagy. Autophagy Reports, 1(1), 576-602.
4. Cavarischia-Rega, C., **Sharma, K.**, Fitzgerald, J.C. & Macek, B. (2025). Proteomic insights into the biology of dopaminergic neurons. Front. Mol. Neurosci. 18:1642519. (review)

5. Personal Contribution.

Manuscript 1: A Novel PINK1 p. F385S Loss-of-Function Mutation in an Indian Family with Parkinson's Disease.

In this manuscript, I used HeLa cells having endogenous PINK1 kinase dead mutation and transfected them with either wildtype or F385S mutant PINK1 to help determine – a. The stability and half-life of PINK1 mutant using a Cycloheximide pulse chase experiment, b. Impaired phospho-ubiquitin at Serine 65 in PINK1 F385S mutant upon CCCP mediated depolarization of mitochondria and c. Performing immunofluorescence to capture images for Parkin translocation to mitochondria and mitochondrial morphology. For the publication, I wrote the first draft of the paper and prepared the final figures.

Manuscript 2: Proteome dynamics in iPSC-derived human dopaminergic neurons.

In this manuscript, I differentiated dopaminergic neurons, cultivated them in microfluidic devices and performed the treatments to have the samples forwarded to our collaborators for mass spectrometry-based proteomics. Additionally, I performed immunofluorescence and imaged the localization of axonal enriched proteins to validate the proteomics finding. I also performed imaging to confirm that the microfluidic devices have fluidic separation with no leakage.

Manuscript 3: PINK1 regulates cholesterol homeostasis via SCAP phosphorylation in human dopaminergic neurons.

In this manuscript, I performed most of the experiments except for the phosphoproteomics, lipidomics and the measurement of cholesterol in PINK1 mice and HeLa cells. For the manuscript submission, I wrote the first draft of the paper and prepared the final figures.

6. Introduction.

6.1 Parkinson's disease

Parkinson's disease (PD) was first described by James Parkinson in 1817 in his treatise "An essay on the Shaking Palsy". He case-studied the symptoms of six men between the age of 50 and 65 years and believed that he had identified a new 'medical species' that has not yet been classified by nosologists. He described the disease as a nervous disorder in which the subjects showed a trembling of their limbs, reduced muscular strength, a stooped posture and difficulty to stop once started to taking steps to walk (Parkinson, 2002).

More than 200 years since the first description, most of James Parkinson's observations still holds true. However, the description and characteristics of the disease are constantly being updated. PD can be broadly described as a neurodegenerative disease characterized by the loss of dopaminergic neurons (DaNs) in the substantia nigra pars compacta (SNpc). This loss of dopamine producing neurons leads to the classical motor symptoms associated with PD – bradykinesia, rigidity, resting tremor and postural instability. These motor symptoms are usually preceded by non-motor symptoms – olfactory loss, sleep dysfunction, autonomics dysfunction, sometimes psychiatric disturbances and cognitive impairment (Armstrong and Okun, 2020). The occurrence of non-motor symptoms can precede the occurrence of the motor symptoms and/or the diagnosis of PD, sometimes by decades (Figure 1). The patients may, however, exhibit a mix of the various symptoms as the disease is altogether heterogenous.

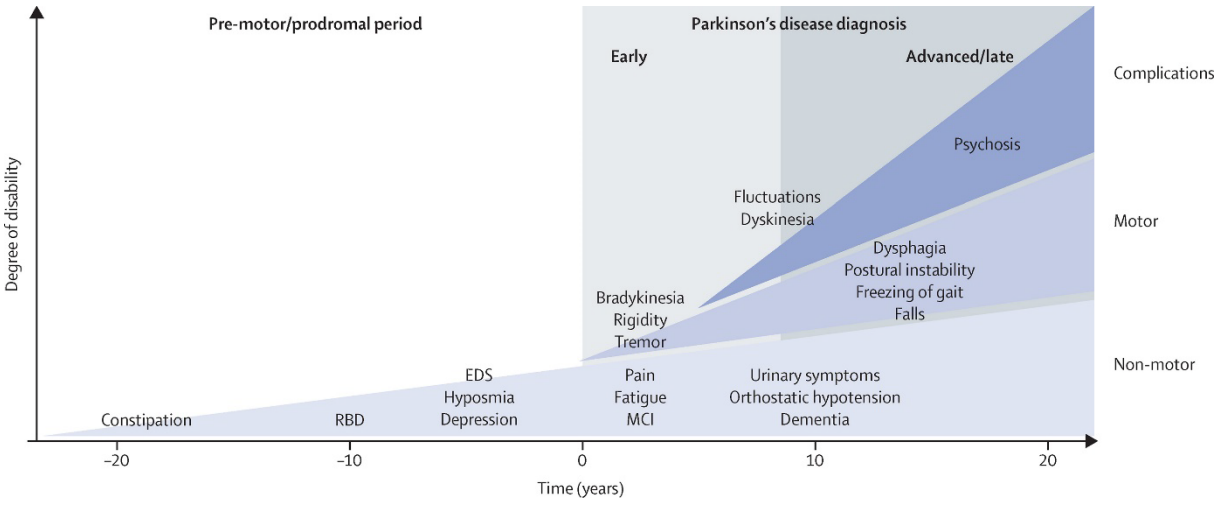

Figure 1: Clinical Symptoms and time course of Parkinson's disease progression. Image taken from (Kalia and Lang, 2015).

6.2 Causes of Parkinson's disease

PD etiology can be broadly categorized as genetic, environmental and/or an interaction of both genetics and environment. Due to technological advancements in sequencing the whole genome of an individual, significant progress has been made in identifying gene mutations that cause PD or those that contribute to PD risk. Understanding environmental contributions, on the other hand, has proven more challenging because exposures vary across a lifetime and are difficult to measure retrospectively. This difficulty is further compounded by PD's long prodromal period, during which clinical symptoms may not yet be evident, making it hard to precisely link early-life exposures to PD onset.

6.2.1 Genetic causes

In the late 1990s, *SNCA* was the first PD gene that was identified in a large Italian kindred and in three unrelated families of Greek origin (Polymeropoulos et al., 1997). Since then, many genes have been associated with monogenic forms of PD. The genes *SNCA, LRRK2 and VPS35* have been linked to autosomal dominant PD while *PRKN, DJ-1 and PINK1* have been linked to autosomal recessive and typically early-onset form of PD. Various other genes – *PLA2G6*, *ATP13A2*, *FBXO7*, *SYNJ1*, *DNAJC6*, *VPS13C*, *PTPA* and *DAGLB* cause early-onset or juvenile-onset parkinsonism and present as PD but are often accompanied by atypical symptoms such as early dementia, intellectual disability, epileptic seizures, pyramidal signs or gaze palsy (Lim et al., 2024).

Despite major advancements, there still lies a major barrier in our knowledge of PD genetics as most of the genome-wide association studies (GWAS) in PD have been performed in populations with European ancestry that account for about 15% of the world's population. Expanding the horizon of PD genetics to a multi-ancestorial global level may help us thoroughly define the complete genetic architecture of PD and guide us in the translatability of genes for precision medicine (Gasser, 2024).

6.2.2 Environmental factors

Before the discovery of the first PD genes through linkage in large families, PD was considered a sporadic disease in which age and environmental factors were known to be the key cause for the disease. An early instance for associating environmental exposures with PD came from an accidental event in 1983 when Langston and his colleagues described individuals who had consumed a bad batch in the illicit production of synthetic analog of the opioid meperidine (Demerol). The resulting analogue synthesized instead was 1-methyl 4—phenyl 1,2,3, 6-tetrahydropyridine (MPTP) (Langston et al., 1983). Our body metabolizes the protoxin MPTP into the active mitochondrial toxin 1-methyl-4-phenylpyridinium ion (MPP+), that crosses the blood brain barrier (BBB) and leads to the selective degeneration of dopaminergic neurons in the substantia nigra (Nonnekes et al., 2018). Since then, numerous environmental toxins have been implicated in the onset of PD, i.e., acetogenins and alkaloids in plants from the Annonaceae family that caused atypical Parkinsonism in the inhabitants of Guadeloupe; and sterol glucosides in cycad seeds that caused Amyotrophic lateral sclerosis-Parkinsonism Dementia complex among the Chamorro people of Guam (Shaw and Höglinger, 2008). There is also consistent and extensive evidence from exposure to pesticides (i.e., paraquat, rotenone), head injuries and traumatic brain injuries (Mackay et al., 2019, Camacho-Soto et al., 2017). Recently, the SARS-CoV2 has also been implicated to parkinsonism and only a careful longitudinal assessment can confirm this association (Brundin et al., 2020).
Additionally, several associations have also been shown to reduce the risk of developing PD such as smoking, drinking coffee, use of non-steroidal anti-inflammatory drugs and physical activity (Noyce et al., 2012). The gut health and other gut-related factors have also been implicated in PD due to inflammation and α-synuclein aggregation via the gut-brain axis (Tan et al., 2022).

6.2.3 Genetic and environmental interaction

Approximately 10-15% of all PD cases are monogenic (pathogenic, disease-causing mutations or copy number variants (CNVs)) and the rest are sporadic (cases arising with no known cause). Sporadic PD is believed to involve a complex interplay with genetic predisposition and environmental influences. In the last decade, many PD

GWAS have been done to identify novel risk genes, variants and single nucleotide polymorphisms (SNPs) that can modify the risk of developing PD. Approximately 5-15% of sporadic PD patients carry a *GBA* mutation with an overall odds ratio of 5.4 (n = 7023) making Glucocerebrosidase (*GBA)* mutations one of the most important risk factor for PD (Mata et al., 2008, Sidranskyl, 2009, Sidransky et al., 2009). The largest PD GWAS to date has identified 90 independent significant risk signals throughout the genome which include *GBA*, *RAB29*, *SNCA*, *LRRK2, TMEM175* among others (Figure 2). These GWAS databases are key in developing a method to attribute polygenic risk scores (PRS) in predicting PD risk for an individual by accounting for their total genetic risk. As of now, between 16-36% of PD heritability can be explained by PRS (Nalls et al., 2019). The identification of genes such as *SNCA* and *LRRK2* risk variants in sporadic PD cases also suggests a link between monogenic and sporadic PD (Bandres-Ciga et al., 2020).

Some studies have associated risk variants with environmental factors and lifestyle. For example, PD risk was reduced to approximately 18% in individuals having variants in *CYP1A2,* involved in caffeine metabolism*,* as they metabolize caffeine slower compared to wildtype *CYP1A2* individuals (Popat et al., 2011). In another study, the risk of developing PD increased in individuals with head injury and those having a long Rep1 (a polymorphic microsatellite) sequence in the promoter region of the *SNCA* gene (Goldman et al., 2012). In a large cross-sectional study using the 23andMe, Inc. research dataset, a significant interaction of PD PRS was associated to type 2 diabetes, body mass index, tobacco consumption and physical activity. The nature of these interactions was mentioned by the authors as not straightforward but only as a proof of principle and should be followed up by further research (Reynoso et al., 2024).

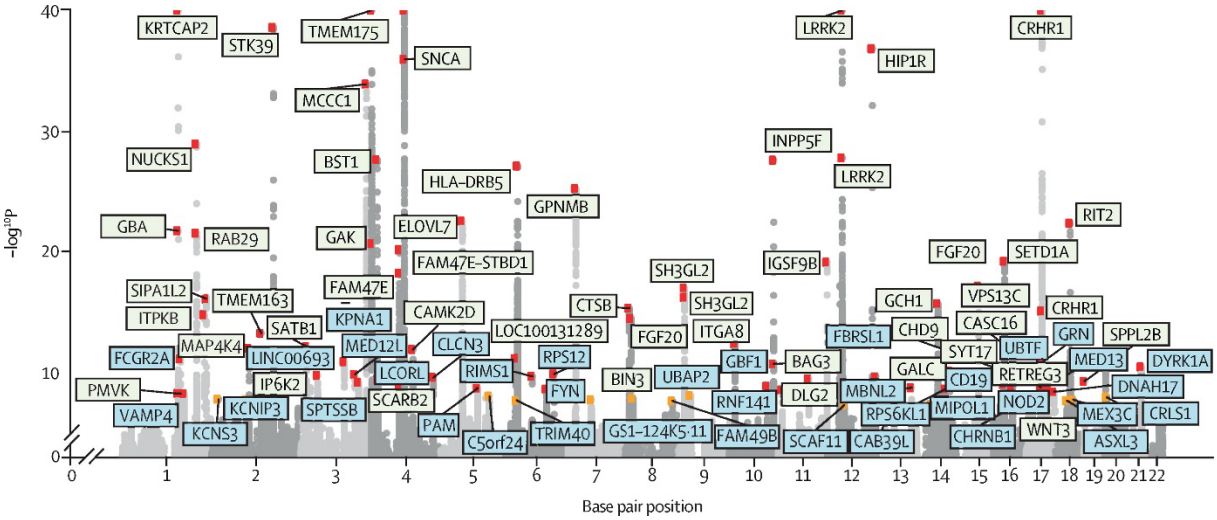

Figure 2: Manhattan Plot showing significant PD risk genes (in light green) and novel genes (in blue) whose variants are associated with Parkinson's disease. Image taken from (Nalls et al., 2019).

6.3 Neuropathology of Parkinson's disease

The most prominent morphological change in a PD brain is observed in the transverse sections of the brainstem, where in most cases there is a loss in the dark pigmented region of SNpc and locus coeruleus. This loss of dark pigmentation is due to the absence of neuromelanin containing DaNs in the SNpc and noradrenergic neurons in the locus coeruleus (Dickson, 2012, Kouli et al., 2018).

Another aspect of PD pathology is the presence of Lewy bodies in the neurons of the ventrolateral part of SNpc. Lewy bodies are localized in the cytoplasm of nerve cells and consist of a fibrillar and granular core with a halo around them. These neurons are accompanied by the degeneration of neurites (mostly axonal) termed as Lewy neurites. A major component of Lewy bodies is the presence of amyloid or amyloid-like filamentous α-Synuclein, especially at the halo. Other components of the Lewy bodies include membranous structures, vesicles, dysmorphic organelles, cytoskeleton elements, ubiquitin, tau and others (Kouli et al., 2018, Shahmoradian et al., 2019, Spillantini et al., 1997, Xia et al., 2008).

However, it is important to note that neither loss of neurons in the SNpc nor the presence of Lewy bodies is specific to PD as similar pathological features can also be observed in Dementia with Lewy bodies, Multiple System Atrophy, Niemann-Pick type C1, Krabbe disease and others. These two pathologies in combination are instead

specifically considered in the diagnosis of idiopathic PD (Halliday et al., 2011, Koga et al., 2021, Dickson, 2012).

6.4 Molecular mechanisms associated with Parkinson's disease.

The molecular mechanisms can be broadly characterized as follows:

6.4.1 α-Synuclein misfolding and aggregation.

Accumulation of misfolded α-Synuclein is one of the hallmarks of Lewy bodies in the dopaminergic neurons of the SNpc. α-Synuclein is a 14kDa protein, comprising 140 amino acids, that is expressed both in the central and peripheral nervous system. The amino acid residues 1-60 at the N-terminus have amphiphatic regions which can form an α-helix structure and are known to facilitate membrane interactions. Residues 61-95 comprises the non-amyloid β-component (NAC) region and is known to be aggregation prone. And the residues 96-140 are negatively charged and are involved in binding to calcium and promote chaperone-like activity (Davidson et al., 1998). The physiological function of α-Synuclein is yet to be completely established. However, since α-Synuclein is associated to presynaptic compartments, it has been shown that α-Synuclein can help in SNARE assembly and is also involved in vesicle trafficking, docking and modulating vesicle interaction leading to the reuptake and release of neurotransmitters (Burre et al., 2010, Calabresi et al., 2023b). Pathological mutations in α-Synuclein or alteration in cellular conditions can cause α-Synuclein to misfold, oligomerize and form aggregated fibrils. Several post-translational modifications, such as phosphorylation at Ser129, can also affect proper folding of α-Synuclein leading to its aggregation (Calabresi et al., 2023a). The accumulation of toxic pathological aggregates is associated to the death of DaNs in PD. α-Synuclein is also present in the nucleus (Maroteaux et al., 1988), endoplasmic reticulum (ER) (Hoozemans et al., 2007), Golgi (Gosavi et al., 2002), mitochondria (Li et al., 2007) and in the endo-lysosomal system (Lee et al., 2004). Misfolded α-Synuclein has been shown to affect the functions of all the above-mentioned organelles.

6.4.2 Mitochondrial dysfunction.

Mitochondria are multifunctional organelles involved in cellular bioenergetics, oxidative balance, calcium buffering, apoptosis, neurotransmitter metabolism, signaling and interactions with other organelles among others (Chakrabarty and Chandel, 2022). Due to their many crucial roles in the brain, their dysfunction is associated with many neurological diseases including PD. Neurons have an elaborate and complex network stretching from the dendrites to the axon terminals. Unlike most other cell types, DaNs have a higher bioenergetic demand as they perform additional functions of neurotransmission, firing and maintenance of their long axons, making them more susceptible to mitochondrial damage. The first evidence of mitochondrial dysfunction in PD came from the accidental consumption of MPTP which was later shown to inhibit complex I of the mitochondrial electron transport chain (ETC) (Langston et al., 1983, Nicklas et al., 1985, Desai et al., 1996). Since then, it has been well established that a disruption of complex-I activity, specifically in dopaminergic neurons of the SNpc, can lead to parkinsonism (Meredith and Rademacher, 2011, Gonzalez-Rodríguez et al., 2021). Impaired activity of the other ETC complexes have also been associated with PD, however the evidence is not consistently reported (Subrahmanian and LaVoie, 2021). Another area of research pointing towards mitochondrial dysfunction in PD comes from the observation of increased aberrations in mitochondrial DNA – deletions and mutations in biospecimens of PD patients compared to age matched healthy individuals (Gu et al., 2002, Bender et al., 2006, Dölle et al., 2016, Puigros et al., 2024, Puigros et al., 2022).

Several PD-linked genes *PINK1*, *PRKN*, *PARK7* among others have a mitochondrial localization and are involved in various processes that help in the maintenance of mitochondrial health. PD-associated mutations in these genes can lead to mitochondrial dysfunction via impaired pathways including mitochondrial fission and fusion, biogenesis of mitochondria and mitochondria derived vesicles, mitophagy, intracellular calcium signaling, impaired activity of ETC complexes and oxidative stress (Lazarou et al., 2015, Deng et al., 2008, Yang et al., 2008, Soubannier et al., 2012a, McLelland et al., 2016, Kumar et al., 2020, Heeman et al., 2011, Morais et al., 2009, Irrcher et al., 2010, Krebiehl et al., 2010, Guzman et al., 2010, Henrich et al., 2023). Findings from PD-associated mitochondrial genes have further demonstrated that multiple mitochondrial pathways are closely linked with PD pathogenesis.

6.4.3 Proteostasis.

The basal steady-state levels of proteins are maintained by synthesis, post-translational modifications, release and degradation. A defect in any part of these processes can cause an impairment in the proteostasis of a system. In PD, there is a strong genetic and molecular evidence of the accumulation of misfolded α-Synuclein and aggregates. Protein clearance is regulated mainly through the ubiquitin-proteasomal system (UPS) and the autophagy lysosomal pathway (ALP) (Hipp et al., 2019, Ebrahimi-Fakhari et al., 2012).

The UPS mainly degrades soluble intracellular proteins in the cytosol, nucleus and ER via a build-up of ubiquitin chains that tag the proteins to be recognized by the proteasome, wherein these proteins are eventually degraded (Goldberg, 2003, Wong and Cuervo, 2010). The involvement of the UPS in PD was initially speculated when the presence of ubiquitin and components of the UPS was discovered in Lewy bodies (Kuzuhara et al., 1988, Lennox et al., 1989, Ii et al., 1997, Kwak et al., 1991, Lowe et al., 1990, Schlossmacher et al., 2002, Zhou et al., 2004). Another line of evidence comes from proteins that are involved in PD, Parkin – an E3 ubiquitin ligase and UCH-L1 – a ubiquitin hydrolase (Kitada et al., 1998, Leroy et al., 1998). Furthermore, reduced proteasomal activity in the SN of PD brain tissues have also been reported (McNaught et al., 2003, Tofaris et al., 2003, McNaught and Jenner, 2001).

The ALP degrades intracellular proteins and organelles in the lysosomes (Wong and Cuervo, 2010). As protein forms like oligomers and fibrils (i.e. α-Synuclein) can be large in size, it has been postulated that many of them cannot pass through the proteasomal barrel and therefore needs to be degraded via the autophagic machineries (Cuervo et al., 2004, Levine and Klionsky, 2004). The accumulation of autophagic vacuoles, membranes and autophagic machineries in the SNpc of PD brain samples are early evidence that suggests the involvement of ALP in PD (Ebrahimi-Fakhari et al., 2012, Anglade et al., 1997, Alvarez-Erviti et al., 2010, Crews et al., 2010, Dehay et al., 2010, Tanji et al., 2011, Chu et al., 2009, Higashi et al., 2011, Li et al., 2011, Tofaris et al., 2011, Shahmoradian et al., 2019). Similarly, an increase in autophagosome marker LC3-II and decrease in marker of lysosomes - LAMP1 have also been identified in PD brain tissues (Ebrahimi-Fakhari et al., 2012). Supporting genetic clues that support ALP dysfunction in PD comes from gene variants and genetic risk factors that are linked to PD that are part of the lysosomes or the endo-

lysosomal system which include *ATP13A2, GBA1, CTSD, CTSB, CTSL, LRRK2* among others (Ramirez et al., 2006, Nalls et al., 2019).
Taken together, the evidence of altered proteostasis may explain abnormal accumulation of misfolded protein aggregates, ruptured organellar membranes and vacuolar vesicles in PD.

6.4.4 Neuroinflammation.

Inflammation, either acute or chronic, is usually a physiological reaction to harmful internal or external stimuli. While acute inflammation could be mainly considered beneficial to a system, sustained chronic inflammation is usually due to persistence presence of toxicity. Multiple cell-types are involved in neuroinflammation which not only include neuronal and non-neuronal glial cells – microglia, astrocytes and oligodendrocytes but also peripheral circulating immune cells - macrophages, monocytes and T-lymphocytes (Kannarkat et al., 2013, MacMahon Copas et al., 2021). Altered cell pathways in DaNs – α-Synuclein aggregation, mitochondrial dysfunction, impaired proteostasis also triggers inflammatory signaling in surrounding immune cells (Arena et al., 2022). This causes the activation of microglia leading to the secretion of high levels of pro-inflammatory mediators (e.g., TNF-α, IL-1β, IL-6, IFN-γ), damaging neurons and perpetuating a cycle of neurodegeneration (Tansey et al., 2007, Fathi et al., 2022, Wang et al., 2015, Arena et al., 2022). Cellular insults from pathogen-associated molecular patterns (PAMPs) and damage-associated molecular patterns (DAMPs) also increase the gene expression of cytokines via the NF-κB pathway. Pathological forms of α-Synuclein can also bind to microglial receptors such as TLR2 and NLRP3 that triggers the NF-κB pathway and the inflammasome assembly which further increases the release of cytokines (Liang et al., 2025).
The brain is typically considered to be isolated from inflammatory molecules via the BBB. However, systemic inflammation can still trigger inflammation in the brain. Insults to the integrity of the BBB can make it become more permeable under conditions due to age, brain injuries and viral infections (Jin et al., 2024, Galea, 2021). Genetics has also been informative in identifying the role of neuroinflammation in PD with the genes *SNCA, PINK1, PRKN, LRRK2, GBA, TMEM175*, all contributing to increasing evidence in the involvement of inflammation in PD (Tansey et al., 2022). Studies of the T-cell subtypes in the PD patients have further associated PD genes in which they found

CD4+ T cells specific to certain α-Synuclein peptides and PINK1, suggesting the presence of adaptive and auto-immunity in PD (Arlehamn et al., 2020, Johansson et al., 2025, Williams et al., 2025).

6.4.5 Gut dysbiosis.

The Braak hypothesis in 2003 introduced a model that PD pathology originates in the gut. The evidence has been backed by gastro-intestinal dysfunction and constipation symptoms that are preceded in PD diagnosis (Braak et al., 2003, Konings et al., 2023, Rietdijk et al., 2017). Since then, the contributions from gut microbiome have been postulated as a mechanism in PD involving the gut-brain axis (Houser and Tansey, 2017, Romano et al., 2021). Molecules from gut microbiota such as bacterial lipopolysaccharides, peptidoglycans, viral double-stranded RNAs that reach the systemic circulation can activate the immune responses thereby releasing pro-inflammatory cytokines such as TNFα, IL-6 and IL-1β can promote neuroinflammatio n (Zhu et al., 2022). Gut dysbiosis can also cause the misfolding and aggregation of α-Synuclein in the enteric nervous system. These aggregates can propagate to the brain via the vagus nerve causing neurodegeneration due to α-Synuclein pathology. Microbial metabolism, such as short-chain fatty acids (SCFAs), that have anti-inflammatory properties, contributes to maintaining the integrity of intestinal barriers. A low number of SCFA-producing bacteria due to gut dysbiosis can cause leakiness of the gut leading to systemic inflammation due to the passage of intestinal pathogens and their products in the blood stream (Aho et al., 2021, Arena et al., 2022, Kalyanaraman et al., 2024, Sun and Shen, 2018).

6.5 Discovery of PINK1.

PINK1 was first identified in 2001 in a screen for genes that are transcriptionally transactivated by the tumor suppressor phosphatase and tensin homolog (PTEN). From the obtained cDNA sequence, it was known that *PINK1* encodes for a 581 amino acid protein having a molecular mass of 62.8 kDa. To gain insights into the function, the motifs of the protein were analyzed using SMART and PSORT II Prediction tools. The results from these protein sequences, localization and secondary structure

prediction tools implied that PINK1 is likely to have a serine/threonine protein kinase catalytic domain. Hence, the name PTEN-induced putative kinase (Unoki and Nakamura, 2001).

In the same year, Valente and colleagues mapped a locus on human chromosome 1p35-p36, named *PARK6*, to autosomal recessive early-onset PD in a large consanguineous family from Sicily, Italy (Valente et al., 2001). Further evidence of *PARK6* linked Parkinsonism was then shown in eight additional families across four European countries (Valente et al., 2002). From these patients' genetic data, the locus of the *PARK6* gene was narrowed down to approximately 40 genes. And based on their putative function and expression in the human SN using cDNA libraries, the candidate genes were prioritized which led to the identification of two homozygous mutations in *PINK1* in three consanguineous families with PD. This study established *PINK1* as a gene that can cause hereditary early-onset PD (Valente et al., 2004). In the same study, due to the presence of mitochondrial targeting sequence in PINK1, it was demonstrated that PINK1 localizes at the mitochondria.

6.6 PINK1 Life Cycle.

The life cycle of PINK1 can be different depending on the state of mitochondria (Figure 3). Under healthy physiological conditions, PINK1 has a very short half-life of ~30 minutes (Lin and Kang, 2008, Ando et al., 2017, Sharma et al., 2024). In the cell it can be found in the cytosol or at the mitochondria(Lin and Kang, 2008). PINK1 is imported to the inner membrane of the mitochondria via the TOM protein complex and TIM (TIM17 and TIM23) proteins. In the mitochondria, PINK1 is cleaved by a protease PARL in the transmembrane domain and released into the cytosol (Jin et al., 2010, Aho et al., 2021, Deas et al., 2011). Due to the cleavage, PINK1 has now an N-terminal phenylalanine which is an N-degron making this cleaved PINK1 follow the N-end rule for degradation. Cleaved PINK1 is now recognized by E3 ubiquitin ligases – UBR1/2/4 which ubiquitinates cleaved PINK1 and targets it to the proteasomes for degradation (Lin and Kang, 2008, Muqit et al., 2006, Yamano and Youle, 2013).

Upon mitochondrial damage, due to membrane depolarization, mitochondrial DNA mutation, increased reactive oxygen species (ROS) or due to misfolded proteins, PINK1 stabilizes at the outer membrane of the mitochondria and forms a complex with TOM proteins (Lazarou et al., 2012, Okatsu et al., 2013, Narendra et al., 2010) and

TIM17-TIM23 (Akabane et al., 2023, Eldeeb et al., 2024). However, mitochondrial depolarization prevents the cleavage of PINK1 by PARL causing it to accumulate at the mitochondria instead (Greene et al., 2012). The accumulation of PINK1 is at the mitochondrial outer membrane (MOM) where it is associated and anchored by the TOM complex proteins. The N-terminus of PINK1 is in complex with TIM17-TIM23 whereas the C-terminus kinase lobe of PINK1 faces the cytosol and undergoes trans-autophosphorylation on serine 228 thereby forming a dimer which triggers it activation (Rasool et al., 2022, Gan et al., 2022, Callegari et al., 2025).

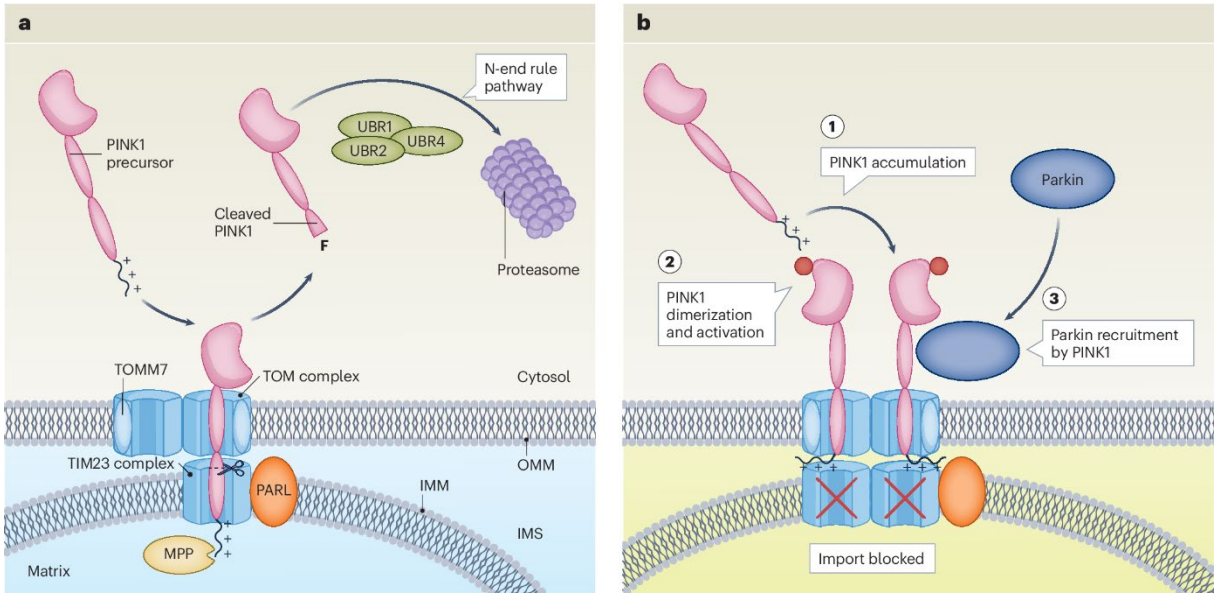

Figure 3: Life cycle of PINK1 under (a) normal physiological conditions and (b) under mitochondrial stress. Image taken from (Narendra and Youle, 2024).

6.7 Role of PINK1.

6.7.1 PINK1/Parkin mitophagy.

Upon sensing mitochondrial damage, the complete import of PINK1 into the mitochondria is halted leading to its stabilization and accumulation at the MOM. Stabilized PINK1 at the mitochondria undergoes autophosphorylation and becomes active. Activated PINK1 phosphorylates both ubiquitin and the E3 ubiquitin ligase Parkin, which is normally found in the cytosol in its inactive form (Kazlauskaite et al.,

2014, Kondapalli et al., 2012, Kane et al., 2014, Koyano et al., 2014). These phosphorylation events trigger Parkin's translocation to damaged mitochondria and activate its E3 ubiquitin ligase activity (Wauer et al., 2015). Parkin ubiquitinates multiple proteins (such as Mfn1/2, VDAC, Miro1 and CISD1) at the MOM (Geisler et al., 2010, Wang et al., 2011, Narendra and Youle, 2024). The ubiquitin chains are further phosphorylated by PINK1, amplifying the signal for mitophagy. The ubiquitinated and phosphorylated mitochondrial surface is then recognized by autophagy adaptors (e.g., p62, NDP52, OPTN) which link damaged mitochondria to the autophagosome membrane via the LC3-family proteins (Lazarou et al., 2015). The damaged mitochondrion is enveloped by an autophagosome, which then fuses with a lysosome leading to degradation of the mitochondria. This sequence of events leading to the clearance of damaged mitochondria is termed as PINK1/Parkin dependent mitophagy.

6.7.2 Mitochondrial Fission.

Mitochondria constantly undergo fission and fusion dynamics to meet the changing metabolic needs of a cell/system. Fission leads to the generation of smaller mitochondria which can help mitochondria traverse larger distances within neurons, potentially reaching dendritic ends. Fusion on the other hand leads to the formation of a larger mitochondrion that has the ability for a higher oxidative phosphorylation efficiency and can help neurons in meeting their bioenergetic needs (van der Bliek et al., 2013, Mishra and Chan, 2016, Kageyama et al., 2012). PINK1 has been shown to play a role in the modulation of fission proteins - Drp1 and Fis1. PINK1 can directly phosphorylate Drp1 at serine 616 (S616), promoting Drp1 activation and its recruitment to mitochondria. The phosphorylation mediated activation of Drp1 causes mitochondrial fission. A loss of PINK1 results in reduced S616 Drp1 phosphorylation, leading to an enlarged mitochondrion, whereas overexpression of PINK1 increases mitochondrial fission and produces smaller, punctate mitochondria (Han et al., 2020, Gao et al., 2022). Yang and colleagues have also shown the interaction of PINK1 with Fis1, another key protein required for fission. They also show that Fis1 acts as mediator between PINK1 and Drp1 for mitochondrial fission (Yang et al., 2008).

6.7.3 Mitochondria-derived vesicles.

Mitochondria-derived vesicles (MDVs) are small (70-150nm), single or double membrane-bound vesicles that bud off from mitochondria to selectively export damaged or oxidized mitochondrial components for degradation. This process is independent of mitochondrial fission machinery and different from mitophagy as only selective chunks of the mitochondria are removed (Sugiura et al., 2014). MDV biogenesis is initiated in response to mild mitochondrial stress during which PINK1 accumulates at sites of damage on the MOM, activating Parkin and via their coordinated action leads to the budding of MDVs. MDVs may contain distinct membrane markers, including TOM20 (outer membrane) or Pyruvate dehydrogenase (inner membrane/matrix). These vesicles traffic to the lysosomes for degradation. Loss of PINK1 can lead to an increase in certain types of MDVs (like TOM20-positive MDVs), suggesting PINK1 may normally repress some MDV formation (Sugiura et al., 2014, McLelland et al., 2014, Soubannier et al., 2012a, Soubannier et al., 2012b).

6.7.4 Calcium homeostasis.

Loss of PINK1 leads to increased ER calcium release via increased activity of the inositol 1,4,5-trisphosphate receptor (IP3R) in neurons which elevate calcium levels in the cytosol and mitochondria. An elevated mitochondrial calcium leads to increased susceptibility to calcium-induced mitochondrial permeability transition that could trigger apoptosis. This regulation of calcium was shown to depend on PINK1's kinase activity, involvement of Parkin and increased IP3R activity due to reduced protein levels of CDGSH iron sulfur domain 1 (CISD1). CISD1 is localized at MOM and has transmembrane and iron-sulfur domains. CISD1 forms a homodimer at MOM and directly interacts with IP3R at the ER-mitochondria contact sites and modulates the activity of IP3R (Ham et al., 2023). PINK1 can also phosphorylate LETM1 at Thr192, a mitochondrial inner membrane protein that facilitates calcium transport. Phosphorylated LETM1 improves both calcium uptake and release in mitochondria, protecting neurons from calcium stress (Huang et al., 2017). Evidence of impaired calcium homeostasis is further supported by multiple independent studies showing a dysregulation of mitochondrial calcium in PINK1 neurons (Bus et al., 2020, Grossmann et al., 2023).

6.7.5 ER Quality.

In addition to the involvement of PINK1 and ER in maintaining calcium homeostasis in neurons, the interaction of mitochondria and ER via contact sites regulates other functions as well. Key ER components such as E3 ligases - gp78 and HRD1, along with proteins like VCP, can help regulate PINK1 levels and maintain mitochondrial quality control by ubiquitinating PINK1 and marking it for proteasomal degradation (Guardia-Laguarta et al., 2019). PINK1 also helps in the selective clearance of the ER via autophagy (ERphagy) by influencing proteins like KEAP1 and ubiquitination of ERphagy receptor, RTNL1 (Wang et al., 2023). PINK1 has also been shown to control RTN3L, another ERphagy receptor via RTN3L-SEC24C dependent ERphagy by regulating and reshaping peripheral tubule junctions (Chidambaram et al., 2024). PINK1 has been proposed to have a dual role in determining the clearance of both mitochondria and ER via Parkin and KEAP1, respectively (Wang et al., 2023). However, the direct association of PINK1 in ERphagy mechanism has not been elucidated yet. This balanced removal of both damaged ER and mitochondria highlights PINK1's broader role in maintaining organelle homeostasis beyond mitochondria.

6.7.6 Mitochondria-ER contacts.

The localization of PINK1 at MOM and in being in close contact with the ER via ER mitochondria contacts has been established by multiple studies that have shown the regulation of PINK1 levels at mitochondria (Guardia-Laguarta et al., 2019), calcium homeostasis (Grossmann et al., 2023, Ham et al., 2023) and ERphagy (Wang et al., 2023). Recently, a study has further shown the local synthesis of PINK1 near ER-associated ribosomes and involving chaperone interactions at the mitochondria ER contact sites. This process aids in the direct delivery of PINK1 protein to the mitochondria (Hees et al., 2024). PINK1 deficiency and loss of kinase function mutations have also been shown to alter mitochondria-ER contacts. However, whether these contacts are increased or decreased is not clear due to contradictory reports (Parrado-Fernández et al., 2018, Grossmann et al., 2023, Bus et al., 2019, Celardo et al., 2016). While it is clear that these contacts are affected, further studies are needed using advanced experimental setup (sensors that get activated only upon close

contacts or interaction using reliable ER and mitochondria markers) and imaging techniques (i.e., super-resolution microscopy) on live DaNs using isogenic PINK1 models to understand the regulation of mitochondria-ER contacts due to the loss of PINK1.

6.7.7 Inflammation.

A loss in PINK1 function can affect the formation of MDVs and lead to the accumulation of DAMPs from damaged mitochondria. In this situation, antigen presenting cells (APC) recognize mitochondrial peptides via major histocompatibility complex I (MHCI) in a process known as mitochondrial antigen presentation (MitAP). MitAP can cause the development of T-cells that are specific to mitochondrial antigens and lead to T-cell dependent autoimmunity in PINK-PD (Matheoud et al., 2016). Other studies have also shown the modulation of immune responses due to oxidative stress and viral infection in the absence of PINK1 (Zhou et al., 2019, Sun et al., 2018). Intestinal infection with Gram-negative bacteria (especially *Citrobacter rodentium*) in PINK1 knockout (KO) mice was also shown to induce $CD8^+$ T-cell autoreactivity providing evidence for the involvement of the gut-brain axis in PINK1-PD (Matheoud et al., 2019). Another study also showed a similar finding due to infection with *Helicobacter pylori* in PINK1 KO mice suggesting the involvement of gene-environment interactions in PD (Kazanova et al., 2024). Both of these studies were able to show motor and cognitive phenotypes in PINK1 KO mice following infection. A follow-up study with *Citrobacter rodentium* infected PINK1 KO mice provided an early-stage characterization for the immunological events in the gut where Recinto and colleagues showed that within one week of infection there was an increase in the differentiation of proinflammatory myeloid cells with enhanced antigen presentation. In the second week post-infection, the presence of T-cell cytotoxic profiles was already evident. Activated myeloid cells also had an upregulation of IL-6 and IL-1β secretion (Recinto et al., 2025). Future work in the identification of specific targeting signals that the T-cells acquire against would be useful in understanding the molecular damages that are associated in PINK1 associated PD.

6.7.8 Apoptosis.

The accumulation of dysfunctional organelles can generate excess ROS and release pro-apoptotic molecules such as cytochrome c (Yang et al., 2024). It has been shown that PINK1 can phosphorylate proteins Bcl-xL and Beclin1, thereby modulating MOM permeabilization and influencing susceptibility to apoptosis (Arena et al., 2013, Brunelli et al., 2022). In addition, loss of PINK1 has been associated with enhanced activation of caspase-3 and caspase-9, indicating a role in the intrinsic apoptotic pathway (Imbriani et al., 2019). Conversely, overexpression of PINK1 has been shown to protect cells from apoptosis induced by oxidative insults, suggesting that PINK1 may act as a direct anti-apoptotic factor (Petit et al., 2005).

6.8 Challenges associated with the study of PINK1 and Parkinson's disease.

6.8.1 Complexity of PINK1 regulation.

Under physiological conditions, PINK1 is continuously imported into mitochondria and rapidly degraded via PARL protease and/or via the ER-associated degradation machinery involving the ubiquitination via gp78 or HRD1, targeting PINK1 for proteasomal degradation (Narendra and Youle, 2024, Guardia-Laguarta et al., 2019). Due to the rapid degradation, PINK1 has an estimated half-life of 30 minutes which makes it difficult to study the role of PINK1. Many studies have had to manipulate cellular conditions by either overexpressing PINK1 or inducing mitochondrial stress or depolarization to study PINK1. This manipulation may miss out in deciphering PINK1 targets under physiological conditions as the cell's metabolism is shifted to respond to the mitochondrial stress and in the elimination of damaged mitochondria. Interventions in stabilizing endogenous PINK1 may further help in our understanding of PINK1.
The structures of isolated kinase domains of PINK1 have been resolved from studies using insects and body louse (Gan et al., 2022, Rasool et al., 2022). However, purification of human PINK1 has proven to be a challenge. A recent study has been successful in purifying human PINK1 that was stalled at the mitochondria after depolarization and have already laid the groundwork for purified human PINK1 studies (Callegari et al., 2025). But the N-terminus of PINK1 which also contain patient

mutations remains unresolved. A full-length structure of human PINK1 may help in the development of PINK1 stabilizers or activators and will be critical in understanding PINK1-PD. *In vitro* kinase assay for purified human PINK1 is also yet to be established. Evolution of PINK1 in the human kinome highlights a unique evolutionary branch and an unusual activity, suggesting the possible requirement of additional unknown cofactors for an *in vitro* kinase assay.

6.8.2 Involvement of other brain cells.

The degeneration of DaNs is a mainstay in the pathology of PD. However, it has been shown that other cell types in the brain are also involved or are affected in PD pathogenesis as there are evidences of neuroinflammation, activation of microglia and the presence of α-Synuclein aggregates in non-neuronal cells such as astrocytes, microglia and pericytes (Tansey et al., 2022, Stevenson et al., 2020). Furthermore, the predominant expression of LRRK2 in microglia compared to neurons also suggests the involvement of non-neuronal cells in PD pathology (Langston et al., 2022). Recent developments in single cell and single nucleus RNA sequencing applications have revolutionized our understanding of cell type changes in postmortem PD midbrain tissues. These studies revealed that glial cells, particularly microglia and astrocytes, show pronounced transcriptional alterations in PD, pointing to their significant role in disease progression, in addition to neuron loss. The loss of oligodendrocytes has also been shown in the midbrain of PD patients further highlighting the gap in our understanding of PD biology (Smajic et al., 2022, Fiorini et al., 2024).

The expression of PINK1 has also been shown to increase during development and differentiation of neural stem cells. The lack of PINK1 can also affect the development of GFAP-positive astrocytes (Choi et al., 2016). Interestingly, Barodia et. al. have shown in a rat model system that PINK1 phosphorylates ubiquitin at Ser65 predominantly in astrocytes, followed by oligodendrocyte precursor cells (OPCs) as compared to neurons, suggesting that the role of PINK1 is not limited to neurons but may rather involve a more complex co-ordination among brain cells for survival (Barodia et al., 2019).

6.8.3 Age-dependent pathology.

PD is widely considered an age-related disorder as the risk for developing PD increases with age. Aging, additionally, introduces factors such as slower metabolism, build-up of toxic misfolded proteins along with acute or chronic exposure to environmental stress. This interplay may produce a more severe and complex phenotype than either aging or PD mutations alone. Additionally, genetic and environmental interactions during aging have not yet been completely understood.
Researchers model PD using various systems which include animals such as flies, mice and primates, human cells, iPSC derived DaNs and brain organoids. No model system has yet to recapitulate the complete PD pathology as they often lack features that can incorporate aging or are not human specific. Animal models have helped us in understanding motor symptoms, inflammation and many PD associated mechanisms, however, the major drawback of using animal models is that they may lack specific cellular mechanisms that are unique to humans. iPSC derived DaNs or organoids also do not fully recapitulate the physiology of human brain because they do not retain aging signatures (Rocha et al., 2023). The involvement of peripheral nervous system and gut have also not been modeled in a system using iPSC derived brain cells/tissues. All model systems, along with data from human biospecimen can instead help us with understanding PD as each of them have their specific advantages and disadvantages.

6.8.4 Incomplete genetic understanding.

PINK1 mutations can cause autosomal-recessive early-onset PD. While homozygous PINK1 mutations are associated with autosomal-recessive PD, many heterozygous variants have been found in both PD patients and healthy individuals. This may raise the question about whether some heterozygous mutations may act as risk factors (Abou-Sleiman et al., 2006).
Heterozygous G411S variant has increased frequency in PD cases and impairs PINK1 kinase activity, suggesting a dominant negative mechanism. Not all carriers of PINK1 mutations develop PD or show symptoms, indicating incomplete penetrance and the influence of genetic and gene-environment interactions, which complicates risk

prediction (Gandhi and Plun-Favreau, 2017). While over 100 mutations in the PINK1 gene have been linked to PD, the precise consequences of many variants are unclear. For example, R98W mutation at the PINK1 transmembrane region alter protein positioning or processing and an increase in mitophagy due to accumulation at the MOM (Brassard et al., 2025). Furthermore, despite evidence that some PINK1 variants contribute to PD risk, PINK1 has not emerged strongly in GWAS, likely due to low variant frequency and/or population differences as majority of these studies have been performed in the Caucasian population. This limits the understanding of PINK1's broader role in sporadic PD. A recent report has found higher frequency of PINK1 variants in populations of Polynesian descent. This study also found that 1 in 1300 West Polynesians carry L347P variant of PINK1, which is well above the typical rarity threshold of 1 in 2200 (Yin and Dieriks, 2025). Their finding further highlights that we may be overlooking some communities and that having a more inclusive approach may help us further in understanding PD.

7. Aims and Objectives.

The overarching aim of this thesis was to investigate the molecular and cellular mechanisms underlying PINK1 associated PD using human DaN models. PD, a progressive neurodegenerative disorder, remains one of the most challenging conditions to treat because its underlying biology is still incompletely understood. Among the various genetic contributors, mutations in the *PINK1* gene are particularly significant, as they cause autosomal recessive early-onset PD. Despite being discovered more than two decades ago, the full spectrum of PINK1's physiological functions have not been fully defined. The main aim of this thesis was therefore to bridge these knowledge gaps by combining gene mutations, molecular and cellular biology and proteomics-based approaches in human DaNs.

The first aim was to extend the genetic understanding of PD beyond European ancestry populations. By characterizing a novel PINK1 mutation (p.F385S) in an Indian family with early-onset PD, we sought to highlight the importance of expanding genetic studies to diverse populations. The genetic analysis was accompanied by functional validation to determine how this mutation destabilizes the DFG kinase activation domain, impairs phosphorylation of ubiquitin at Ser65, prevents Parkin recruitment and ultimately impairs canonical PINK1/Parkin mitophagy.

The second aim was to capture the dynamic proteomic landscape of human DaNs. Unlike proliferative cells, neurons have long lifespans and unique proteome dynamics. We aimed to provide comprehensive datasets on protein turnover, subcellular trafficking, and compartment-specific proteostasis in DaNs. The use of microfluidic devices allowed separation of axonal compartments, enabling a method to study protein synthesis and trafficking. This approach aimed to provide a methodological advancement in studying neurological disorders and to provide a resource for the proteome dynamics in human DaNs.

The third aim was to study PINK1 biology beyond its canonical role in mitochondrial quality control. While PINK1/Parkin-dependent mitophagy is well established, most previous research relied on using non-physiological mitochondrial depolarization agents. This work aimed to explore PINK1 LOF under basal physiological conditions, revealing a previously unrecognized regulatory role in cholesterol metabolism. By identifying that PINK1 loss stabilizes SCAP, enhances cholesterol biosynthesis, and

disrupts dopamine transporter localization, we found cholesterol imbalance as an early cellular phenotype in the pathogenesis of PINK1 associated PD.

In summary, the aims of this dissertation were to: (1) expand the genetic architecture of PD through genetic studies in the Indian population; (2) provide mechanistic validation of a novel PINK1 mutation; (3) map the proteomic dynamics of human DaNs; (4) identify a novel regulatory role of PINK1 cholesterol metabolism and (5) evaluate the potential therapeutic role of cholesterol modulating drugs.

8. Results and Discussion.

8.1 Manuscript 1: A Novel PINK1 p.F385S Loss-of-Function Mutation in an Indian Family with Parkinson's Disease.

Much of the genetic landscape of PD has been derived from the European populations, leaving significant gaps in our understanding of how PD manifests in genetically diverse groups globally. The transferability of findings from European cohorts to other populations is limited, partly due to differences in genetic background, founder effects, and gene-environment interactions. This lack of representation has implications that may restrict diagnostic accuracy and limit the global applicability of potential gene targeted therapies.

Despite recent advances, the genetic architecture of PD remains incompletely defined worldwide. The South Asian population, comprising India with its vast genetic diversity and unique environmental exposures, provides an important region for expanding PD genetics. Previous large-scale studies have shown that loci identified in European GWAS often do not replicate completely with Indian cohorts, highlighting the possibility of unidentified population specific variants.

In this study, we aimed to bridge this gap by investigating a well characterized Indian family with multiple members affected by early-onset PD.

8.1.2 Identification of a novel PINK1 p. F385S mutation in an Indian family.

Using exome sequencing, we identified a previously unreported mutation in the PINK1 gene: a homozygous missense substitution p.F385S in three individuals of an Indian family across two generations who have been affected by early-onset PD (Fig 1A). Clinically, all affected carriers presented with early-onset PD. They exhibited classical motor features of PD - bradykinesia, rigidity and tremor along with psychiatric symptoms. Importantly, their symptoms responded well to levodopa therapy, consistent with the clinical profile of PINK1 associated PD.

The mutation was located at chromosome 1:20648535 (GRCh38). At the protein level, this resulted in the replacement of phenylalanine with serine at position 385 (p.F385S)

within exon 6. This substitution was present in homozygous form in affected individuals but absent in unaffected family members.

Analysis of runs of homozygosity (ROH) around the PINK1 locus revealed a 2.26 Mb shared segment across affected individuals. This provided genomic evidence consistent with consanguinity, even though none was reported at the time of family recruitment. Such findings explained the apparent pseudodominant mode of inheritance in this family where autosomal recessive disorders appear to follow a dominant inheritance pattern due to shared ancestry.

The p.F385S substitution was absent in over 1,000 Indian genomes cataloged in the IndiGenomes project, as well as in large global datasets such as gnomAD, which includes genomic sequences from diverse populations. This confirmed that the variant is not a common polymorphism but rather a rare, likely pathogenic mutation that is unique to this family.

8.1.3 In Silico Modeling Predicts Disruption of Kinase Activation.

Following genetic identification, the structural and biochemical implications of the F385S substitution were investigated through computational modeling. PINK1's full-length 3D structure was predicted by AlphaFold2 and used as a template. F385 lies within the highly conserved DFG motif that regulates ATP binding and catalysis (Fig 1B-D).

Structural models revealed that the serine substitution disrupted hydrophobic interactions needed to maintain the DFG-in conformation associated with kinase activity. The predicted change in free energy (ddG) for the mutant was significantly higher than that for WT, reflecting higher structural instability. Importantly, this destabilization was more evident in the active conformation ($P = 9.25 \times 10^{-18}$), whereas the inactive conformation was less destabilized ($P = 4.7 \times 10^{-4}$), suggesting a strong shift in the conformation towards the inactive state which could impair kinase activation (Fig 1E).

8.1.4 F385S mutant PINK1 has reduced stability.

Under normal conditions, full-length PINK1 (~63 kDa) is imported into mitochondria where its N-terminal targeting sequence is cleaved, producing a ~53 kDa fragment (ΔN1). Another truncated product (~45 kDa, ΔN2) arises through cleavage and is rapidly degraded by the proteasome. Cells expressing the F385S mutant showed a similar processing profile. This indicated that the mutation did not prevent import into mitochondria or the cleavage by mitochondrial proteases (Fig 1F).
However, treatment with cycloheximide to inhibit protein synthesis revealed that full-length F385S PINK1 had a slight but significantly shorter half-life (26.2 minutes) compared to WT PINK1 (30 minutes). Although the reduction was small, it showed a tendency towards increased degradation (Fig 1G).

8.1.5 F385S Mutation Abolishes Phosphorylation of Ubiquitin at Ser65.

The most widely accepted function of PINK1 is phosphorylation of ubiquitin at Ser65 which serves as the trigger for Parkin activation and PINK1/Parkin mitophagy. To test this, we reconstituted the PINK1/Parkin system in HeLa cells lacking functional endogenous PINK1 and Parkin (Fig 2 A-C).
When WT PINK1 was expressed with Parkin, treatment with the mitochondrial uncoupler CCCP induced phosphorylation of ubiquitin at Ser65. However, cells expressing the F385S mutant exhibited almost complete loss of ubiquitin phosphorylation. Only a residual signal was detected after CCCP treatment, amounting to less than 10% of WT levels (Fig 2D-E). Under basal conditions without CCCP, phosphorylation was entirely absent. Importantly, levels of Parkin itself was unchanged, confirming that the effect was due to impaired PINK1 activity.

8.1.6 F385S Mutation Impairs Parkin Recruitment.

As the phosphorylation of ubiquitin was impaired, the downstream consequences for parkin recruitment and mitochondrial morphology were examined. In cells expressing WT PINK1 and Parkin, CCCP induced mitochondrial depolarization led to significant changes in/at the mitochondria. The mitochondrial marker SSBP1 aggregated into large clusters, reflecting active mitophagy (Fig 2F). Correspondingly, parkin translocated to mitochondria in the majority of cells (83%). However, in cells expressing

the F385S mutant, mitochondria retained a dispersed morphology with many small foci of SSBP1, similar to our control lacking PINK1. Quantitative image analysis confirmed that the mean mitochondrial size was significantly reduced and the number of mitochondrial foci per cell significantly increased compared with WT PINK1 (Fig 2 G-H). Parkin remained largely cytosolic, with only ~1% of cells showing mitochondrial localization (Fig 2I).
These findings show that the F385S impairs PINK1/Parkin mitophagy, as Parkin is not recruited and the mitochondria do not cluster into mitoaggresomes.

Taken together, substitution of phenylalanine with serine at 385 within the DFG motif destabilizes PINK1, reduces stability and kinase activity. This leads to almost complete loss of ubiquitin phosphorylation at Ser65, absence of Parkin recruitment and failure to initiate mitophagy. Importantly, these findings extend the database of pathogenic PINK1 mutations beyond those already reported in European ancestry populations.

8.2 Manuscript 2: Proteome Dynamics in Human iPSC Derived Dopaminergic Neurons.

DaNs, characterized by their ability to synthesize and release dopamine, constitute a vital subset of neurons within the central nervous system, particularly concentrated in the SNpc and the ventral tegmental area. Their degeneration in the SNpc is closely associated with Parkinsonian syndromes. Despite extensive characterization of their electrophysiological properties and synaptic connectivity, comprehensive insights into the temporal dynamics of their proteome remain limited. Unlike proliferative cells, neurons must maintain a delicate balance of protein synthesis, degradation and transport over prolonged lifespans requiring the need for proper regulation of proteostasis. Using iPSC derived human dopaminergic neurons (hDaNs), we can circumvent the limited inaccessibility of primary human neuronal tissue and apply quantitative proteomics to probe into their dynamic proteome landscape.

To characterize the proteome dynamics of iPSC derived hDaNs, we implemented a workflow combining in-depth proteome profiling, measurement of protein turnover rates using dynamic SILAC labeling (Stable Isotope Labeling by Amino acids in Cell culture) and spatio-temporal analysis of axonal and somatodendritic proteomes using microfluidic devices.

8.2.1 Proteome coverage of iPSC derived hDaNs.

We assessed the global proteomic landscape of mature hDaNs, harvested at day 23 of differentiation and performed peptide fractionation and analyzed using data-independent acquisition (DIA) mass spectrometry. Across three independent differentiation replicates, we identified a total of 9,409 protein groups. Our data is one of the deepest proteomic coverages that have been reported for iPSC derived neurons. To evaluate the depth of this dataset, we used MitoCarta3.0 as a reference and detected 913 mitochondrial proteins which is a coverage of ~81%, underscoring the extensive representation of subcellular compartments in our dataset. This suggests that the proteome coverage achieved a good representation of the cellular proteome in these neurons (Fig S1A-B).

Next, we stratified proteins into five abundance bins based on DIA intensities and performed enrichment analysis using the Panther database. Proteins with the highest

intensities were enriched in pathways including PD, Huntington's disease, cytoskeletal regulation by Rho GTPases and glycolysis. Lower intensity bins still showed strong representation of pathways relevant to dopaminergic function, such as ubiquitin proteasome signaling, synaptic vesicle trafficking, dopamine receptor signaling, Hedgehog signaling and axon guidance (Fig S1C). These results confirm that our hDaN cultures dataset could recapitulate the molecular hallmarks of midbrain DaNs.

8.2.2 Protein turnover in hDaNs.

To measure protein turnover, we used dynamic SILAC labeling. hDaNs were pulsed with heavy isotope-labeled lysine and arginine containing medium at day 18, and harvested at five time points (6, 12, 48, 72, and 120 hours). High pH fractionation followed by LC-MS/MS enabled quantification of approximately 6,000 protein groups per time point. Using this method, we determined the half-lives of 4,397 proteins, including 554 mitochondrial proteins and 59 MOM proteins (Fig 2A). Protein half lives in hDaNs ranged from ~1 day to over 20 days, with a median half-life of ~97 hours (~4 days). This range is broadly consistent with values reported in other mammalian neurons, but our dataset represents the first turnover study in human specific DaNs (Fig S2B-C).

Mitochondrial and ribosomal proteins tend to be long lived, with half-lives significantly higher than the population average, whereas synaptic proteins were significantly short lived. These findings align with the high metabolic stability of mitochondria and the need for rapid metabolism at the synapses.

Pathway enrichment analysis revealed that proteins with short half-lives (<3 days) were enriched in synaptic vesicle trafficking, Wnt signaling, and Alzheimer's disease associated pathways. Proteins with intermediate half-lives (3-7 days) were enriched in dopamine receptor mediated signaling, DNA replication and PDGF pathways. While long lived proteins (>7 days) were associated with central metabolism, TCA cycle, cholesterol metabolism and purine synthesis (Fig S2D).

8.2.3 Dynamics of respiratory chain complexes.

Given the central role of mitochondrial dysfunction in PD, we quantified turnover rates of respiratory chain complexes. We observed variations in turnover rates across complexes and even among subunits of the same complex. Complex I, which has 44 subunits (7 mitochondrial encoded) displayed particularly heterogeneous turnover with peripheral subunits turning over faster than core subunits. In contrast, Complex V (ATP synthase) subunits tended to be long-lived (Fig 2D).
Comparative analysis with proliferative cancer cells revealed that respiratory complex subunits turned over more slowly in hDaNs. This difference was mainly confined to nuclear encoded subunits as mitochondrial DNA encoded subunits showed similar turnover between the two cell types. These findings highlight the distinct proteostasis demands of post mitotic neurons compared to highly proliferative cancer cells.

8.2.4 Validation of microfluidic devices for axonal analysis.

To spatially resolve soma and axon proteomes, we cultured hDaNs in microfluidic devices separated by 900 µm microgroove barriers. To confirm fluidic isolation, we performed control experiments where heavy SILAC amino acids were added only to the distal (axonal) chamber before axons had crossed the barrier. After 48 hours, <0.02% of proximal proteins showed labeling less than the 1% FDR threshold, confirming negligible diffusion (Fig 3A-C, S4A). Additional live imaging with mitochondrial and lipid dyes further showed the absence of leakage, with only intracellular trafficking observed across the barrier (Fig S5D-F).

8.2.5 Somatodendritic and axonal proteomes.

Using differential SILAC labeling, we quantified up to 3,400 proteins in the soma-enriched chamber and ~500 proteins in the axonal chamber across four time points. In total, we identified 3,915 unique proteins, of which 1,279 were shared between both compartments, 2,576 were exclusive to the soma, and 60 were detected only in the axons (Fig 3E-G). Principal component analysis clearly separated axonal from somatodendritic proteomes. For validation, nuclear protein NeuN was enriched in somatic samples, while known axonal markers MAPT and MAP1B were enriched in axonal samples (Fig 3H-I, Fig S4D).

We further examined proteins enriched at least fourfold in the axon, yielding a set of 127 candidate axonal proteins (Fig S4E-F). Among these, 22 were annotated as axonal by Gene Ontology, including canonical markers MAPT and MAP1B. The remaining 105 proteins represent putative novel axonal markers of hDaNs (Fig S4F). We validated the axonal localization of GAP43 and STMN2 using immunofluorescence microscopy, confirming their enrichment in axons (Fig S5G-H). Enrichment analysis of axon specific proteins revealed representation of synaptic vesicle membranes, SNARE complexes and exocytic vesicles (Fig S4G).

8.2.6 Local protein synthesis and trafficking between soma and axons.

Proteins labeled with medium SILAC in axons were interpreted as soma synthesized and transported anterogradely, while proteins labeled with heavy SILAC in soma were interpreted as axon synthesized and transported retrogradely. Overall, we identified 269 trafficking proteins of which 141 were soma synthesized and trafficked to axons, 154 were axon synthesized and trafficked to soma and 26 were detected moving in both directions (Fig 3G).
To validate active protein synthesis, we inhibited translation with CHX. As expected, CHX in the soma abolished medium labeling and reduced heavy labeling in the axonal chamber, indicating that soma translation contributes to axonal proteins. Also, CHX in the axonal chamber had negligible impact, likely due to the lower protein abundance in axonal samples (Fig 4B).

To biologically associate our findings with the proteomic dataset, we used a few examples:
KIF5C (kinesin heavy chain): Synthesized in soma and transported to axons (Fig 5A).
KLC1 (kinesin light chain): Showed similar soma-to-axon transport dynamics, consistent with its role in kinesin-1 complexes (Fig 5B).
DHX30 (RNA helicase): Synthesized in axons and retrogradely transported to soma (Fig 5C).
ADAR1 (RNA editing enzyme): Also synthesized in axons and trafficked to soma, but at a slower rate (Fig 5D).
SEC24A (COPII vesicle protein): Primarily synthesized in axons and transported to soma, suggesting localized vesicle assembly functions (Fig 5E).

RAB11B (small GTPase): Detected as bidirectionally trafficked, consistent with its roles in vesicle recycling and mitophagy regulation (Fig 5F).
These examples demonstrate that dopaminergic axons have local translation capacity and can synthesize proteins implicated in RNA editing, mitochondrial function and vesicle trafficking.

The study's findings provide a thorough understanding of neuronal proteome dynamics, integrating global turnover measurements, compartment specific protein profiling and microfluidic based synthesis and transport analyses. The identification of previously uncharacterized axonal markers and locally synthesized proteins underscores the complexity of protein regulation in neurons and highlights the importance of spatially resolved proteomics for understanding neuronal function. Moreover, the use of microfluidic separation chambers with quantitative proteomics provides a methodological advance enabling the analysis of compartment specific protein dynamics.

8.3 Manuscript 3: PINK1 regulates cholesterol homeostasis via SCAP phosphorylation in human dopaminergic neurons.

PINK1 has long been primarily recognized as a regulator of mitochondrial quality control, mostly through PINK1/Parkin mediated mitophagy. However, most of these studies have been performed under mitochondrial depolarizing conditions that may not mimic physiological conditions. Therefore, to bridge this gap in our understanding of PINK1-PD, we aimed to study the effects of PINK1 LOF without the use of depolarizing agents in iPSC derived hDaNs.

8.3.1 PINK1 LOF Reduces SCAP Phosphorylation at Ser822 and Ser838.

To investigate molecular alterations arising from the loss of PINK1, we performed an unbiased, mass-spectrometry–based phosphoproteomics in iPSC derived hDaNs. We used two independent PINK1 LOF systems: a PINK1 knockout (KO) model and neurons derived from PD patient carrying the pathogenic PINK1 Q456X mutation. Each was compared against its respective isogenic control lines (Fig 1A-C, Fig S1A-D). This approach ensured that the observed effects were not influenced by an individual's genetic predisposition.

Across all samples, we quantified approximately 2000 proteins, with no significant global changes in total protein abundance between mutants and control DaNs (Fig S1A). From over 13,000 phosphorylation sites identified with high localization confidence, around 6500 sites were quantified per condition (Fig S1B). Among these, we found reduced phosphorylation of sterol regulatory element-binding protein cleavage-activating protein (SCAP) at two serine residues, Ser822 and Ser838, in both PINK1 KO and PINK1 Q456X DaNs. Manual inspection of annotated MS/MS spectra confirmed the precise localization of these phosphorylation sites (Fig S2). Mapping the peptide sequence to the canonical SCAP sequence (UniProt Q12770-1) further validated the detected residues.

Other phosphoproteins with altered phosphorylation included CLASP1/2, MAP1B and KLC4 (involved in microtubule regulation), PAK2 and DAB2IP (linked to dendritic development) and proteins regulating the endo-lysosomal system and metabolic pathways (Fig 1B-C).

8.3.2 PINK1 LOF Enhances Cholesterol Biosynthesis by Stabilizing SCAP.

As SCAP is involved in the regulation of cholesterol biosynthesis, we probed into other essential proteins that are involved in the cholesterol biosynthesis pathway. Immunocytochemical analysis revealed increased nuclear localization of SREBP2 in PINK1 KO DaNs compared to controls (Fig 1D-E). The accumulation of SREBP2 puncta in the nucleus can increase transcriptional activation of cholesterol biosynthesis genes.

Using immunoblot analysis, we observed elevated expression of squalene monooxygenase (SQLE), a rate limiting enzyme in the cholesterol pathway, and decreased expression of the inhibitory regulator INSIG2. Interestingly, HMG-CoA reductase (HMGCR), another rate limiting enzyme, did not show significant changes in abundance (Fig 1F-I). These changes overall suggest that PINK1 LOF regulates cholesterol biosynthesis.

To rule out clonal artifacts, we reintroduced WT PINK1 into KO neurons using lentiviral expression. This intervention normalized SQLE levels and partially restored INSIG2, while HMGCR remained unchanged. In contrast, a kinase-dead (3xKD) PINK1 mutant failed to rescue these phenotypes, emphasizing that PINK1's kinase activity is essential for maintaining cholesterol biosynthetic homeostasis (Fig S3A-E).

Impaired SCAP phosphorylation had previously been shown to increase its stability due to reduced degradation. To test whether SCAP stability was altered, we performed a CHX pulse chase experiment. In PINK1 KO DaNs, SCAP levels did not reduce over time with CHX treatment, indicating increased stability of SCAP (Fig 1J-K). Importantly, total SCAP abundance and PKCλ/ι levels remained unchanged (Fig S4A-C), and co-immunoprecipitation assays showed no direct interaction between PINK1 and SCAP (Fig S4D).

Together, these results demonstrate that PINK1 indirectly regulates SCAP phosphorylation and stability and that its LOF increases cholesterol biosynthesis.

8.3.3 PINK1 LOF Increases Neuronal Cholesterol in a Domain and Neuron Specific Manner.

We next examined whether the altered regulation of cholesterol biosynthesis is reflected in total cholesterol levels. Using biochemical assays, we found significantly elevated free cholesterol in both PINK1 KO and PINK1 Q456X DaNs. In contrast, neurons carrying the PINK1 Q126P mutation, which affects the N-terminal domain rather than the kinase domain, showed no cholesterol increase. Similarly, HeLa cells harboring an endogenous PINK1 W437X mutation did not display cholesterol accumulation (Fig 2B-F). These results highlight that the cholesterol phenotype is specific to PINK1 mutations in the kinase domain and to DaNs or non-proliferating cells.

We also measured free cholesterol levels in PINK1 KO mice. In the striatum of young (4 month old) KO mice, cholesterol was elevated compared to WT controls. However, in older (16 month old) mice, cholesterol levels showed no difference (Fig 2G). We hypothesize that increased cholesterol may be an early phenotype in PINK1-PD DaNs. This is also consistent with the literature that only young developing neurons synthesize cholesterol. Interestingly, cholesterol levels in the ventral midbrain remained unchanged in both young and old mice, which is consistent with the fact that DaNs in the ventral midbrain are unaffected in PD (Fig 2H).

Lipidomics analyses revealed no significant changes in other major lipid classes (Fig S5). This specificity shows disruption of cholesterol regulation rather than a general lipid imbalance.

8.3.4 Cholesterol Accumulates at the Plasma Membrane and in Flotillin-Rich Lipid Rafts.

To determine the localization of excess cholesterol, we used live cell staining with NR12A, a dye specific for plasma membrane cholesterol composition which revealed increased fluorescence intensity in PINK1 KO DaNs (Fig 2I). Quantification of lipid order using a plate reader assay further confirmed a significant increase, indicating enrichment of cholesterol in the plasma membrane. Importantly, cholesterol-lowering treatments with Simvastatin or β-cyclodextrin (βCD) rescued the lipid order ratio (Fig 2J).

To determine cholesterol levels inside the neurons, we used perfringolysin O (PFO), a cholesterol binding toxin, which revealed increased cholesterol intensities that colocalized with flotillin-1 (FLOT1), a marker of lipid rafts. Both PFO intensity and

FLOT1 staining were elevated in PINK1 KO DaNs, indicating accumulation of cholesterol within internalized lipid rafts (Fig 2K).
Together, these observations establish that PINK1 LOF leads to the accumulation of cholesterol at the plasma membrane and in FLOT1-rich lipid rafts.

8.3.5 Excess Cholesterol Disrupts DAT Distribution and Neurotransmitter Uptake.

Since cholesterol rich lipid rafts regulate trafficking of the dopamine transporter (DAT), we next investigated the functional consequences of cholesterol accumulation. In PINK1 KO DaNs, DAT accumulated at the perinuclear regions, partially colocalizing with PFO stained cholesterol. Cholesterol lowering agents - simvastatin or βCD restored DAT distribution, similar to WT hDaNs (Fig 4A).
To test whether altered distribution of DAT affects its function at the plasma membrane, we performed a neurotransmitter uptake assay (Fig 4B). PINK1 KO DaNs exhibited significantly reduced uptake rate compared to WT hDaNs. This deficit was rescued by treatment with cholesterol lowering agents - Simvastatin or βCD. Moreover, pharmacological inhibition of DAT almost completely abolished neurotransmitter uptake, confirming that this defect was largely DAT dependent (Fig 4C).

Overall, our findings identify reduced phosphorylation of SCAP at Ser822 and Ser838 as a critical early defect in PINK1 LOF neurons. This alteration stabilizes SCAP, enhances cholesterol biosynthesis and drives cholesterol accumulation at the plasma membrane and within FLOT1-rich lipid rafts. These altered cholesterol levels disrupt DAT trafficking and impair neurotransmitter uptake, providing a mechanistic link between PINK1 loss, cholesterol dysregulation and dopaminergic dysfunction.

9. Conclusion and Future Perspectives.

In this thesis, the research opened up a deeper understanding of PINK1 associated PD using genetics, cellular and molecular and proteomic approaches in hDaN models. This work revealed novel insights and expands the mechanistic repertoire of PINK1 biology.

First, the identification and functional validation of the PINK1 p.F385S mutation in an Indian family not only expanded the list of pathogenic PINK1 variants but also addressed a critical gap in the representation of non-European ancestry populations in PD genetics. Functional assays demonstrated that this mutation destabilizes the DFG kinase domain, disrupts phosphorylation of ubiquitin at Ser65 and prevents Parkin recruitment thereby impairing canonical PINK1/Parkin mitophagy. This provides additional validation between PINK1 mutations and mitochondrial dysfunction. This also highlights the need for inclusive genetic studies that incorporate diverse populations to ensure precision medicine.

Second, the exploration of proteome dynamics in iPSC derived hDaNs established a resource that benefits researchers working on diseases associated with DaNs, including PD. By mapping global protein turnover, compartment specific protein dynamics and axonal trafficking, this work provides a thorough protein characterization of hDaNs. For example, the observation that synaptic proteins are among the most short-lived, whereas mitochondrial and ribosomal proteins are long-lived, underscores the fine balance that post-mitotic neurons maintain to preserve function over longer periods. In addition, the methodological advance, integrating microfluidic device-based culture methods with proteomics also provides a framework for future studies that seek to dissect neuron compartmentalization at the molecular level.

Third, this work uncovered a novel role of PINK1 in the regulation of cholesterol metabolism. Through phosphoproteomics and functional validation, we showed that PINK1 LOF reduces phosphorylation of SCAP, stabilizing the protein and enhancing cholesterol biosynthesis. This in turn leads to cholesterol accumulation in neuronal plasma membranes and lipid rafts, disrupts dopamine transporter distribution and

impairs neurotransmitter uptake. This finding showed additional roles of PINK1 beyond mitochondrial quality control.

Overall, these findings open up multiple research avenues.

The identification of a novel pathogenic *PINK1* mutation in the Indian population highlights that there are potentially many novel variants or mutations that remains to be identified in the global population. Population specific variants may reveal new mechanistic insights or therapeutic targets. Such discoveries will broaden the conceptual landscape of PD genetics and biology and facilitate the development of effective therapies that are globally applicable. Additionally, the inclusive genetic approach taken in this work highlights the need for population specific screening tools. Incorporating diverse genetic variants into diagnostic panels will improve the accuracy of early detection and risk stratification globally.

The proteome dynamics dataset also raises important questions. For instance, identifying regulatory networks that determine the distinct half-lives of synaptic versus mitochondrial proteins. Or the presence of neuron specific chaperones or degradation pathways that selectively protects long-lived proteins. The proteomic approach and resource also open up translational cues. Proteins with altered turnover or compartment specific enrichment in neurons associated with neurological disorder may serve as biomarkers of early dysfunction. For example, axonal proteins that are differentially expressed, mislocalized or that fail to traffic efficiently could be studied in patient biospecimens such as cerebrospinal fluid (CSF) or blood. This would provide a bridge between cellular phenotypes and clinically identifiable biomarkers.

The cholesterol finding identifies a mechanistic understanding on how SCAP phosphorylation is regulated by PINK1. The discovery that cholesterol imbalance occurs early in PINK1 LOF hDaNs suggests opportunities for therapeutic intervention before disease manifestation. Statins, cyclodextrins or other cholesterol lowering agents could be tested in human neuronal models and preclinical settings. Importantly, these interventions should be assessed not only for their ability to normalize cholesterol levels but also for their impact in disease manifestation and/or progression.

Finally, future work embracing interdisciplinary integration and convergence of multiple methodological applications, including proteomics, lipidomics, genomics and advanced imaging will be essential to capture the complexity of PD biology. Moreover, coupling human iPSC derived models with organoid systems, *in vivo* imaging and computational modeling could provide conserved, reproducible and meaningful insights in PD pathology.

10. References.

ABOU-SLEIMAN, P. M., MUQIT, M. M. K., MCDONALD, N. Q., YANG, Y. X., GANDHI, S., HEALY, D. G., HARVEY, K., HARVEY, R. J., DEAS, E., HATIA, K., QUINN, N., LEES, A., LATCHMAN, D. S. & WOOD, N. W. 2006. A heterozygous effect for PINK1 mutations in Parkinson's disease? *Annals of Neurology,* 60**,** 414-419.

AHO, V. T. E., HOUSER, M. C., PEREIRA, P. A. B., CHANG, J. J., RUDI, K., PAULIN, L., HERTZBERG, V., AUVINEN, P., TANSEY, M. G. & SCHEPERJANS, F. 2021. Relationships of gut microbiota, short-chain fatty acids, inflammation, and the gut barrier in Parkinson's disease. *Molecular Neurodegeneration,* 16.

AKABANE, S., WATANABE, K., KOSAKO, H., YAMASHITA, S. I., NISHINO, K., KATO, M., SEKINE, S., KANKI, T., MATSUDA, N., ENDO, T. & OKA, T. 2023. TIM23 facilitates PINK1 activation by safeguarding against OMA1-mediated degradation in damaged mitochondria. *Cell Reports,* 42.

ALVAREZ-ERVITI, L., RODRIGUEZ-OROZ, M. C., COOPER, J. M., CABALLERO, C., FERRER, I., OBESO, J. A. & SCHAPIRA, A. H. V. 2010. Chaperone-Mediated Autophagy Markers in Parkinson Disease Brains. *Archives of Neurology,* 67**,** 1464-1472.

ANDO, M., FIESEL, F. C., HUDEC, R., CAULFIELD, T. R., OGAKI, K., GORKA-SKOCZYLAS, P., KOZIOROWSKI, D., FRIEDMAN, A., CHEN, L., DAWSON, V. L., DAWSON, T. M., BU, G., ROSS, O. A., WSZOLEK, Z. K. & SPRINGER, W. 2017. The PINK1 p.I368N mutation affects protein stability and ubiquitin kinase activity. *Mol Neurodegener,* 12**,** 32.

ANGLADE, P., VYAS, S., JAVOYAGID, F., HERRERO, M. T., MICHEL, P. P., MARQUEZ, J., MOUATTPRIGENT, A., RUBERG, M., HIRSCH, E. C. & AGID, Y. 1997. Apoptosis and autophagy in nigral neurons of patients with Parkinson's disease. *Histology and Histopathology,* 12**,** 25-31.

ARENA, G., GELMETTI, V., TOROSANTUCCI, L., VIGNONE, D., LAMORTE, G., DE ROSA, P., CILIA, E., JONAS, E. A. & VALENTE, E. M. 2013. PINK1 protects against cell death induced by mitochondrial depolarization, by phosphorylating Bcl-xL and impairing its pro-apoptotic cleavage. *Cell Death and Differentiation,* 20**,** 920-930.

ARENA, G., SHARMA, K., AGYEAH, G., KRÜGER, R., GRÜNEWALD, A. & FITZGERALD, J. C. 2022. Neurodegeneration and Neuroinflammation in Parkinson's Disease: a Self-Sustained Loop. *Current Neurology and Neuroscience Reports,* 22**,** 427-440.

ARLEHAMN, C. S. L., DHANWANI, R., PHAM, J., KUAN, R., FRAZIER, A., DUTRA, J. R., PHILLIPS, E., MALLAL, S., ROEDERER, M., MARDER, K. S., AMARA, A. W., STANDAERT, D. G., GOLDMAN, J. G., LITVAN, I., PETERS, B., SULZER, D. & SETTE, A. 2020. α-Synuclein-specific T cell reactivity is associated with preclinical and early Parkinson's disease. *Nature Communications,* 11.

ARMSTRONG, M. J. & OKUN, M. S. 2020. Diagnosis and Treatment of Parkinson Disease A Review. *Jama-Journal of the American Medical Association,* 323**,** 548-560.

BANDRES-CIGA, S., DIEZ-FAIREN, M., KIM, J. J. & SINGLETON, A. B. 2020. Genetics of Parkinson's disease: An introspection of its journey towards precision medicine. *Neurobiol Dis,* 137**,** 104782.
BARODIA, S. K., MCMEEKIN, L. J., CREED, R. B., QUINONES, E. K., COWELL, R. M. & GOLDBERG, M. S. 2019. PINK1 phosphorylates ubiquitin predominantly in astrocytes. *Npj Parkinsons Disease,* 5.
BENDER, A., KRISHNAN, K. J., MORRIS, C. M., TAYLOR, G. A., REEVE, A. K., PERRY, R. H., JAROS, E., HERSHESON, J. S., BETTS, J., KLOPSTOCK, T., TAYLOR, R. W. & TURNBULL, D. M. 2006. High levels of mitochondrial DNA deletions in substantia nigra neurons in aging and Parkinson disease. *Nature Genetics,* 38**,** 515-517.
BRAAK, H., DEL TREDICI, K., RÜB, U., DE VOS, R. A. I., STEUR, E. N. H. J. & BRAAK, E. 2003. Staging of brain pathology related to sporadic Parkinson's disease. *Neurobiology of Aging,* 24**,** 197-211.
BRASSARD, R., ARUTYUNOVA, E., TAKYI, E., ESPINOZA-FONSECA, L. M., YOUNG, H. S., TOURET, N. & LEMIEUX, M. J. 2025. Transmembrane Parkinson's disease mutation of PINK1 leads to altered mitochondrial anchoring. *Journal of Biological Chemistry,* 301.
BRUNDIN, P., NATH, A. & BECKHAM, J. D. 2020. Is COVID-19 a Perfect Storm for Parkinson's Disease? *Trends Neurosci,* 43**,** 931-933.
BRUNELLI, F., TOROSANTUCCI, L., GELMETTI, V., FRANZONE, D., GRUNEWALD, A., KRUGER, R., ARENA, G. & VALENTE, E. M. 2022. PINK1 Protects against Staurosporine-Induced Apoptosis by Interacting with Beclin1 and Impairing Its Pro-Apoptotic Cleavage. *Cells,* 11.
BURRE, J., SHARMA, M., TSETSENIS, T., BUCHMAN, V., ETHERTON, M. R. & SÜDHOF, T. C. 2010. α-Synuclein Promotes SNARE-Complex Assembly in Vivo and in Vitro. *Science,* 329**,** 1663-1667.
BUS, C., GEISLER, S., FELDKAEMPER, M., FLORES-ROMERO, H., SCHAEDLER, A., ZITTLAU, K., ZARANI, M., UYSAL, B., CASADEI, N., FALLIER-BECKER, P., SCHWARZ, L., BROUWERS, J. F., KOCH, H., UGUN-KLUSEK, A., MARUSZCZAK, K., VOGT WEISENHORN, D. M., WURST, W., SCHMIDT, B., MARTENS, G., BRÜGGER, B., RAPAPORT, D., GARCIA, A., MACEK, B., KRÜGER, R., GASSER, T., KAHLE, P. & FITZGERALD, J. C. 2019. PINK1 Regulates Dopamine and Lipids at Mitochondria to Maintain Synapses and Neuronal Function. *bioRxiv***,** 814343.
BUS, C., ZIZMARE, L., FELDKAEMPER, M., GEISLER, S., ZARANI, M., SCHAEDLER, A., KLOSE, F., ADMARD, J., MAGEEAN, C. J., ARENA, G., FALLIER-BECKER, P., UGUN-KLUSEK, A., MARUSZCZAK, K. K., KAPOLOU, K., SCHMID, B., RAPAPORT, D., UEFFING, M., CASADEI, N., KRUGER, R., GASSER, T., VOGT WEISENHORN, D. M., KAHLE, P. J., TRAUTWEIN, C., GLOECKNER, C. J. & FITZGERALD, J. C. 2020. Human Dopaminergic Neurons Lacking PINK1 Exhibit Disrupted Dopamine Metabolism Related to Vitamin B6 Co-Factors. *iScience,* 23**,** 101797.
CALABRESI, P., DI LAZZARO, G., MARINO, G., CAMPANELLI, F. & GHIGLIERI, V. 2023a. Advances in understanding the function of alpha-synuclein: implications for Parkinson's disease. *Brain,* 146**,** 3587-3597.
CALABRESI, P., MECHELLI, A., NATALE, G., VOLPICELLI-DALEY, L., DI LAZZARO, G. & GHIGLIERI, V. 2023b. Alpha-synuclein in Parkinson's disease and other synucleinopathies: from overt neurodegeneration back to early synaptic dysfunction. *Cell Death & Disease,* 14.

CALLEGARI, S., KIRK, N. S., GAN, Z. Y., DITE, T., COBBOLD, S. A., LEIS, A., DAGLEY, L. F., GLUKHOVA, A. & KOMANDER, D. 2025. Structure of human PINK1 at a mitochondrial TOM-VDAC array. *Science,* 388**,** 303-310.
CAMACHO-SOTO, A., WARDEN, M. N., SEARLES NIELSEN, S., SALTER, A., BRODY, D. L., PRATHER, H. & RACETTE, B. A. 2017. Traumatic brain injury in the prodromal period of Parkinson's disease: A large epidemiological study using medicare data. *Annals of Neurology,* 82**,** 744-754.
CELARDO, I., COSTA, A. C., LEHMANN, S., JONES, C., WOOD, N., MENCACCI, N. E., MALLUCCI, G. R., LOH, S. H. & MARTINS, L. M. 2016. Mitofusin-mediated ER stress triggers neurodegeneration in pink1/parkin models of Parkinson's disease. *Cell Death Dis,* 7**,** e2271.
CHAKRABARTY, R. P. & CHANDEL, N. S. 2022. Beyond ATP, new roles of mitochondria. *Biochem (Lond),* 44**,** 2-8.
CHIDAMBARAM, R., KUMAR, K., PARASHAR, S., RAMACHANDRAN, G., CHEN, S. L. & FERRO-NOVICK, S. 2024. PINK1 controls RTN3L-mediated ER autophagy by regulating peripheral tubule junctions. *Journal of Cell Biology,* 223.
CHOI, I., CHOI, D. J., YANG, H., WOO, J. H., CHANG, M. Y., KIM, J. Y., SUN, W., PARK, S. M., JOU, I., LEE, S. H. & JOE, E. H. 2016. PINK1 expression increases during brain development and stem cell differentiation, and affects the development of GFAP-positive astrocytes. *Molecular Brain,* 9.
CHU, Y. P., DODIYA, H., AEBISCHER, P., OLANOW, C. W. & KORDOWER, J. H. 2009. Alterations in lysosomal and proteasomal markers in Parkinson's disease: Relationship to alpha-synuclein inclusions. *Neurobiology of Disease,* 35**,** 385-398.
CREWS, L., SPENCER, B., DESPLATS, P., PATRICK, C., PAULINO, A., ROCKENSTEIN, E., HANSEN, L., ADAME, A., GALASKO, D. & MASLIAH, E. 2010. Selective Molecular Alterations in the Autophagy Pathway in Patients with Lewy Body Disease and in Models of α-Synucleinopathy. *Plos One,* 5.
CUERVO, A. M., STEFANIS, L., FREDENBURG, R., LANSBURY, P. T. & SULZER, D. 2004. Impaired degradation of mutant α-synuclein by chaperone-mediated autophagy. *Science,* 305**,** 1292-1295.
DAVIDSON, W. S., JONAS, A., CLAYTON, D. F. & GEORGE, J. M. 1998. Stabilization of α-synuclein secondary structure upon binding to synthetic membranes. *Journal of Biological Chemistry,* 273**,** 9443-9449.
DEAS, E., PLUN-FAVREAU, H., GANDHI, S., DESMOND, H., KJAER, S., LOH, S. H. Y., RENTON, A. E. M., HARVEY, R. J., WHITWORTH, A. J., MARTINS, L. M., ABRAMOV, A. Y. & WOOD, N. W. 2011. PINK1 cleavage at position A103 by the mitochondrial protease PARL. *Human Molecular Genetics,* 20**,** 867-879.
DEHAY, B., BOVÉ, J., RODRÍGUEZ-MUELA, N., PERIER, C., RECASENS, A., BOYA, P. & VILA, M. 2010. Pathogenic Lysosomal Depletion in Parkinson's Disease. *Journal of Neuroscience,* 30**,** 12535-12544.
DENG, H. S., DODSON, M. W., HUANG, H. X. & GUO, M. 2008. The Parkinson's disease genes
and
promote mitochondrial fission and/or inhibit fusion in. *Proceedings of the National Academy of Sciences of the United States of America,* 105**,** 14503-14508.

DESAI, V. G., FEUERS, R. J., HART, R. W. & ALI, S. F. 1996. MPP(+)-induced neurotoxicity in mouse is age-dependent: Evidenced by the selective inhibition of complexes of electron transport. *Brain Research,* 715**,** 1-8.

DICKSON, D. W. 2012. Parkinson's Disease and Parkinsonism: Neuropathology. *Cold Spring Harbor Perspectives in Medicine,* 2.

DÖLLE, C., FLONES, I., NIDO, G. S., MILETIC, H., OSUAGWU, N., KRISTOFFERSEN, S., LILLENG, P. K., LARSEN, J. P., TYSNES, O. B., HAUGARVOLL, K., BINDOFF, L. A. & TZOULIS, C. 2016. Defective mitochondrial DNA homeostasis in the substantia nigra in Parkinson disease. *Nature Communications,* 7.

EBRAHIMI-FAKHARI, D., WAHLSTER, L. & MCLEAN, P. J. 2012. Protein degradation pathways in Parkinson's disease: curse or blessing. *Acta Neuropathol,* 124**,** 153-72.

ELDEEB, M. A., BAYNE, A. N., FALLAHI, A., GOIRAN, T., MACDOUGALL, E. J., SOUMBASIS, A., ZORCA, C. E., TABAH, J. J., THOMAS, R. A., KARPILOVSKY, N., MATHUR, M., DURCAN, T. M., TREMPE, J. F. & FON, E. A. 2024. Tom20 gates PINK1 activity and mediates its tethering of the TOM and TIM23 translocases upon mitochondrial stress. *Proceedings of the National Academy of Sciences of the United States of America,* 121.

FATHI, M., VAKILI, K., YAGHOOBPOOR, S., QADIRIFARD, M. S., KOSARI, M., NAGHSH, N., TAEI, A. A., KLEGERIS, A., DEHGHANI, M., BAHRAMI, A., TAHERI, H., MOHAMADKHANI, A., HAJIBEYGI, R., TAVIRANI, M. R. & SAYEHMIRI, F. 2022. Pre-clinical Studies Identifying Molecular Pathways of Neuroinflammation in Parkinson's Disease: A Systematic Review. *Frontiers in Aging Neuroscience,* 14.

FIORINI, M. R., DILLIOTT, A. A., THOMAS, R. A. & FARHAN, S. M. K. 2024. Transcriptomics of Human Brain Tissue in Parkinson's Disease: a Comparison of Bulk and Single-cell RNA Sequencing. *Molecular Neurobiology,* 61**,** 8996-9015.

GALEA, I. 2021. The blood-brain barrier in systemic infection and inflammation. *Cellular & Molecular Immunology,* 18**,** 2489-2501.

GAN, Z. Y., CALLEGARI, S., COBBOLD, S. A., COTTON, T. R., MLODZIANOSKI, M. J., SCHUBERT, A. F., GEOGHEGAN, N. D., ROGERS, K. L., LEIS, A., DEWSON, G., GLUKHOVA, A. & KOMANDER, D. 2022. Activation mechanism of PINK1. *Nature,* 602**,** 328-335.

GANDHI, S. & PLUN-FAVREAU, H. 2017. Mutations and mechanism: how may contribute to risk of sporadic Parkinson's disease. *Brain,* 140**,** 2-5.

GAO, Q. T., TIAN, R. Y., HAN, H. L., SLONE, J., WANG, C. F., KE, X., ZHANG, T. M., LI, X. Y., HE, Y. H., LIAO, P. L., WANG, F., CHEN, Y., FU, S. Q., ZHANG, K. X., ZENG, F. F., YANG, Y. X., LI, Z., TAN, J. Q., LI, J. D., LU, Y. M., HUANG, T. S., HU, Z. H. & ZHANG, Z. H. 2022. PINK1-mediated Drp1 phosphorylation modulates synaptic development and plasticity via promoting mitochondrial fission. *Signal Transduction and Targeted Therapy,* 7.

GASSER, T. 2024. The global dimension of Parkinson's disease genetics. *Lancet Neurology,* 23**,** 1178-1179.

GEISLER, S., HOLMSTROM, K. M., SKUJAT, D., FIESEL, F. C., ROTHFUSS, O. C., KAHLE, P. J. & SPRINGER, W. 2010. PINK1/Parkin-mediated mitophagy is dependent on VDAC1 and p62/SQSTM1. *Nature Cell Biology,* 12**,** 119-U70.

GOLDBERG, A. L. 2003. Protein degradation and protection against misfolded or damaged proteins. *Nature,* 426**,** 895-899.

GOLDMAN, S. M., KAMEL, F., ROSS, G. W., JEWELL, S. A., BHUDHIKANOK, G. S., UMBACH, D., MARRAS, C., HAUSER, R. A., JANKOVIC, J., FACTOR, S. A., BRESSMAN, S., LYONS, K. E., MENG, C., KORELL, M., ROUCOUX, D. F., HOPPIN, J. A., SANDLER, D. P., LANGSTON, J. W. & TANNER, C. M. 2012. Head injury, alpha-synuclein Rep1, and Parkinson's disease. *Annals of Neurology,* 71**,** 40-48.

GONZALEZ-RODRÍGUEZ, P., ZAMPESE, E., STOUT, K. A., GUZMAN, J. N., ILIJIC, E., YANG, B., TKATCH, T., STAVARACHE, M. A., WOKOSIN, D. L., GAO, L., KAPLITT, M. G., LÓPEZ-BARNEO, J., SCHUMACKER, P. T. & SURMEIER, D. J. 2021. Disruption of mitochondrial complex I induces progressive parkinsonism. *Nature,* 599**,** 650-+.

GOSAVI, N., LEE, H. J., LEE, J. S., PATEL, S. & LEE, S. J. 2002. Golgi fragmentation occurs in the cells with prefibrillar α-synuclein aggregates and precedes the formation of fibrillar inclusion. *Journal of Biological Chemistry,* 277**,** 48984-48992.

GREENE, A. W., GRENIER, K., AGUILETA, M. A., MUISE, S., FARAZIFARD, R., HAQUE, M. E., MCBRIDE, H. M., PARK, D. S. & FON, E. A. 2012. Mitochondrial processing peptidase regulates PINK1 processing, import and Parkin recruitment. *Embo Reports,* 13**,** 378-385.

GROSSMANN, D., MALBURG, N., GLASS, H., WEEREN, V., SONDERMANN, V., PFEIFFER, J. F., PETTERS, J., LUKAS, J., SEIBLER, P., KLEIN, C., GRUNEWALD, A. & HERMANN, A. 2023. Mitochondria-Endoplasmic Reticulum Contact Sites Dynamics and Calcium Homeostasis Are Differentially Disrupted in PINK1-PD or PRKN-PD Neurons. *Mov Disord,* 38**,** 1822-1836.

GU, G. Y., REYES, P. F., GOLDEN, G. T., WOLTJER, R. L., HULETTE, C., MONTINE, T. J. & ZHANG, J. 2002. Mitochondrial DNA deletions/rearrangements in Parkinson disease and related neurodegenerative disorders. *Journal of Neuropathology and Experimental Neurology,* 61**,** 634-639.

GUARDIA-LAGUARTA, C., LIU, Y. H., LAURITZEN, K. H., ERDJUMENT-BROMAGE, H., MARTIN, B., SWAYNE, T. C., JIANG, X. J. & PRZEDBORSKI, S. 2019. PINK1 Content in Mitochondria is Regulated by ER-Associated Degradation. *Journal of Neuroscience,* 39**,** 7074-7085.

GUZMAN, J. N., SANCHEZ-PADILLA, J., WOKOSIN, D., KONDAPALLI, J., ILIJIC, E., SCHUMACKER, P. T. & SURMEIER, D. J. 2010. Oxidant stress evoked by pacemaking in dopaminergic neurons is attenuated by DJ-1. *Nature,* 468**,** 696-U119.

HALLIDAY, G. M., HOLTON, J. L., REVESZ, T. & DICKSON, D. W. 2011. Neuropathology underlying clinical variability in patients with synucleinopathies. *Acta Neuropathologica,* 122**,** 187-204.

HAM, S. J., YOO, H., WOO, D., LEE, D. H., PARK, K. S. & CHUNG, J. 2023. PINK1 and Parkin regulate IP(3)R-mediated ER calcium release. *Nat Commun,* 14**,** 5202.

HAN, H. L., TAN, J. D. O., WANG, R. X., WAN, H. D., HE, Y. H., YAN, X. X., GUO, J. F., GAO, Q. T., LI, J., SHAN, S., CHEN, F., TIAN, R. Y., LIU, W., LIAO, L. J., TANG, B. S. & ZHANG, Z. H. 2020. PINK1 phosphorylates Drp1 to regulate mitophagy-independent mitochondrial dynamics. *Embo Reports,* 21.

HEEMAN, B., VAN DEN HAUTE, C., AELVOET, S. A., VALSECCHI, F., RODENBURG, R. J., REUMERS, V., DEBYSER, Z., CALLEWAERT, G.,

KOOPMAN, W. J. H., WILLEMS, P. H. G. M. & BAEKELANDT, V. 2011. Depletion of PINK1 affects mitochondrial metabolism, calcium homeostasis and energy maintenance. *Journal of Cell Science,* 124**,** 1115-1125.
HEES, J. T., SEGURA, I., SCHNEIDER, A., SCHIFFERER, M., MISGELD, T. & HARBAUER, A. B. 2024. ER-associated biogenesis of PINK1 preprotein for neuronal mitophagy. *bioRxiv***,** 2024.06.21.600039.
HENRICH, M. T., OERTEL, W. H., SURMEIER, D. J. & GEIBL, F. F. 2023. Mitochondrial dysfunction in Parkinson's disease - a key disease hallmark with therapeutic potential. *Molecular Neurodegeneration,* 18.
HIGASHI, S., MOORE, D. J., MINEGISHI, M., KASANUKI, K., FUJISHIRO, H., KABUTA, T., TOGO, T., KATSUSE, O., UCHIKADO, H., FURUKAWA, Y., HINO, H., KOSAKA, K., SATO, K., ARAI, H., WADA, K. & ISEKI, E. 2011. Localization of MAP1-LC3 in Vulnerable Neurons and Lewy Bodies in Brains of Patients With Dementia With Lewy Bodies. *Journal of Neuropathology and Experimental Neurology,* 70**,** 264-280.
HIPP, M. S., KASTURI, P. & HARTL, F. U. 2019. The proteostasis network and its decline in ageing. *Nature Reviews Molecular Cell Biology,* 20**,** 421-435.
HOOZEMANS, J. J. M., VAN HAASTERT, E. S., EIKELENBOOM, P., DE VOS, R. A. I., ROZEMULLER, J. M. & SCHEPER, W. 2007. Activation of the unfolded protein response in Parkinson's disease. *Biochemical and Biophysical Research Communications,* 354**,** 707-711.
HOUSER, M. C. & TANSEY, M. G. 2017. The gut-brain axis: is intestinal inflammation a silent driver of Parkinson's disease pathogenesis? *NPJ Parkinsons Dis,* 3**,** 3.
HUANG, E., QU, D. B., HUANG, T. W., RIZZI, N., BOONYING, W., KROLAK, D., CIANA, P., WOULFE, J., KLEIN, C., SLACK, R. S., FIGEYS, D. & PARK, D. S. 2017. PINK1-mediated phosphorylation of LETM1 regulates mitochondrial calcium transport and protects neurons against mitochondrial stress. *Nature Communications,* 8.
II, K., ITO, H., TANAKA, K. & HIRANO, A. 1997. Immunocytochemical co-localization of the proteasome in ubiquitinated structures in neurodegenerative diseases and the elderly. *Journal of Neuropathology and Experimental Neurology,* 56**,** 125-131.
IMBRIANI, P., TASSONE, A., MERINGOLO, M., PONTERIO, G., MADEO, G., PISANI, A., BONSI, P. & MARTELLA, G. 2019. Loss of Non-Apoptotic Role of Caspase-3 in the PINK1 Mouse Model of Parkinson's Disease. *International Journal of Molecular Sciences,* 20.
IRRCHER, I., ALEYASIN, H., SEIFERT, E. L., HEWITT, S. J., CHHABRA, S., PHILLIPS, M., LUTZ, A. K., ROUSSEAUX, M. W. C., BEVILACQUA, L., JAHANI-ASL, A., CALLAGHAN, S., MACLAURIN, J. G., WINKLHOFER, K. F., RIZZU, P., RIPPSTEIN, P., KIM, R. H., CHEN, C. X., FON, E. A., SLACK, R. S., HARPER, M. E., MCBRIDE, H. M., MAK, T. W. & PARK, D. S. 2010. Loss of the Parkinson's disease-linked gene DJ-1 perturbs mitochondrial dynamics. *Human Molecular Genetics,* 19**,** 3734-3746.
JIN, H., LI, M. T., JEONG, E., CASTRO-MARTINEZ, F. & ZUKER, C. S. 2024. A body-brain circuit that regulates body inflammatory responses. *Nature,* 630.
JIN, S. M., LAZAROU, M., WANG, C., KANE, L. A., NARENDRA, D. P. & YOULE, R. J. 2010. Mitochondrial membrane potential regulates PINK1 import and proteolytic destabilization by PARL. *J Cell Biol,* 191**,** 933-42.

JOHANSSON, E., FREUCHET, A., WILLIAMS, G. P., MICHEALIS, T., FRAZIER, A., LITVAN, I., GOLDMAN, J. G., ALCALAY, R. N., STANDAERT, D. G., AMARA, A. W., STOVER, N., FON, E. A., POSTUMA, R. B., SIDNEY, J., SULZER, D., ARLEHAMN, C. S. L. & SETTE, A. 2025. T cell responses towards PINK1 and α-synuclein are elevated in prodromal Parkinson's disease. *Npj Parkinsons Disease,* 11.

KAGEYAMA, Y., ZHANG, Z., RODA, R., FUKAYA, M., WAKABAYASHI, J., WAKABAYASHI, N., KENSLER, T. W., REDDY, P. H., IIJIMA, M. & SESAKI, H. 2012. Mitochondrial division ensures the survival of postmitotic neurons by suppressing oxidative damage. *Journal of Cell Biology,* 197**,** 535-551.

KALIA, L. V. & LANG, A. E. 2015. Parkinson's disease. *Lancet,* 386**,** 896-912.

KALYANARAMAN, B., CHENG, G. & HARDY, M. 2024. Gut microbiome, short-chain fatty acids, alpha-synuclein, neuroinflammation, and ROS/RNS: Relevance to Parkinson's disease and therapeutic implications. *Redox Biology,* 71.

KANE, L. A., LAZAROU, M., FOGEL, A. I., LI, Y., YAMANO, K., SARRAF, S. A., BANERJEE, S. & YOULE, R. J. 2014. PINK1 phosphorylates ubiquitin to activate Parkin E3 ubiquitin ligase activity. *Journal of Cell Biology,* 205**,** 143-153.

KANNARKAT, G. T., BOSS, J. M. & TANSEY, M. G. 2013. The Role of Innate and Adaptive Immunity in Parkinson's Disease. *Journal of Parkinsons Disease,* 3**,** 493-514.

KAZANOVA, A., SUNG, J., OLIVEIRA, N., GAVINO, C., RECINTO, S., BESSAIAH, H., PEI, J., BURNS, L., MILLER, W., BROUILLARD-GALIPEAU, M., ZHU, L., GUERRA, L., ELEMEERY, M. N., MACDONALD, A., LANOIX, J., THIBAULT, P., MCBRIDE, H., DESJARDINS, M., STRATTON, J. A., LABRECQUE, N. & GRUENHEID, S. 2024. Modeling gene-environment interactions in Parkinson’s Disease: Helicobacter pylori infection of Pink1^{−/−} mice induces CD8 T cell-dependent motor and cognitive dysfunction. *bioRxiv***,** 2024.02.25.580545.

KAZLAUSKAITE, A., KONDAPALLI, C., GOURLAY, R., CAMPBELL, D. G., RITORTO, M. S., HOFMANN, K., ALESSI, D. R., KNEBEL, A., TROST, M. & MUQIT, M. M. 2014. Parkin is activated by PINK1-dependent phosphorylation of ubiquitin at Ser65. *Biochem J,* 460**,** 127-39.

KITADA, T., ASAKAWA, S., HATTORI, N., MATSUMINE, H., YAMAMURA, Y., MINOSHIMA, S., YOKOCHI, M., MIZUNO, Y. & SHIMIZU, N. 1998. Mutations in the

gene cause autosomal recessive juvenile parkinsonism. *Nature,* 392**,** 605-608.

KOGA, S., SEKIYA, H., KONDRU, N., ROSS, O. A. & DICKSON, D. W. 2021. Neuropathology and molecular diagnosis of Synucleinopathies. *Molecular Neurodegeneration,* 16.

KONDAPALLI, C., KAZLAUSKAITE, A., ZHANG, N., WOODROOF, H. I., CAMPBELL, D. G., GOURLAY, R., BURCHELL, L., WALDEN, H., MACARTNEY, T. J., DEAK, M., KNEBEL, A., ALESSI, D. R. & MUQIT, M. M. K. 2012. PINK1 is activated by mitochondrial membrane potential depolarization and stimulates Parkin E3 ligase activity by phosphorylating Serine 65. *Open Biology,* 2.

KONINGS, B., VILLATORO, L., VAN DEN EYNDE, J., BARAHONA, G., BURNS, R., MCKNIGHT, M., HUI, K., YENOKYAN, G., TACK, J. & PASRICHA, P. J. 2023. Gastrointestinal syndromes preceding a diagnosis of Parkinson's disease:

testing Braak's hypothesis using a nationwide database for comparison with Alzheimer's disease and cerebrovascular diseases. *Gut,* 72**,** 2103-+.
KOULI, A., TORSNEY, K. M. & KUAN, W. L. 2018. Parkinson's Disease: Etiology, Neuropathology, and Pathogenesis. *In:* STOKER, T. B. & GREENLAND, J. C. (eds.) *Parkinson's Disease: Pathogenesis and Clinical Aspects.* Brisbane (AU).
KOYANO, F., OKATSU, K., KOSAKO, H., TAMURA, Y., GO, E., KIMURA, M., KIMURA, Y., TSUCHIYA, H., YOSHIHARA, H., HIROKAWA, T., ENDO, T., FON, E. A., TREMPE, J. F., SAEKI, Y., TANAKA, K. & MATSUDA, N. 2014. Ubiquitin is phosphorylated by PINK1 to activate parkin. *Nature,* 510**,** 162-+.
KREBIEHL, G., RUCKERBAUER, S., BURBULLA, L. F., KIEPER, N., MAURER, B., WAAK, J., WOLBURG, H., GIZATULLINA, Z., GELLERICH, F. N., WOITALLA, D., RIESS, O., KAHLE, P. J., PROIKAS-CEZANNE, T. & KRÜGER, R. 2010. Reduced Basal Autophagy and Impaired Mitochondrial Dynamics Due to Loss of Parkinson's Disease-Associated Protein DJ-1. *Plos One,* 5.
KUMAR, M., ACEVEDO-CINTRÓN, J., JHALDIYAL, A., WANG, H., ANDRABI, S. A., EACKER, S., KARUPPAGOUNDER, S. S., BRAHMACHARI, S., CHEN, R., KIM, H., KO, H. S., DAWSON, V. L. & DAWSON, T. M. 2020. Defects in Mitochondrial Biogenesis Drive Mitochondrial Alterations in
-Deficient Human Dopamine Neurons. *Stem Cell Reports,* 15**,** 629-645.
KUZUHARA, S., MORI, H., IZUMIYAMA, N., YOSHIMURA, M. & IHARA, Y. 1988. Lewy Bodies Are Ubiquitinated - a Light and Electron-Microscopic Immunocytochemical Study. *Acta Neuropathologica,* 75**,** 345-353.
KWAK, S., MASAKI, T., ISHIURA, S. & SUGITA, H. 1991. Multicatalytic Proteinase Is Present in Lewy Bodies and Neurofibrillary Tangles in Diffuse Lewy Body Disease Brains. *Neuroscience Letters,* 128**,** 21-24.
LANGSTON, J. W., BALLARD, P., TETRUD, J. W. & IRWIN, I. 1983. Chronic Parkinsonism in Humans Due to a Product of Meperidine-Analog Synthesis. *Science,* 219**,** 979-980.
LANGSTON, R. G., BEILINA, A., REED, X., KAGANOVICH, A., SINGLETON, A. B., BLAUWENDRAAT, C., GIBBS, J. R. & COOKSON, M. R. 2022. Association of a common genetic variant with Parkinson's disease is mediated by microglia. *Science Translational Medicine,* 14.
LAZAROU, M., JIN, S. M., KANE, L. A. & YOULE, R. J. 2012. Role of PINK1 binding to the TOM complex and alternate intracellular membranes in recruitment and activation of the E3 ligase Parkin. *Dev Cell,* 22**,** 320-33.
LAZAROU, M., SLITER, D. A., KANE, L. A., SARRAF, S. A., WANG, C. X., BURMAN, J. L., SIDERIS, D. P., FOGEL, A. I. & YOULE, R. J. 2015. The ubiquitin kinase PINK1 recruits autophagy receptors to induce mitophagy. *Nature,* 524**,** 309-+.
LEE, H. J., KHOSHAGHIDEH, F., PATEL, S. & LEE, S. J. 2004. Clearance of α-synuclein oligomeric intermediates via the lysosomal degradation pathway. *Journal of Neuroscience,* 24**,** 1888-1896.
LENNOX, G., LOWE, J., MORRELL, K., LANDON, M. & MAYER, R. J. 1989. Anti-Ubiquitin Immunocytochemistry Is More Sensitive Than Conventional Techniques in the Detection of Diffuse Lewy Body Disease. *Journal of Neurology Neurosurgery and Psychiatry,* 52**,** 67-71.
LEROY, E., BOYER, R., AUBURGER, G., LEUBE, B., ULM, G., MEZEY, E., HARTA, G., BROWNSTEIN, M. J., JONNALAGADA, S., CHERNOVA, T., DEHEJIA,

A., LAVEDAN, C., GASSER, T., STEINBACH, P. J., WILKINSON, K. D. & POLYMEROPOULOS, M. H. 1998. The ubiquitin pathway in Parkinson's disease. *Nature,* 395**,** 451-452.
LEVINE, B. & KLIONSKY, D. J. 2004. Development by self-digestion: Molecular mechanisms and biological functions of autophagy. *Developmental Cell,* 6**,** 463-477.
LI, L. Y., WANG, X. X., FEI, X. F., XIA, L. P., QIN, Z. H. & LIANG, Z. Q. 2011. Parkinson's disease involves autophagy and abnormal distribution of cathepsin L. *Neuroscience Letters,* 489**,** 62-67.
LI, W. W., YANG, R., GUO, J. C., REN, H. M., ZHA, X. L., CHENG, J. S. & CAI, D. F. 2007. Localization of α-synuclein to mitochondria within midbrain of mice. *Neuroreport,* 18**,** 1543-1546.
LIANG, J. Y., YUAN, X. L., JIANG, J. M., ZHANG, P. & TAN, K. 2025. Targeting the NLRP3 inflammasome in Parkinson's disease: From molecular mechanism to therapeutic strategy. *Experimental Neurology,* 386.
LIM, S. Y., TAN, A. H., AHMAD-ANNUAR, A., OKUBADEJO, N. U., LOHMANN, K., MORRIS, H. R., TOH, T. S., TAY, Y. W., LANGE, L. M., BANDRES-CIGA, S., MATA, I., FOO, J. N., SAMMLER, E., OOI, J. C. E., NOYCE, A. J., BAHR, N., LUO, W., OJHA, R., SINGLETON, A. B., BLAUWENDRAAT, C. & KLEIN, C. 2024. Uncovering the genetic basis of Parkinson's disease globally: from discoveries to the clinic. *Lancet Neurology,* 23**,** 1267-1280.
LIN, W. & KANG, U. J. 2008. Characterization of PINK1 processing, stability, and subcellular localization. *Journal of Neurochemistry,* 106**,** 464-474.
LOWE, J., MCDERMOTT, H., LANDON, M., MAYER, R. J. & WILKINSON, K. D. 1990. Ubiquitin Carboxyl-Terminal Hydrolase (Pgp 9.5) Is Selectively Present in Ubiquitinated Inclusion-Bodies Characteristic of Human Neurodegenerative Diseases. *Journal of Pathology,* 161**,** 153-160.
MACKAY, D. F., RUSSELL, E. R., STEWART, K., MACLEAN, J. A., PELL, J. P. & STEWART, W. 2019. Neurodegenerative Disease Mortality among Former Professional Soccer Players. *New England Journal of Medicine,* 381**,** 1801-1808.
MACMAHON COPAS, A. N., MCCOMISH, S. F., FLETCHER, J. M. & CALDWELL, M. A. 2021. The Pathogenesis of Parkinson's Disease: A Complex Interplay Between Astrocytes, Microglia, and T Lymphocytes? *Front Neurol,* 12**,** 666737.
MAROTEAUX, L., CAMPANELLI, J. T. & SCHELLER, R. H. 1988. Synuclein - a Neuron-Specific Protein Localized to the Nucleus and Presynaptic Nerve-Terminal. *Journal of Neuroscience,* 8**,** 2804-2815.
MATA, I. F., SAMII, A., SCHNEER, S. H., ROBERTS, J. W., GRIFFITH, A., LEIS, B. C., SCHELLENBERG, G. D., SIDRANSKY, E., BIRD, T. D., LEVERENZ, J. B., TSUANG, D. & ZABETIAN, C. P. 2008. Glucocerebrosidase gene mutations: a risk factor for Lewy body disorders. *Arch Neurol,* 65**,** 379-82.
MATHEOUD, D., CANNON, T., VOISIN, A., PENTTINEN, A. M., RAMET, L., FAHMY, A. M., DUCROT, C., LAPLANTE, A., BOURQUE, M. J., ZHU, L., CAYROL, R., LE CAMPION, A., MCBRIDE, H. M., GRUENHEID, S., TRUDEAU, L. E. & DESJARDINS, M. 2019. Intestinal infection triggers Parkinson's disease-like symptoms in

mice. *Nature,* 571**,** 565-+.

MATHEOUD, D., SUGIURA, A., BELLEMARE-PELLETIER, A., LAPLANTE, A., RONDEAU, C., CHEMALI, M., FAZEL, A., BERGERON, J. J., TRUDEAU, L. E., BURELLE, Y., GAGNON, E., MCBRIDE, H. M. & DESJARDINS, M. 2016. Parkinson's Disease-Related Proteins PINK1 and Parkin Repress Mitochondrial Antigen Presentation. *Cell,* 166**,** 314-327.

MCLELLAND, G. L., LEE, S. A., MCBRIDE, H. M. & FON, E. A. 2016. Syntaxin-17 delivers PINK1/parkin-dependent mitochondrial vesicles to the endolysosomal system. *Journal of Cell Biology,* 214**,** 275-291.

MCLELLAND, G. L., SOUBANNIER, V., CHEN, C. X., MCBRIDE, H. M. & FON, E. A. 2014. Parkin and PINK1 function in a vesicular trafficking pathway regulating mitochondrial quality control. *Embo Journal,* 33**,** 282-295.

MCNAUGHT, K. S., BELIZAIRE, R., ISACSON, O., JENNER, P. & OLANOW, C. W. 2003. Altered proteasomal function in sporadic Parkinson's disease. *Experimental Neurology,* 179**,** 38-46.

MCNAUGHT, K. S. P. & JENNER, P. 2001. Proteasomal function is impaired in substantia nigra in Parkinson's disease. *Neuroscience Letters,* 297**,** 191-194.

MEREDITH, G. E. & RADEMACHER, D. J. 2011. MPTP Mouse Models of Parkinson's Disease: An Update. *Journal of Parkinsons Disease,* 1**,** 19-33.

MISHRA, P. & CHAN, D. C. 2016. Metabolic regulation of mitochondrial dynamics. *Journal of Cell Biology,* 212**,** 379-387.

MORAIS, V. A., VERSTREKEN, P., ROETHIG, A., SMET, J., SNELLINX, A., VANBRABANT, M., HADDAD, D., FREZZA, C., MANDEMAKERS, W., VOGT-WEISENHORN, D., VAN COSTER, R., WURST, W., SCORRANO, L. & DE STROOPER, B. 2009. Parkinson's disease mutations in PINK1 result in decreased Complex I activity and deficient synaptic function. *Embo Molecular Medicine,* 1**,** 99-111.

MUQIT, M. M. K., ABOU-SLEIMAN, P. M., SAURIN, A. T., HARVEY, K., GANDHI, S., DEAS, E., EATON, S., SMITH, M. D. P., VENNER, K., MATILLA, A., HEALY, D. G., GILKS, W. P., LEES, A. J., HOLTON, J., REVESZ, T., PARKER, P. J., HARVEY, R. J., WOOD, N. W. & LATCHMAN, D. S. 2006. Altered cleavage and localization of PINK1 to aggresomes in the presence of proteasomal stress. *Journal of Neurochemistry,* 98**,** 156-169.

NALLS, M. A., BLAUWENDRAAT, C., VALLERGA, C. L., HEILBRON, K., BANDRES-CIGA, S., CHANG, D., TAN, M., KIA, D. A., NOYCE, A. J., XUE, A., BRAS, J., YOUNG, E., VON COELLN, R., SIMÓN-SÁNCHEZ, J., SCHULTE, C., SHARMA, M., KROHN, L., PIHLSTROM, L., SIITONEN, A., IWAKI, H., LEONARD, H., FAGHRI, F., GIBBS, J. R., HERNANDEZ, D. G., SCHOLZ, S. W., BOTIA, J. A., MARTINEZ, M., CORVOL, J. C., LESAGE, S., JANKOVIC, J., SHULMAN, L. M., SUTHERLAND, M., TIENARI, P., MAJAMAA, K., TOFT, M., ANDREASSEN, O. A., BANGALE, T., BRICE, A., YANG, J., GAN-OR, Z., GASSER, T., HEUTINK, P., SHULMAN, J. M., WOOD, N. W., HINDS, D. A., HARDY, J. A., MORRIS, H. R., GRATTEN, J., VISSCHER, P. M., GRAHAM, R. R., SINGLETON, A. B., TEAM, M. R., DIS, S. G. P. S. & GENOMICS, I. P. S. D. 2019. Identification of novel risk loci, causal insights, and heritable risk for Parkinson's disease: a meta-analysis of genome-wide association studies. *Lancet Neurology,* 18**,** 1091-1102.

NARENDRA, D. P., JIN, S. M., TANAKA, A., SUEN, D. F., GAUTIER, C. A., SHEN, J., COOKSON, M. R. & YOULE, R. J. 2010. PINK1 Is Selectively Stabilized on Impaired Mitochondria to Activate Parkin. *Plos Biology,* 8.

NARENDRA, D. P. & YOULE, R. J. 2024. The role of PINK1-Parkin in mitochondrial quality control. *Nature Cell Biology,* 26**,** 1639-1651.
NICKLAS, W. J., VYAS, I. & HEIKKILA, R. E. 1985. Inhibition of Nadh-Linked Oxidation in Brain Mitochondria by 1-Methyl-4-Phenyl-Pyridine, a Metabolite of the Neurotoxin, 1-Methyl-4-Phenyl-1,2,5,6-Tetrahydropyridine. *Life Sciences,* 36**,** 2503-2508.
NONNEKES, J., POST, B., TETRUD, J. W., LANGSTON, J. W. & BLOEM, B. R. 2018. MPTP-induced parkinsonism: an historical case series. *Lancet Neurology,* 17**,** 300-301.
NOYCE, A. J., BESTWICK, J. P., SILVEIRA-MORIYAMA, L., HAWKES, C. H., GIOVANNONI, G., LEES, A. J. & SCHRAG, A. 2012. Meta-analysis of early nonmotor features and risk factors for Parkinson disease. *Ann Neurol,* 72**,** 893-901.
OKATSU, K., UNO, M., KOYANO, F., GO, E., KIMURA, M., OKA, T., TANAKA, K. & MATSUDA, N. 2013. A Dimeric PINK1-containing Complex on Depolarized Mitochondria Stimulates Parkin Recruitment. *Journal of Biological Chemistry,* 288**,** 36372-36384.
PARKINSON, J. 2002. An essay on the shaking palsy (Reprinted). *Journal of Neuropsychiatry and Clinical Neurosciences,* 14**,** 223-236.
PARRADO-FERNÁNDEZ, C., SCHNEIDER, B., ANKARCRONA, M., CONTI, M. M., COOKSON, M. R., KIVIPELTO, M., CEDAZO-MÍNGUEZ, A. & SANDEBRING-MATTON, A. 2018. Reduction of PINK1 or DJ-1 impair mitochondrial motility in neurites and alter ER-mitochondria contacts. *Journal of Cellular and Molecular Medicine,* 22**,** 5439-5449.
PETIT, A., KAWARAI, T., PAITEL, E., SANJO, N., MAJ, M., SCHEID, M., CHEN, F. S., GU, Y. J., HASEGAWA, H., SALEHI-RAD, S., WANG, L., ROGAEVA, E., FRASER, P., ROBINSON, B., ST GEORGE-HYSLOP, P. & TANDON, A. 2005. Wild-type PINK1 prevents basal and induced neuronal apoptosis, a protective effect abrogated by Parkinson disease-related mutations. *Journal of Biological Chemistry,* 280**,** 34025-34032.
POLYMEROPOULOS, M. H., LAVEDAN, C., LEROY, E., IDE, S. E., DEHEJIA, A., DUTRA, A., PIKE, B., ROOT, H., RUBENSTEIN, J., BOYER, R., STENROOS, E. S., CHANDRASEKHARAPPA, S., ATHANASSIADOU, A., PAPAPETROPOULOS, T., JOHNSON, W. G., LAZZARINI, A. M., DUVOISIN, R. C., DIIORIO, G., GOLBE, L. I. & NUSSBAUM, R. L. 1997. Mutation in the alpha-synuclein gene identified in families with Parkinson's disease. *Science,* 276**,** 2045-2047.
POPAT, R. A., VAN DEN EEDEN, S. K., TANNER, C. M., KAMEL, F., UMBACH, D. M., MARDER, K., MAYEUX, R., RITZ, B., ROSS, G. W., PETROVITCH, H., TOPOL, B., MCGUIRE, V., COSTELLO, S., MANTHRIPRAGADA, A. D., SOUTHWICK, A., MYERS, R. M. & NELSON, L. M. 2011. Coffee,
, and
: the caffeine connection in Parkinson's disease. *European Journal of Neurology,* 18**,** 756-765.
PUIGROS, M., CALDERON, A., MARTIN-RUIZ, D., SERRADELL, M., FERNANDEZ, M., MUNOZ-LOPETEGI, A., MAYA, G., SANTAMARIA, J., GAIG, C., COLELL, A., TOLOSA, E., IRANZO, A. & TRULLAS, R. 2024. Mitochondrial DNA deletions in the cerebrospinal fluid of patients with idiopathic REM sleep behaviour disorder. *EBioMedicine,* 102**,** 105065.

PUIGROS, M., CALDERON, A., PEREZ-SORIANO, A., DE DIOS, C., FERNANDEZ, M., COLELL, A., MARTI, M. J., TOLOSA, E. & TRULLAS, R. 2022. Cell-free mitochondrial DNA deletions in idiopathic, but not LRRK2, Parkinson's disease. *Neurobiol Dis,* 174**,** 105885.

RAMIREZ, A., HEIMBACH, A., GRUENDEMANN, J., STILLER, B., HAMPSHIRE, D., CID, L. P., GOEBEL, I., MUBAIDIN, A. F., WRIEKAT, A. L., ROEPER, J., AL-DIN, A., HILLMER, A. M., KARSAK, M., LISS, B., WOODS, C. G., BEHRENS, M. I. & KUBISCH, C. 2006. Hereditary parkinsonism with dementia is caused by mutations in

, encoding a lysosomal type 5 P-type ATPase. *Nature Genetics,* 38**,** 1184-1191.

RASOOL, S., VEYRON, S., SOYA, N., ELDEEB, M. A., LUKACS, G. L., FON, E. A. & TREMPE, J. F. 2022. Mechanism of PINK1 activation by autophosphorylation and insights into assembly on the TOM complex. *Molecular Cell,* 82**,** 44-+.

RECINTO, S. J., KAZANOVA, A., LIU, L., CORDEIRO, B., PREMACHANDRAN, S., BESSAIAH, H., ALLOT, A., AFANASIEV, E., MUKHERJEE, S., PEI, J., MACDONALD, A., YAQUBI, M., MCBRIDE, H. M., MATHEOUD, D., TRUDEAU, L. E., GRUENHEID, S. & STRATTON, J. A. 2025. PINK1 deficiency rewires early immune responses in a mouse model of Parkinson's disease triggered by intestinal infection. *Npj Parkinsons Disease,* 11.

REYNOSO, A., TORRICELLI, R., JACOBS, B. M., SHI, J. C. Z., ASLIBEKYAN, S., NORCLIFFE-KAUFMANN, L., NOYCE, A. J. & HEILBRON, K. 2024. Gene-Environment Interactions for Parkinson's Disease. *Annals of Neurology,* 95**,** 677-687.

RIETDIJK, C. D., PEREZ-PARDO, P., GARSSEN, J., VAN WEZEL, R. J. & KRANEVELD, A. D. 2017. Exploring Braak's Hypothesis of Parkinson's Disease. *Front Neurol,* 8**,** 37.

ROCHA, E., CHAMOLI, M., CHINTA, S. J., ANDERSEN, J. K., WALLIS, R., BEZARD, E., GOLDBERG, M., GREENAMYRE, T., HIRST, W., KUAN, W. L., KIRIK, D., NIEDERNHOFER, L., RAPPLEY, I., PADMANABHAN, S., TRUDEAU, L. E., SPILLANTINI, M., SCOTT, S., STUDER, L., BELLANTUONO, I. & MORTIBOYS, H. 2023. Aging, Parkinson's Disease, and Models: What Are the Challenges? *Aging Biol,* 1.

ROMANO, S., SAVVA, G. M., BEDARF, J. R., CHARLES, I. G., HILDEBRAND, F. & NARBAD, A. 2021. Meta-analysis of the Parkinson's disease gut microbiome suggests alterations linked to intestinal inflammation. *Npj Parkinsons Disease,* 7.

SCHLOSSMACHER, M. G., FROSCH, M. P., GAI, W. P., MEDINA, M., SHARMA, N., FORNO, L., OCHIISHI, T., SHIMURA, H., SHARON, R., HATTORI, N., LANGSTON, J. W., MIZUNO, Y., HYMAN, B. T., SELKOE, D. J. & KOSIK, K. S. 2002. Parkin localizes to the Lewy bodies of Parkinson disease and dementia with Lewy bodies. *American Journal of Pathology,* 160**,** 1655-1667.

SHAHMORADIAN, S. H., LEWIS, A. J., GENOUD, C., HENCH, J., MOORS, T. E., NAVARRO, P. P., CASTAÑO-DÍEZ, D., SCHWEIGHAUSER, G., GRAFF-MEYER, A., GODIE, K. N., SÜTTERLIN, R., HUISMAN, E., INGRASSIA, A., DE GIER, Y., ROZEMULLER, A. J. M., WANG, J., DE PAEPE, A., ERNY, J., STAEMPFLI, A., HOERNSCHEMEYER, J., GROSSERÜSCHKAMP, F., NIEDIEKER, D., EL-MASHTOLY, S. F., QUADRI, M., VAN IJCKEN, W. F. J., BONIFATI, V., GERWERT, K., BOHRMANN, B., FRANK, S., BRITSCHGI, M., STAHLBERG, H., VAN DE BERG, W. D. J. & LAUER, M. E. 2019. Lewy

pathology in Parkinson's disease consists of crowded organelles and lipid membranes. *Nature Neuroscience,* 22**,** 1099-+.
SHARMA, K., KISHORE, A., LECHADO-TERRADAS, A., PASSANNANTI, R., RAIMONDI, F., STURM, M., SREELATHA, A. A. K., PUTHENVEEDU, D. K., SARMA, G., CASADEI, N., KRÜGER, R., GASSER, T., KAHLE, P., RIESS, O., FITZGERALD, J. C. & SHARMA, M. 2024. A Novel p.F385S Loss-of-Function Mutation in an Indian Family with Parkinson's Disease. *Movement Disorders,* 39**,** 1217-1225.
SHAW, C. A. & HÖGLINGER, G. U. 2008. Neurodegenerative diseases:: Neurotoxins as sufficient etiologic agents? *Neuromolecular Medicine,* 10**,** 1-9.
SIDRANSKY, E., NALLS, M. A., AASLY, J. O., AHARON-PERETZ, J., ANNESI, G., BARBOSA, E. R., BAR-SHIRA, A., BERG, D., BRAS, J., BRICE, A., CHEN, C. M., CLARK, L. N., CONDROYER, C., DE MARCO, E. V., DURR, A., EBLAN, M. J., FAHN, S., FARRER, M. J., FUNG, H. C., GAN-OR, Z., GASSER, T., GERSHONI-BARUCH, R., GILADI, N., GRIFFITH, A., GUREVICH, T., JANUARIO, C., KROPP, P., LANG, A. E., LEE-CHEN, G. J., LESAGE, S., MARDER, K., MATA, I. F., MIRELMAN, A., MITSUI, J., MIZUTA, I., NICOLETTI, G., OLIVEIRA, C., OTTMAN, R., ORR-URTREGER, A., PEREIRA, L. V., QUATTRONE, A., ROGAEVA, E., ROLFS, A., ROSENBAUM, H., ROZENBERG, R., SAMII, A., SAMADDAR, T., SCHULTE, C., SHARMA, M., SINGLETON, A., SPITZ, M., TAN, E. K., TAYEBI, N., TODA, T., TROIANO, A. R., TSUJI, S., WITTSTOCK, M., WOLFSBERG, T. G., WU, Y. R., ZABETIAN, C. P., ZHAO, Y. & ZIEGLER, S. G. 2009. Multicenter analysis of glucocerebrosidase mutations in Parkinson's disease. *N Engl J Med,* 361**,** 1651-61.
SIDRANSKYL, E. 2009. International Multi-Center Analysis of Glucocerebrosidase Mutations in Parkinson Disease. *Molecular Genetics and Metabolism,* 98**,** 85-85.
SMAJIC, S., PRADA-MEDINA, C. A., LANDOULSI, Z., GHELFI, J., DELCAMBRE, S., DIETRICH, C., JARAZO, J., HENCK, J., BALACHANDRAN, S., PACHCHEK, S., MORRIS, C. M., ANTONY, P., TIMMERMANN, B., SAUER, S., PEREIRA, S. L., SCHWAMBORN, J. C., MAY, P., GRÜNEWALD, A. & SPIELMANN, M. 2022. Single-cell sequencing of human midbrain reveals glial activation and a Parkinson-specific neuronal state. *Brain,* 145**,** 964-978.
SOUBANNIER, V., MCLELLAND, G. L., ZUNINO, R., BRASCHI, E., RIPPSTEIN, P., FON, E. A. & MCBRIDE, H. M. 2012a. A Vesicular Transport Pathway Shuttles Cargo from Mitochondria to Lysosomes. *Current Biology,* 22**,** 135-141.
SOUBANNIER, V., RIPPSTEIN, P., KAUFMAN, B. A., SHOUBRIDGE, E. A. & MCBRIDE, H. M. 2012b. Reconstitution of Mitochondria Derived Vesicle Formation Demonstrates Selective Enrichment of Oxidized Cargo. *Plos One,* 7.
SPILLANTINI, M. G., SCHMIDT, M. L., LEE, V. M. Y., TROJANOWSKI, J. Q., JAKES, R. & GOEDERT, M. 1997. alpha-synuclein in Lewy bodies. *Nature,* 388**,** 839-840.
STEVENSON, T. J., MURRAY, H. C., TURNER, C., FAULL, R. L. M., DIERIKS, B. V. & CURTIS, M. A. 2020. α-synuclein inclusions are abundant in non-neuronal cells in the anterior olfactory nucleus of the Parkinson's disease olfactory bulb. *Scientific Reports,* 10.

SUBRAHMANIAN, N. & LAVOIE, M. J. 2021. Is there a special relationship between complex I activity and nigral neuronal loss in Parkinson's disease? A critical reappraisal. *Brain Res,* 1767**,** 147434.
SUGIURA, A., MCLELLAND, G. L., FON, E. A. & MCBRIDE, H. M. 2014. A new pathway for mitochondrial quality control: mitochondrial-derived vesicles. *Embo Journal,* 33**,** 2142-2156.
SUN, L. K., SHEN, R. F., AGNIHOTRI, S. K., CHEN, Y., HUANG, Z. W. & BÜELER, H. 2018. Lack of PINK1 alters glia innate immune responses and enhances inflammation-induced, nitric oxide-mediated neuron death. *Scientific Reports,* 8.
SUN, M. F. & SHEN, Y. Q. 2018. Dysbiosis of gut microbiota and microbial metabolites in Parkinson's Disease. *Ageing Research Reviews,* 45**,** 53-61.
TAN, A. H., LIM, S. Y. & LANG, A. E. 2022. The microbiome-gut-brain axis in Parkinson disease - from basic research to the clinic. *Nature Reviews Neurology,* 18**,** 476-495.
TANJI, K., MORI, F., KAKITA, A., TAKAHASHI, H. & WAKABAYASHI, K. 2011. Alteration of autophagosomal proteins (LC3, GABARAP and GATE-16) in Lewy body disease. *Neurobiology of Disease,* 43**,** 690-697.
TANSEY, M. G., MCCOY, M. K. & FRANK-CANNON, T. C. 2007. Neuroinflammatory mechanisms in Parkinson's disease: Potential environmental triggers, pathways, and targets for early therapeutic intervention. *Experimental Neurology,* 208**,** 1-25.
TANSEY, M. G., WALLINGS, R. L., HOUSER, M. C., HERRICK, M. K., KEATING, C. E. & JOERS, V. 2022. Inflammation and immune dysfunction in Parkinson disease. *Nature Reviews Immunology,* 22**,** 657-673.
TOFARIS, G. K., KIM, H. T., HOUREZ, R., JUNG, J. W., KIM, K. P. & GOLDBERG, A. L. 2011. Ubiquitin ligase Nedd4 promotes α-synuclein degradation by the endosomal-lysosomal pathway. *Proceedings of the National Academy of Sciences of the United States of America,* 108**,** 17004-17009.
TOFARIS, G. K., RAZZAQ, A., GHETTI, B., LILLEY, K. S. & SPILLANTINI, M. G. 2003. Ubiquitination of alpha-synuclein in Lewy bodies is a pathological event not associated with impairment of proteasome function. *J Biol Chem,* 278**,** 44405-11.
UNOKI, M. & NAKAMURA, Y. 2001. Growth-suppressive effects of
and
, two genes involved in the
signaling pathway. *Oncogene,* 20**,** 4457-4465.
VALENTE, E. M., ABOU-SLEIMAN, P. M., CAPUTO, V., MUQIT, M. M., HARVEY, K., GISPERT, S., ALI, Z., DEL TURCO, D., BENTIVOGLIO, A. R., HEALY, D. G., ALBANESE, A., NUSSBAUM, R., GONZALEZ-MALDONADO, R., DELLER, T., SALVI, S., CORTELLI, P., GILKS, W. P., LATCHMAN, D. S., HARVEY, R. J., DALLAPICCOLA, B., AUBURGER, G. & WOOD, N. W. 2004. Hereditary early-onset Parkinson's disease caused by mutations in PINK1. *Science,* 304**,** 1158-60.
VALENTE, E. M., BENTIVOGLIO, A. R., DIXON, P. H., FERRARIS, A., IALONGO, T., FRONTALI, M., ALBANESE, A. & WOOD, N. W. 2001. Localization of a novel locus for autosomal recessive early-onset parkinsonism, PARK6, on human chromosome 1p35-p36. *American Journal of Human Genetics,* 68**,** 895-900.

VALENTE, E. M., BRANCATI, F., FERRARIS, A., GRAHAM, E. A., DAVIS, M. B., BRETELER, M. M. B., GASSER, T., BONIFATI, V., BENTIVOGLIO, A. R., DE MICHELE, G., DÜRR, A., CORTELLI, P., WASSILOWSKY, D., HARHANGI, B. S., RAWAL, N., CAPUTO, V., FILLA, A., MECO, G., OOSTRA, B. A., BRICE, A., ALBANESE, A., DALLAPICCOLA, B., WOOD, N. W. & SUSCEP, E. C. G. 2002. PARK6-linked parkinsonism occurs in several European families. *Annals of Neurology,* 51**,** 14-18.

VAN DER BLIEK, A. M., SHEN, Q. F. & KAWAJIRI, S. 2013. Mechanisms of Mitochondrial Fission and Fusion. *Cold Spring Harbor Perspectives in Biology,* 5.

WANG, Q. Q., LIU, Y. J. & ZHOU, J. W. 2015. Neuroinflammation in Parkinson's disease and its potential as therapeutic target. *Translational Neurodegeneration,* 4.

WANG, R., FORTIER, T. M., CHAI, F., MIAO, G., SHEN, J. L., RESTREPO, L. J., DIGIACOMO, J. J., VELENTZAS, P. D. & BAEHRECKE, E. H. 2023. PINK1, Keap1, and Rtnl1 regulate selective clearance of endoplasmic reticulum during development. *Cell,* 186**,** 4172-4188 e18.

WANG, X., WINTER, D., ASHRAFI, G., SCHLEHE, J., WONG, Y. L., SELKOE, D., RICE, S., STEEN, J., LAVOIE, M. J. & SCHWARZ, T. L. 2011. PINK1 and Parkin target Miro for phosphorylation and degradation to arrest mitochondrial motility. *Cell,* 147**,** 893-906.

WAUER, T., SIMICEK, M., SCHUBERT, A. & KOMANDER, D. 2015. Mechanism of phospho-ubiquitin-induced PARKIN activation. *Nature,* 524**,** 370-+.

WILLIAMS, G. P., FREUCHET, A., MICHAELIS, T., FRAZIER, A., TRAN, N. K., LIMA-JUNIOR, J. R., PHILLIPS, E. J., MALLAL, S. A., LITVAN, I., GOLDMAN, J. G., ALCALAY, R. N., SIDNEY, J., SULZER, D., SETTE, A. & ARLEHAMN, C. S. L. 2025. PINK1 is a target of T cell responses in Parkinson's disease. *Journal of Clinical Investigation,* 135.

WONG, E. & CUERVO, A. M. 2010. Integration of Clearance Mechanisms: The Proteasome and Autophagy. *Cold Spring Harbor Perspectives in Biology,* 2.

XIA, Q. W., LIAO, L. J., CHENG, D. M., DUONG, D. M., GEARING, M., LAH, J. J., LEVEY, A. I. & PENG, J. M. 2008. Proteomic identification of novel proteins associated with Lewy bodies. *Frontiers in Bioscience-Landmark,* 13**,** 3850-3856.

YAMANO, K. & YOULE, R. J. 2013. PINK1 is degraded through the N-end rule pathway. *Autophagy,* 9**,** 1758-1769.

YANG, M. L., WEI, X., YI, X. & JIANG, D. S. 2024. Mitophagy-related regulated cell death: molecular mechanisms and disease implications. *Cell Death & Disease,* 15.

YANG, Y. F., OUYANG, Y. S., YANG, L. C., BCAL, M. F., MCQUIBBAN, A., VOGEL, H. & LU, B. W. 2008. Pink1 regulates mitochondrial dynamics through interaction with the fission/fusion machinery (vol 105, pg 7070, 2008). *Proceedings of the National Academy of Sciences of the United States of America,* 105**,** 17585-17587.

YIN, E. P. & DIERIKS, B. V. 2025. Rethinking 'rare' Parkinson's disease: A meta-analysis of geographical prevalence, phenotypic diversity, and α-synuclein pathology. *Journal of Parkinsons Disease,* 15**,** 41-65.

ZHOU, J., YANG, R., ZHANG, Z. R., LIU, Q. R., ZHANG, Y. Y., WANG, Q. Q. & YUAN, H. B. 2019. Mitochondrial Protein PINK1 Positively Regulates RLR Signaling. *Frontiers in Immunology,* 10.

ZHOU, Y., GU, G. Y., GOODLETT, D. R., ZHANG, T., PAN, C., MONTINE, T. J., MONTINE, K. S., AEBERSOLD, R. H. & ZHANG, J. 2004. Analysis of α-synuclein-associated proteins by quantitative proteomics. *Journal of Biological Chemistry,* 279**,** 39155-39164.

ZHU, M. L., LIU, X., YE, Y. R., YAN, X. M., CHENG, Y. W., ZHAO, L. Y., CHEN, F. & LING, Z. X. 2022. Gut Microbiota: A Novel Therapeutic Target for Parkinson's Disease. *Frontiers in Immunology,* 13.

11. Appendix.

Manuscript 1:

Sharma, K., Kishore, A., Lechado-Terradas, A., Passannanti, R., Raimondi, F., Sturm, M., ... & Sharma, M. (2024). A Novel PINK1 p. F385S Loss-of-Function Mutation in an Indian Family with Parkinson's Disease. Movement Disorders, 39(7), 1217-1225.

Manuscript 2:

Cavarischia-Rega, C., **Sharma, K.**, Fitzgerald, J. C., & Macek, B. (2024). Proteome dynamics in iPSC-derived human dopaminergic neurons. Molecular & Cellular Proteomics, 23(10).

Manuscript 3:

Sharma, K., Cavarischia-Rega, C., Ivaniuk, D., Bus, C., Brouwers, J. F... & Fitzgerald, J. C. (2025). PINK1 regulates cholesterol homeostasis via SCAP phosphorylation in human dopaminergic neurons. (BioRxiv preprint)

BRIEF REPORT

A Novel *PINK1* p.F385S Loss-of-Function Mutation in an Indian Family with Parkinson's Disease

Karan Sharma, MSc,[1] Asha Kishore, MD,[2,3] Anna Lechado-Terradas, PhD,[1] Raffaele Passannanti, PhD,[4] Francesco Raimondi, PhD,[4] Marc Sturm, PhD,[5] Ashwin Ashok Kumar Sreelatha, MSc, MTech,[6] Divya Kalikavila Puthenveedu, MD,[2] Gangadhara Sarma, MD,[2] Nicolas Casadei, PhD,[7] Rejko Krüger, MD,[8] Thomas Gasser, MD,[1,9] Philipp Kahle, PhD,[1,9,10] Olaf Riess, MD,[7] Julia C. Fitzgerald, PhD,[1] and Manu Sharma, PhD[6*]

[1]*Department of Neurodegeneration, Hertie Institute for Clinical Brain Research, University of Tübingen, Tübingen, Germany* [2]*Department of Neurology, Sree Chitra Tirunal Institute for Medical Sciences and Technology, Thiruvananthapuram, India* [3]*Parkinson and Movement Disorder Centre, Aster Medicity, Kochi, India* [4]*Laboratorio di Biologia Bio@SNS, Scuola Normale Superiore, Pisa, Italy* [5]*Institute of Medical Genetics and Applied Genomics, University of Tübingen, Tübingen, Germany* [6]*Centre for Genetic Epidemiology, Institute for Clinical Epidemiology and Applied Biometry, University of Tübingen, Tübingen, Germany* [7]*Institute of Medical Genetics and Applied Genomics & Core Facility for Applied Genomics, University of Tübingen, Tübingen, Germany* [8]*Translational Neuroscience, Luxembourg Center for Systems Biomedicine, University of Luxembourg, Luxembourg, Transversal Translational Medicine, Luxembourg Institute of Health, Strassen, Luxembourg & Centre Hospitalier de Luxembourg, Esch-sur-Alzette, Luxembourg* [9]*German Centre for Neurodegenerative Diseases, Tübingen, Germany* [10]*Department of Biochemistry, University of Tübingen, Tübingen, Germany*

ABSTRACT: Background: Most Parkinson's disease (PD) loci have shown low prevalence in the Indian population, highlighting the need for further research.
Objective: The aim of this study was to characterize a novel phosphatase tensin homolog-induced serine/threonine kinase 1 (*PINK1*) mutation causing PD in an Indian family.
Methods: Exome sequencing of a well-characterized Indian family with PD. A novel *PINK1* mutation was studied by in silico modeling using AlphaFold2, expression of mutant PINK1 in human cells depleted of functional endogenous PINK1, followed by quantitative image analysis and biochemical assessment.
Results: We identified a homozygous chr1:20648535–20648535 T>C on GRCh38 (p.F385S) mutation in exon 6 of *PINK1*, which was absent in 1029 genomes from India and in other known databases. PINK1 F385S lies within the highly conserved Deutsche Forschungsgemeinschaft (DFG) motif, destabilizes its active state, and impairs phosphorylation of ubiquitin at serine 65 and proper engagement of parkin upon mitochondrial depolarization.
Conclusions: We characterized a novel non-conservative mutation in the DFG motif of *PINK1*, which causes loss of its ubiquitin kinase activity and inhibition of mitophagy. © 2024 The Authors. *Movement Disorders* published by Wiley Periodicals LLC on behalf of International Parkinson and Movement Disorder Society.

Key Words: PINK1; genome sequencing; phosphorylation; ubiquitin; mitophagy; Parkinson's disease

***Correspondence to:** Dr. Manu Sharma, Centre for Genetic Epidemiology, Institute for Clinical Epidemiology and Applied Biometry, University of Tübingen, Silcherstr. 5 72076, Tübingen, Germany; E-mail: manu.sharma@uni-tuebingen.de

Karan Sharma, Asha Kishore, and Anna Lechado-Terradas contributed equally to this work.

Relevant conflicts of interest/financial disclosures: Nothing to report.

Funding agencies: This study was supported by The Michael J. Fox Foundation, USA, GP2, and the German Research Council–Deutsche Forschungsgemeinschaft (DFG). M.S. was supported by funding from The Michael J. Fox Foundation and GP2 (Grants MJFF-11879, 17473, 009411, and 023430) and DFG (Grant SH599/16-1). P.K., J.C.F., A.L.-T., and K.S. acknowledge support from the DFG, German Research Council, Research Training Group (MOMbrane 654651/GRK2364).

Full financial disclosures and author roles may be found in the online version of this article.

Received: 14 November 2023; **Revised:** 1 February 2024; **Accepted:** 11 March 2024

Published online in Wiley Online Library (wileyonlinelibrary.com). DOI: 10.1002/mds.29792

Introduction

Mutations in phosphatase tensin homolog-induced serine/threonine kinase 1 gene (*PINK1*) cause autosomal recessive Parkinson's disease (PD).[1] PINK1-PD is usually of early onset, is slowly progressive, and shows excellent response to levodopa treatment.[2] The discovery of *PINK1* as a cause of familial PD, together with several other mutations, led to the identification of disturbed mitochondrial quality control as a molecular mechanism underlying PD. Most, if not all, monogenetic causes of PD have been identified in the European population, and there is a lack transferability to other ethnically diverse populations. In our study, we found a novel PINK1 mutation. The p.F385S mutation lies in the highly conserved DFG motif of PINK1, which is

important for its ATP binding and kinase activity.[3] Kinase activity is required for PINK1 to initiate the clearance of damaged mitochondria via PINK1/Parkin mitophagy.[4] Upon mitochondrial stress, PINK1 forms a dimer at the mitochondrial outer membrane (MOM) and autophosphorylates itself, enabling self-activation.[5,6] This activation frees its ubiquitin recognition site and helps in the recruitment of parkin by phosphorylation of ubiquitin at Ser65 and the ubiquitin-like domain of parkin.[7-16] PINK1 further phosphorylates proteins of the MOM, and parkin ubiquitinates them in a cascade to promote outside-in mitophagy.[17-19] Previously described mutations in PINK1 in the Caucasian population, particularly the G386A mutation, also localize in the DFG motif.[11,20] Our aim was to functionally characterize a novel PINK1 mutation causing PD identified in an Indian family.

Subjects and Methods

Monogenetic PD Cohort

Sixty families with PD were compiled over 10 years as part of Cataloging Genetic Architecture of PD and Genomic Registry of Parkinson Disease in the Movement Disorder Centre of Sree Chitra Tirunal Institute for Medical Sciences and Technology, India. All affected and nonaffected individuals were interviewed and examined by a movement disorder specialist. The ethics committee of Sree Chitra Tirunal Institute for Medical Sciences and Technology approved the study. All participants gave written informed consent.

Exome Sequencing

Genomic DNA was extracted using the salting-out method for targeted resequencing and whole-genome analysis. Exome sequencing was performed at the Core Facility of Applied Transcriptomics and Genomics at the Institute of Medical Genetics (University of Tübingen, Tübingen, Germany). The data analysis was performed using a medical genetics sequence analysis pipeline (see Supporting Information Methods: Data S1). We first searched for known mutations in our cohorts, and to find novel PD variants, we filtered the detected variants using two main criteria: (1) the variant must be protein altering or in a splice region; and (2) the variant should have a maximum allele frequency of 0.01% in gnomAD, including subpopulations.

IndiGenomes

A publicly available database was used to search for putative variants in the control genomes ascertained from different regions of India. In brief, a total of 1029 self-declared healthy individuals underwent whole-genome sequencing to develop a comprehensive compendium of genetic variants in the Indian population.[21,22]

Molecular Modeling

We used the full-length (FL) structure of human *PINK1* predicted via AlphaFold2,[23] which is available through accession number Q9BXM7 (https://alphafold.ebi.ac.uk/entry/Q9BXM7), maintained at the European Bioinformatics Institute.[24] We assessed the effect of the *PINK1* F385S mutation through the ddg_monomer protocol[25] from the RosettaCommons molecular modeling suite (https://www.rosettacommons.org/). For further details, see Supporting Information Methods: Data S1. We calculated the statistical significance of energetic calculations through the "ranksums" method of the Python (v3.10.4) scipy (v1.7.3) and seaborn (v0.12.2) libraries.

Site-Directed Mutagenesis

Plasmid pcDNA/V5-His A with wild-type (WT) *PINK1* gene at the multiple cloning site was used to introduce the Phe385Ser (F385S) mutation by altering T>C at position 1154 of the gene with QuikChange II Site-Directed Mutagenesis Kit (200523; Agilent Technologies Deutschland GmbH, Waldbronn, Germany). The primers used were 5′-gcagcagccagaatctgcgatcaccagcca-3′ and 5′-tggctggtgatcgcagattctggctgctgc-3′. The polymerase chain reaction, cycle parameters, and procedure were followed according to the manufacturer's instructions.

Cell Culture and Transfection

WT and PINK1 W437X HeLa cells[26] (Sigma-Aldrich Chemie GmbH, Taufkirchen, Germany) were maintained in Dulbecco's Modified Eagles Medium: 4.5 g/L glucose (D6429; Sigma-Aldrich) supplemented with 10% fetal bovine serum and 1% penicillin/streptomycin. For DNA transfection (Thermo Fisher Scientific, Waltham, MA, USA) with WT-PINK1 pcDNA/V5-His A or F385S-PINK1 pcDNA/V5-His A and WT parkin-3XFLAG pcDNA3.1, cells were seeded at least 24 h before transfecting with Lipofectamine 3000 reagent (L3000008; Invitrogen) according to the manufacturer's instructions.

Cell Culture Treatments

For half-life and stability assays, cells were treated with 100 µM cycloheximide solution (CHX; 239765; Calbiochem, Merck Chemicals GmbH, an affiliate of Merck KGaA, Darmstadt, Germany) and/or 10 µM MG132 (sc210270; Santa Cruz Biotechnology, Inc., Heidelberg, Germany) resuspended in dimethylsulfoxide (DMSO) with an equal volume of DMSO used as a vehicle. For the stability assay, cells were pretreated with MG132 for 2 hours and maintained in the media throughout the 6-hour time course. For the mitophagy initiation assay, 40 µM carbonyl cyanide chlorophenylhydrazone (CCCP) (C2759; Sigma-Aldrich) resuspended in DMSO was used with an equal volume of DMSO as a vehicle.

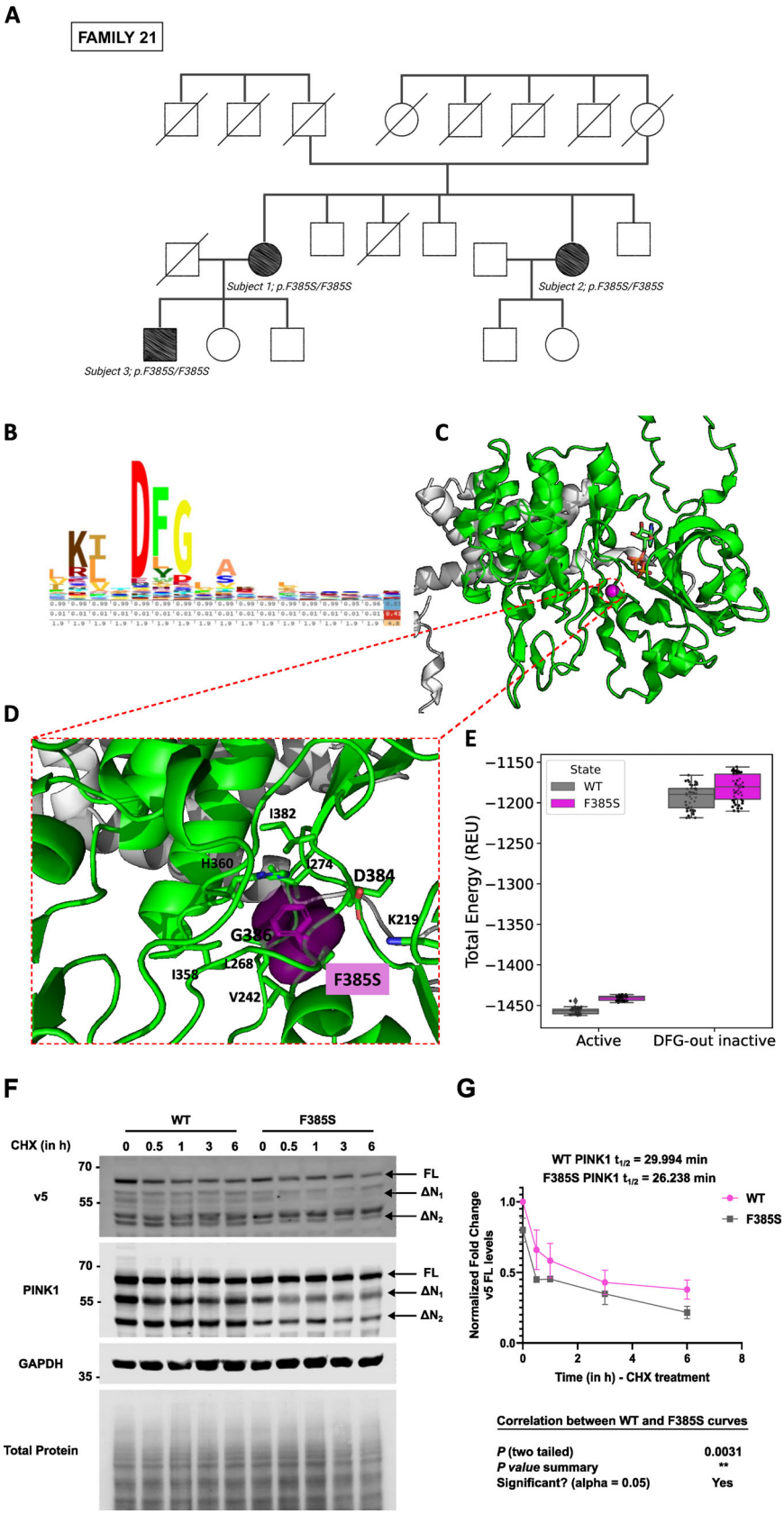

FIG. 1. Legend on next page.

Immunofluorescence

Cells were fixed in 4% paraformaldehyde solution and washed with PBS. Permeabilization and blocking were done using 0.3% Triton X-100 + 1% bovine serum albumin and incubated for 1 hour at room temperature. Antibodies were added in 0.1% Triton X-100 + 1% bovine serum albumin overnight at room temperature inside a humidifier chamber. Primary antibodies were used at 1:1000 for Parkin (2132, rabbit; Cell Signaling Technology Europe B.V. Leiden, The Netherlands), 1:500 for v5 (sc271944, mouse; Santa Cruz), and 1:500 for single-stranded DNA binding protein (SSBP1; AF6588, sheep; R&D Systems- Bio-Techne GmbH, Wiesbaden Nordenstadt, Germany). The secondary antibodies were all used at 1:1000 and included donkey anti-sheep Alexa 488 (A-11015; Invitrogen), donkey anti-mouse Alexa 568 (A10037; Life Technologies, Thermo Fisher Scientific), and goat anti-rabbit Alexa 647 (A21245; Life Technologies). Hoechst (H3569; Molecular Devices, GmbH, Munich, Germany) was used to stain nuclei before mounting with Dako fluorescent mounting medium (S3023; Agilent).

Immunoblotting

Cells were lysed in 1% Triton X-100 + 1% SDS in PBS containing cOmplete protease inhibitor (Millipore 89, 11873580001; Sigma) and PhosStop phosphatase inhibitor (4906837001; Sigma-Aldrich). SDS-PAGE gel and protein transfer was followed by incubation with primary antibodies used at 1:500 for v5 (sc271944, mouse; Santa Cruz), 1:1000 for PINK1 (BC100-494, rabbit; Novus Biologicals, - Bio-Techne GmbH, Wiesbaden Nordenstadt, Germany), 1:1000 for Parkin (ab15954, rabbit; Abcam Limited, Cambridge, United Kingdom), 1:10,000 for GAPDH (CB1001, mouse; Sigma), and 1:500 for phospho-ubiquitin Ser65 (62802S, rabbit; Cell Signaling). Secondary antibodies were used at 1:10,000 (926-32211 and 926-68070; LI-COR Biotechnology - GmbH, Bad Homburg, Germany) and detected with Odyssey CLx (LI-COR) using Image Studio software (LI-COR). Mitochondrial fragmentation analysis used CellProfiler. For semiquantitative image analysis, CellProfiler (4.2.1 version) software was used. In all transfected conditions, a minimum of 169 cells were assessed combining all three replicates, with each replicate including between 37 and 81 cells. In nontransfected cells, a minimum of 157 cells were analyzed per replicate. In all cases, individual cells were recognized with the nuclear staining, and the cytoplasmic area was established using PINK1 and parkin staining. Nuclei were not considered as part of the cytoplasm. For details, see Supporting Information Methods: Data S1.

Parkin Translocation Analysis

Parkin localization was assessed manually using the same raw images and cell number used for SSBP1 morphology analysis (see earlier). In this study, transfected cells were classified as either positive or negative for parkin translocation only when the parkin signal colocalized with SSBP1.

Statistical Analysis and Interpretation

For statistical analyses, GraphPad Prism version 8.4.0 was used. Data are presented as mean average ± standard error of the mean (SEM) ($^{*}P < 0.05$; $^{**}P < 0.005$; $^{***}P < 0.0005$; $^{****}P < 0.0001$; $^{ns}P > 0.05$, where ns represents nonsignificant). For details, see the figure legends and Supporting Information Methods: Data S1.

Results

Identification of a Novel *PINK1* p.F385S Mutation

For exome sequencing, the mean sequencing depth was 124×. On average, 94.82% of the 50-Mb target region was covered with at least 20× depth. The exome sequencing identified a novel missense mutation, homozygous *PINK1* p.F385S, in three affected carriers spanning two consecutive generations, but not in healthy subjects (Fig. 1A). Analysis of the sum of runs of homozygosity (ROHs) larger than 500 Kb in the three carriers showed likely consanguinity implicating a pseudodominant inheritance. When looking at the ROHs around *PINK1*, they share an ROH of 2.26 Mb at chr1:19713608–21974391 (hg38) (see Supporting Information Methods: Data S1). Using publicly available IndiGenomes and gnomad databases, the mutation was not present in the Indian and the European population,

FIG. 1. (**A**) The Indian family pedigree showed a pseudodominant mode of inheritance. (**B**) Consensus logo of the Hidden Markov Model of the Kinase domain (https://www.ebi.ac.uk/interpro/entry/pfam/PF00069/logo/) showing the conservation profile of the DFG motif. (**C**) Cartoon three-dimensional representations of the predicted full-length structure of PINK1 in complex with ATP. (**D**) Zoomed view of the contacts mediated by the F385 residue. (**E**) Bar plots showing the predicted ddG for the wild-type (WT) and F385S mutant of PINK1 predicted in its active conformation (left) and DFG-out, inactive conformation (right). (**F**) HeLa cells expressing WT or mutant (F385S) PINK1 were untreated or treated with 100 μM cycloheximide (CHX) for 0.5, 1, 3, or 6 hours. Western blot probed for V5-tagged PINK1 (v5), PINK1, and GAPDH loading control. The Western blot was stained for total protein using the Ponceau stain. Full-length PINK1, N-terminal processed PINK1 (ΔN1), and further N-terminal processed PINK1 (ΔN2) are observed. A representative Western blot is shown (n = 3). (**G**) Quantified levels of V5-tagged full-length PINK1 normalized to total protein levels at 0, 0.5, 1, 3, and 6 hours of CHX treatment. Half-lives (T1/2) of full-length WT and mutant F385S PINK1 are shown (minutes). Error bars show the standard error of the mean (SEM) (n = 3). The correlation of WT and mutant F385S PINK1 levels over time using Pearson's *r* test (2-tailed) is shown. FL, full-length PINK1. [Color figure can be viewed at wileyonlinelibrary.com]

indicating its rarity. Clinically, all affected carriers showed early-onset, typical motor symptoms and psychiatric symptoms with good response to levodopa (see Supporting Information Data S2). *PINK1* was analyzed by multiplex-ligation dependent probe amplification (MLPA), and no gene dosage change was detected.

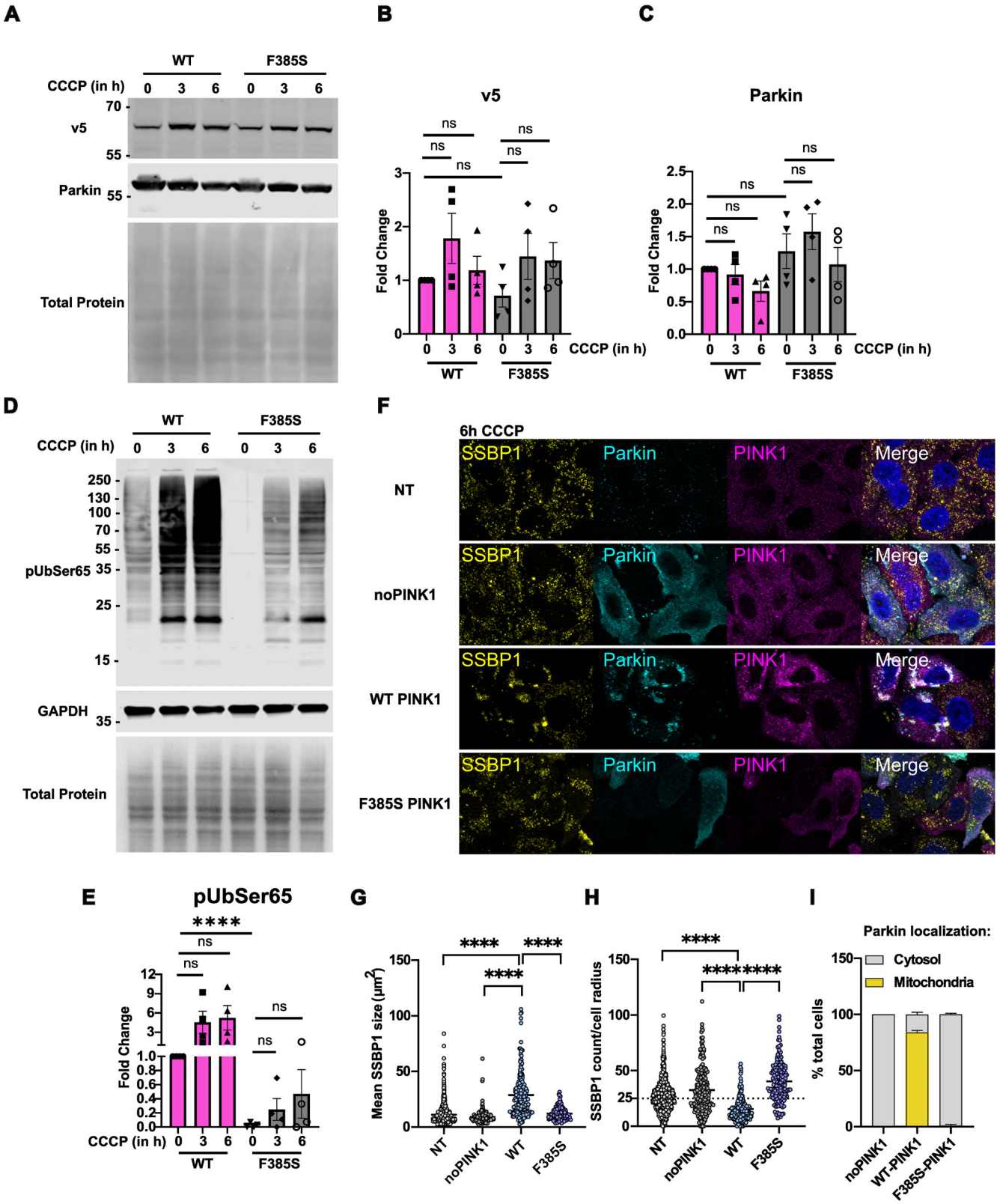

FIG. 2. Legend on next page.

In Silico Modeling Predicts the PINK1 F385S Mutation to Disrupt Kinase Activation

PINK1 F385 is part of the highly conserved DFG motif, which is a master regulator of the kinase domain activation (Fig. 1B). We have modeled the functional consequences of the F385S mutation in silico using the structure of monomeric PINK1, predicted by AlphaFold2 (Fig. 1C,D). We predicted the effect of the mutation via energy calculations, which showed a higher ddG for the mutant versus the WT in its active ($P = 9.25E{-}18$) and inactive state ($P = 0.00047$) (Fig. 1E). This suggested a much greater overall destabilization of PINK1, particularly in its active state, and consequently impairment of its kinase function.

Expression and Processing of F385S Mutant PINK1

Under basal conditions, FL PINK1 is efficiently imported into mitochondria. The N-terminal mitochondrial targeting sequence is removed by mitochondrial processing proteases to yield ΔN1. PINK1 is then further N-terminally truncated to yield ΔN2, which is rapidly degraded via the proteasome.[27] Overexpressed WT PINK1-V5 showed this processing pattern: FL, 63-kDa; ΔN1, 53-kDa; and ΔN2, 45-kDa bands, which are consistent with the literature.[28,29] F385S-PINK1-V5 showed the same pattern (Fig. 1F), indicating intact processing of mutant PINK1. To determine protein half-life, we blocked translation with CHX and chased the cells for a time ranging from 0.5 to 6 hours. When probed for anti-V5 and with anti-PINK1 directly, FL-F385S-PINK1 had a slightly but significantly reduced half-life of 26.238 minutes compared with FL-WT-PINK1, which had a half-life of 29.994 minutes (Fig. 1G). To investigate protein stability, we treated the cells with CHX for 0.5 to 6 hours in the presence of MG132 followed by probing with anti-V5 and anti-PINK1 (Supporting Information Fig. S1A) and quantified the levels of FL (Fig. S1B), ΔN1 (Fig. S1C), and ΔN1/FL ratio of v5-tagged PINK1 (Fig. S1D). There were no differences in the WT and F385S-PINK1 levels, suggesting no impact of F385S mutation on PINK1 stability and processing. The reduced half-life of F385S-PINK1 observed in Figure 1G is due to slightly faster degradation of FL-F385S compared with the WT protein, as confirmed by the proteasomal inhibition with MG132. The observed half-life of FL-WT-PINK1 is in line with other studies.[28-30]

F385S-PINK1 Disrupts Phosphorylation of Ubiquitin at Ser65

To confirm that the F385S mutation abolishes PINK1 kinase activity, we assessed a well-known substrate of PINK1 in stressed cells: phospho-ubiquitin Ser65.[8,9,11] We used HeLa cells that lack endogenous parkin,[31] which were gene edited to remove functional, endogenous PINK1.[26] The PINK1-parkin system was reconstituted in the cell culture model by cotransfection of FLAG-tagged parkin ubiquitin ligase and either WT or F385S PINK1-V5. PINK1-parkin–dependent mitophagy was induced by the addition of CCCP to the culture medium. CCCP treatment led to the stabilization of WT-PINK1, with a reduction tendency of F385S-PINK1 over a time course of 6 hours (Fig. 2A–C). FLAG-parkin levels did not alter significantly in this time frame (Fig. 2A–C).

Under basal conditions (no CCCP treatment), there was no phosphorylation of ubiquitin at S65 in F385S-PINK1–expressing cells. However, when treated with CCCP, there is some residual phosphorylation of ubiquitin at Ser65 in F385S-PINK1 cells, yet still ∼90% less phosphorylated compared with WT-PINK1–expressing cells (Fig. 2D,E).

F385S-PINK1 Affects Parkin Recruitment and Mitochondrial Fragmentation

To investigate the implications of the F385S mutation on PINK1 function, we performed mitophagy induction using CCCP as a depolarizing agent. Upon cotransfection with WT-PINK1-V5 and FLAG-parkin, a strong mitochondrial phenotype was observed after 6-hour CCCP treatment, with the matrix mitochondrial marker SSBP1 appearing in big clusters instead of localized foci (Fig. 2F). In contrast, dispersed SSBP1 foci were observed upon transfection with parkin alone, as well as in the parkin and F385S-PINK1 cotransfected cells (Fig. 2F), indicating that F385S mutant PINK1 impairs initiation of PINK1-parkin–dependent mitophagy.[19]

FIG. 2. HeLa cells expressing parkin and either wild-type (WT) or mutant (F385S) PINK1 were untreated or treated with 40 μM CCCP for 3 or 6 hours. (**A**) Western blot probed for V5-tagged PINK1 (v5) and parkin. The Western blot was stained for total protein using Ponceau stain. Full-length PINK1 is shown. A representative Western blot is shown (n = 4). (**B**, **C**) Quantified fold change of V5-tagged PINK1 (B) and parkin levels (C) after CCCP treatment compared with the untreated control. Error bars show mean ± SEM (n = 4). Statistical test: ordinary one-way ANOVA with multiple comparisons using Dunnett's multiple comparison test. (**D**) Western blot probed for phospho-ubiquitin Ser65 (pUbSer65) and loading control GAPDH. The Western blot was stained for total protein using the Ponceau stain. A representative Western blot is shown (n = 4). (**E**) Quantified fold change of pUbSer65 after CCCP treatment compared with the untreated WT control. Error bars show mean ± SEM (n = 4). Statistical test: ordinary one-way ANOVA with multiple comparisons using Dunnett's multiple comparison test. (**F**) Representative images of HeLa cells transfected with parkin (blue) only or together with WT PINK1 or F385S PINK1 (pink) upon 6 hours of CCCP treatment showing SSBP1 marker of mitochondria (yellow). Scale bar: 10 μm. (**G**, **H**) Mean mitochondrial size of SSBP1 foci after 6 hours of CCCP treatment (G); normalized count of the number of SSBP1 foci per cell (H). In both panels (G, H), each dot represents a single-cell value. (**I**) Percentage of cells with mitochondrial or cytosolic parkin after 6 hours of CCCP treatment. Error bars: mean ± SEM. NT, nontransfected (n = 3). [Color figure can be viewed at wileyonlinelibrary.com]

CellProfiler image analysis allowed for an unbiased, automated quantification.[19,32] Upon expression of WT-PINK1, there was a significant increase in the mean size of SSBP1 profiles compared with nontransfected, parkin-only, and F385S-PINK1 plus parkin transfected conditions, indicating successful mitochondrial clustering as a consequence of mitophagy initiation only in WT-PINK1 conditions (Fig. 2G). Concomitantly, SSBP1 mean foci count was significantly reduced as mitochondria coalesced into mitoaggresomes only in WT-PINK1–expressing cells, again suggesting impaired mitochondrial clustering (Fig. 2H). Because translocation of active parkin to mitochondria depends on PINK1 kinase activity, we analyzed parkin localization upon mitochondrial depolarization (Fig. 2I). Strikingly, upon coexpression of parkin and WT-PINK1, parkin was found on mitochondria in 83% of the cells, whereas only 1% of the cells showed mitochondrial parkin in F385S-PINK1 conditions (Fig. 2I). Overall, our data indicate an impaired mitophagy initiation upon expression of F385S-PINK1, confirming F385S to be a loss-of-kinase-function mutation.

Discussion

Addressing the issue of global genetic disparity in genomic research, we are developing a large PD genetic catalog for the Indian population. The identification of novel loci or novel variants in known monogenic PD genes would help to understand the molecular mechanisms. Future therapeutics targeting monogenic forms of PD might not be equally generalizable for every population.[33] Further, this would also allow the possibility of linking risk variants with environmental factors in that region because they are believed to work synergistically to modify PD risk.[34] Here, in our ongoing monogenic project, we report a novel homozygous mutation in the *PINK1* gene. Interestingly, the underlying disease inheritance highlighted a pseudodominant mode in this family, a phenomenon that has been reported previously in European and North African patients with parkinsonism.[20] Although there was no consanguinity reported at the time of sampling, analysis of ROHs predicts likely consanguinity, indicating the pseudodominant mode of inheritance. The majority of the phenotypic features in this family were similar to typical PINK1 PD, with onset in the fourth decade in two affected individuals and slightly later in the third. There was sustained levodopa responsiveness, early fluctuations and dyskinesias, and the common nonmotor symptoms reported with this mutation.[35] The atypical features were cognitive involvement and the occurrence of mild dysphagia for liquids, after a decade from the onset of the disease in this family. Cognitive impairment is considered rare in PINK1 mutation carriers but was reported in 14% of 65 PINK1 mutation carriers in a recent systematic review.[35]

Duplication or deletion of PINK1 was ruled out by sequencing and MLPA, and we designed the functional experiments accordingly by expressing F385S-PINK1 in cells lacking any functional, endogenous PINK1. PINK1/Parkin mitophagy is one of the most widely studied pathways to functionally characterize the role of both PINK1 and parkin in cell culture systems, with PD-associated mutations in PINK1 having a compromised canonical mitophagy.[36] To functionally characterize F385S-PINK1, we employed this assay and found the F385S PINK1 mutation to be detrimental to PINK1 kinase activity because there is absence of phosphorylated ubiquitin at Ser65. Consequently, parkin activation is also affected, observed by reduced parkin translocation and mitoaggresome formation in F385S-PINK1 cells, which are unable to initiate mitophagy under depolarizing conditions. F385S-PINK1 has a slightly shorter half-life than WT PINK1. Thus, the reduced kinase activity of F385S mutant PINK1 could also be attributed partially to the reduced half-life of FL-PINK1. Our quantifications of PINK1 half-life were restricted to the FL form for reliability.

In summary, we identified a novel p.F385S PINK1 mutation in an Indian family. We characterized the mutation both structurally and functionally and concluded that this mutation results in a severe loss of its kinase activity. Our work provides an understanding of pathological events that are governed by PINK1 loss-of-function mutations in PD and highlights the importance of including diversity in PD genetics. ■

Acknowledgments: We acknowledge Olmo Ruiz (Graduate Training Centre of Neuroscience, University of Tübingen) for performing site-directed mutagenesis and Jana Staib (Interfaculty Institute for Cell Biology, University of Tübingen) for helping with the plating and transfection of cells. We thank Roland L. Dunbrack (Fox Chase Cancer Center, Philadelphia, PA, USA) for assisting us with the usage of KinCore and Ann-Kathrin Hauser (Hertie Institute for Clinical Brain Research, University of Tübingen) for performing the MLPA analysis. We thank the HIH-CIN Imaging Cluster of Microscopy Core Facility of the Medical Faculty at the University of Tübingen for providing support (especially Olga Oleksiuk) and instrumentation. Open Access funding enabled and organized by Projekt DEAL.

Data Availability

The information on genetic variants from the Cataloging Genetic Architecture of PD cohort is available upon request from the corresponding author.

References

1. Valente EM, Abou-Sleiman PM, Caputo V, et al. Hereditary early-onset Parkinson's disease caused by mutations in PINK1. Science 2004; 304(5674):1158–1160. https://doi.org/10.1126/science.1096284
2. Schneider SA, Klein C. PINK1 type of young-onset Parkinson disease. In: Adam MP, Mirzaa GM, Pagon RA, eds. Seattle (WA): GeneReviews®; 1993.

3. Trempe JF, Gehring K. Structural mechanisms of mitochondrial quality control mediated by PINK1 and Parkin. J Mol Biol 2023; 435(12):168090. https://doi.org/10.1016/j.jmb.2023.168090
4. Youle RJ, Narendra DP. Mechanisms of mitophagy. Nat Rev Mol Cell Biol 2011;12(1):9–14. https://doi.org/10.1038/nrm3028
5. Gan ZY, Callegari S, Cobbold SA, et al. Activation mechanism of PINK1. Nature 2022;602(7896):328–335. https://doi.org/10.1038/s41586-021-04340-2
6. Rasool S, Veyron S, Soya N, et al. Mechanism of PINK1 activation by autophosphorylation and insights into assembly on the TOM complex. Mol Cell 2022;82(1):44. https://doi.org/10.1016/j.molcel.2021.11.012
7. Gladkova C, Maslen SL, Skehel JM, et al. Mechanism of parkin activation by PINK1. Nature 2018;559(7714):410–414. https://doi.org/10.1038/s41586-018-0224-x
8. Kane LA, Lazarou M, Fogel AI, et al. PINK1 phosphorylates ubiquitin to activate Parkin E3 ubiquitin ligase activity. J Cell Biol 2014;205(2):143–153. https://doi.org/10.1083/jcb.201402104
9. Kazlauskaite A, Kondapalli C, Gourlay R, et al. Parkin is activated by PINK1-dependent phosphorylation of ubiquitin at Ser65. Biochem J 2014;460(1):127–139. https://doi.org/10.1042/BJ20140334
10. Kondapalli C, Kazlauskaite A, Zhang N, et al. PINK1 is activated by mitochondrial membrane potential depolarization and stimulates Parkin E3 ligase activity by phosphorylating serine 65. Open Biol 2012;2(5). https://doi.org/10.1098/rsob.120080
11. Koyano F, Okatsu K, Kosako H, et al. Ubiquitin is phosphorylated by PINK1 to activate parkin. Nature 2014;510(7503):162. https://doi.org/10.1038/nature13392
12. Ordureau A, Sarraf SA, Duda DM, et al. Quantitative proteomics reveal a feedforward mechanism for mitochondrial PARKIN translocation and ubiquitin chain synthesis. Mol Cell 2014;56(3):360–375. https://doi.org/10.1016/j.molcel.2014.09.007
13. Lazarou M, Jin SM, Kane LA, et al. Role of PINK1 binding to the TOM complex and alternate intracellular membranes in recruitment and activation of the E3 ligase Parkin. Dev Cell 2012;22(2):320–333. https://doi.org/10.1016/j.devcel.2011.12.014
14. Okatsu K, Oka T, Iguchi M, et al. PINK1 autophosphorylation upon membrane potential dissipation is essential for Parkin recruitment to damaged mitochondria. Nat Commun 2012;3. https://doi.org/10.1038/ncomms2016
15. Shiba-Fukushima K, Imai Y, Yoshida S, et al. PINK1-mediated phosphorylation of the Parkin ubiquitin-like domain primes mitochondrial translocation of Parkin and regulates mitophagy. Sci Rep-UK 2012;2. https://doi.org/10.1038/srep01002
16. Wauer T, Simicek M, Schubert A, et al. Mechanism of phospho-ubiquitin-induced PARKIN activation. Nature 2015;524(7565):370. https://doi.org/10.1038/nature14879
17. Geisler S, Holmstrom KM, Skujat D, et al. PINK1/Parkin-mediated mitophagy is dependent on VDAC1 and p62/SQSTM1. Nat Cell Biol 2010;12(2):119–170. https://doi.org/10.1038/ncb2012
18. Wang X, Winter D, Ashrafi G, et al. PINK1 and Parkin target Miro for phosphorylation and degradation to arrest mitochondrial motility. Cell 2011;147(4):893–906. https://doi.org/10.1016/j.cell.2011.10.018
19. Lechado-Terradas A, Schepers S, Zittlau KI, et al. Parkin-dependent mitophagy occurs via proteasome-dependent steps sequentially targeting separate mitochondrial sub-compartments for autophagy. Autophagy Rep 2022;1(1):576–602. https://doi.org/10.1080/27694127.2022.2143214
20. Ibanez P, Lesage S, Lohmann E, et al. Mutational analysis of the PINK1 gene in early-onset parkinsonism in Europe and North Africa. Brain 2006;129(3):686–694. https://doi.org/10.1093/brain/awl005
21. Bajaj A, Senthivel V, Bhoyar R, et al. 1029 genomes of self-declared healthy individuals from India reveal prevalent and clinically relevant cardiac ion channelopathy variants. Hum Genomics 2022; 16(1):30. https://doi.org/10.1186/s40246-022-00402-2
22. Jain A, Bhoyar RC, Pandhare K, et al. IndiGenomes: a comprehensive resource of genetic variants from over 1000 Indian genomes. Nucleic Acids Res 2021;49(D1):D1225–D1232. https://doi.org/10.1093/nar/gkaa923
23. Jumper J, Evans R, Pritzel A, et al. Highly accurate protein structure prediction with AlphaFold. Nature 2021;596(7873):583–589. https://doi.org/10.1038/s41586-021-03819-2
24. Varadi M, Anyango S, Deshpande M, et al. AlphaFold protein structure database: massively expanding the structural coverage of protein-sequence space with high-accuracy models. Nucleic Acids Res 2022; 50(D1):D439–D444. https://doi.org/10.1093/nar/gkab1061
25. Kellogg EH, Leaver-Fay A, Baker D. Role of conformational sampling in computing mutation-induced changes in protein structure and stability. Proteins 2011;79(3):830–838. https://doi.org/10.1002/prot.22921
26. Wettengel J, Reautschnig P, Geisler S, et al. Harnessing human ADAR2 for RNA repair – recoding a PINK1 mutation rescues mitophagy. Nucleic Acids Res 2017;45(5):2797–2808. https://doi.org/10.1093/nar/gkw911
27. Greene AW, Grenier K, Aguileta MA, et al. Mitochondrial processing peptidase regulates PINK1 processing, import and Parkin recruitment. EMBO Rep 2012;13(4):378–385. https://doi.org/10.1038/embor.2012.14
28. Lin W, Kang UJ. Characterization of PINK1 processing, stability, and subcellular localization. J Neurochem 2008;106(1):464–474. https://doi.org/10.1111/j.1471-4159.2008.05398.x
29. Deas E, Plun-Favreau H, Gandhi S, et al. PINK1 cleavage at position A103 by the mitochondrial protease PARL. Hum Mol Genet 2011; 20(5):867–879. https://doi.org/10.1093/hmg/ddq526
30. Ando M, Fiesel FC, Hudec R, et al. The PINK1 p.I368N mutation affects protein stability and ubiquitin kinase activity. Mol Neurodegener 2017;12(1):32. https://doi.org/10.1186/s13024-017-0174-z
31. Denison SR, Wang F, Becker NA, et al. Alterations in the common fragile site gene Parkin in ovarian and other cancers. Oncogene 2003;22(51):8370–8378. https://doi.org/10.1038/sj.onc.1207072
32. Zittlau KI, Lechado-Terradas A, Nalpas N, et al. Temporal analysis of protein Ubiquitylation and phosphorylation during Parkin-dependent Mitophagy. Mol Cell Proteomics 2022;21(2):100191. https://doi.org/10.1016/j.mcpro.2021.100191
33. Blauwendraat C, Nalls MA, Singleton AB. The genetic architecture of Parkinson's disease. Lancet Neurol 2020;19(2):170–178. https://doi.org/10.1016/S1474-4422(19)30287-X
34. Perinan MT, Brolin K, Bandres-Ciga S, et al. Effect modification between genes and environment and Parkinson's disease risk. Ann Neurol 2022;92(5):715–724. https://doi.org/10.1002/ana.26467
35. Kasten M et al. Genotype-phenotype relations for the Parkinson's disease genes Parkin, PINK1, DJ1: MDSGene systematic review. Mov Disord 2018;33(5):730–741.
36. Geisler S, Holmstrom KM, Treis A, et al. The PINK1/Parkin-mediated mitophagy is compromised by PD-associated mutations. Autophagy 2010;6(7):871–878. https://doi.org/10.4161/auto.6.7.13286

Supporting Data

Additional Supporting Information may be found in the online version of this article at the publisher's web-site.

SGML and CITI Use Only
DO NOT PRINT

Author Roles

Karan Sharma: validation, formal analysis, investigation, writing—original draft, writing—review and editing, and visualization. Asha Kishore: investigation, resources, writing—review and editing, and funding acquisition. Anna Lechado-Terradas: validation, formal analysis, investigation, writing—original draft, writing—review and editing, and visualization. Raffaele Passannanti: formal analysis, investigation, and visualization. Francesco Raimondi: formal analysis, investigation, visualization, supervision, and writing—original draft. Marc Sturm: methodology, software, formal analysis, investigation, and writing—review and editing. Ashwin Ashok Kumar Sreelatha: methodology, software, formal analysis, and visualization. Divya Kalikavila Puthenveedu: resources and investigation. Gangadhara Sarma: resources and investigation. Nicolas Casadei: methodology, software, validation, formal analysis, and investigation. Rejko Krüger: resources and writing—review and editing. Thomas Gasser: resources and validation. Philipp Kahle: methodology, resources, writing—original draft, writing—review and editing, and supervision. Olaf Riess: resources and writing—review and editing. Julia C. Fitzgerald: conceptualization, methodology, investigation, formal analysis, resources, writing—original draft, writing—review and editing, and supervision. Manu Sharma: conceptualization, methodology, resources, validation, formal analysis, writing—review and editing, project administration, supervision, and funding acquisition.

Financial Disclosures

This study was supported by The Michael J. Fox Foundation, USA, GP2, and The German Research Council–Deutsche Forschungsgemeinschaft (DFG). M.S. was supported by funding from The Michael J. Fox Foundation and GP2 (Grants MJFF-11879, 17473, 009411, and 023430) and DFG (Grant SH599/16-1). P.K., J.C.F., A.L.-T., and K.S. acknowledge support from the DFG, German Research Council, Research Training Group (MOMbrane 654651/GRK2364). The authors declare that there are no conflicts of interest relevant to this work. The authors declare that there are no additional disclosures to report.

Proteome Dynamics in iPSC-Derived Human Dopaminergic Neurons

Authors

Claudia Cavarischia-Rega, Karan Sharma, Julia C. Fitzgerald, and Boris Macek

Correspondence

Julia.Fitzgerald@uni-tuebingen.de; boris.macek@uni-tuebingen.de

In Brief

Our study provides in-depth proteome analysis of iPSC-derived human dopaminergic neurons (hDaNs). We use dynamic SILAC to measure half-lives of ~4300 proteins. We apply differential SILAC labeling in microfluidic chambers to reveal axon-specific proteome and provide evidence for local protein synthesis and trafficking between axons and the soma. This dataset serves as a reference for studying axonal proteins and a resource for researchers working on protein biology of hDaNs.

Graphical Abstract

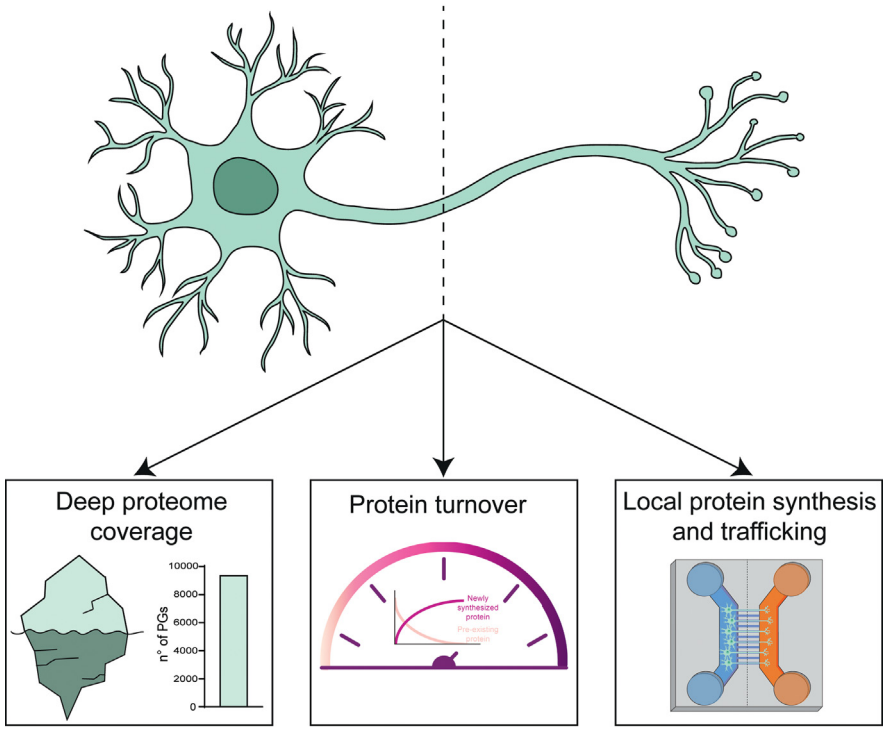

Highlights

- Deep proteome analysis of human iPSC-derived dopaminergic neurons.
- Determination of half-life of more than 4300 proteins by dynamic SILAC.
- Measurement of local protein synthesis and trafficking between axons and soma.
- Resource for future applications of quantitative proteomics in neurons.

2024, Mol Cell Proteomics *23*(*10*), 100838

https://doi.org/10.1016/j.mcpro.2024.100838

Proteome Dynamics in iPSC-Derived Human Dopaminergic Neurons

Claudia Cavarischia-Rega[1,‡], Karan Sharma[2,‡], Julia C. Fitzgerald[2,*], and Boris Macek[1,*]

Dopaminergic neurons participate in fundamental physiological processes and are the cell type primarily affected in Parkinson's disease. Their analysis is challenging due to the intricate nature of their function, involvement in diverse neurological processes, and heterogeneity and localization in deep brain regions. Consequently, most of the research on the protein dynamics of dopaminergic neurons has been performed in animal cells *ex vivo*. Here we use iPSC-derived human mid-brain–specific dopaminergic neurons to study general features of their proteome biology and provide datasets for protein turnover and dynamics, including a human axonal translatome. We cover the proteome to a depth of 9409 proteins and use dynamic SILAC to measure the half-life of more than 4300 proteins. We report uniform turnover rates of conserved cytosolic protein complexes such as the proteasome and map the variable rates of turnover of the respiratory chain complexes in these cells. We use differential dynamic SILAC labeling in combination with microfluidic devices to analyze local protein synthesis and transport between axons and soma. We report 105 potentially novel axonal markers and detect translocation of 269 proteins between axons and the soma in the time frame of our analysis (120 h). Importantly, we provide evidence for local synthesis of 154 proteins in the axon and their retrograde transport to the soma, among them several proteins involved in RNA editing such as ADAR1 and the RNA helicase DHX30, involved in the assembly of mitochondrial ribosomes. Our study provides a workflow and resource for the future applications of quantitative proteomics in iPSC-derived human neurons.

Dopaminergic neurons are a subset of neurons within the central nervous system characterized by their synthesis and release of dopamine, a pivotal neurotransmitter (1). They are predominantly localized in discrete brain regions, notably the *substantia nigra* (SN) and the ventral tegmental area (2), and they participate in fundamental physiological processes that include motor control, reward mechanisms, motivation, and mood regulation (3). The study of dopaminergic neurons poses significant challenges owing to their heterogeneity and localization in deep brain structures, impeding direct access for experimental interventions (2, 4). Dopaminergic neurons are especially relevant in the context of Parkinson's disease (PD), which is characterized by their selective loss in the SN region of the midbrain (5). Recently, extensive investigations into the proteome of this specific neuronal subtype in PD was performed using *post mortem* brain tissue from patients (6), but there are no dynamic studies of cultured human dopaminergic neurons, which are a mainstay model system.

Quantitative proteomics has long since contributed to our understanding of proteomic alterations associated with neurodegenerative disorders, including PD, Huntington's disease, Schizophrenia, and Alzheimer's disease (AD) (6–10). Several proteomics studies have scrutinized the bulk proteome and post-translational modification (PTMome) (11) of human induced pluripotent stem cell (iPSC)-derived mid-brain–specific dopaminergic neurons (hDaNs) models of familial (12–15) and sporadic PD (16). Other studies have focused on the synaptic proteome of striatal dopaminergic terminals in mice (17) and, recently, the distinct protein expression profiles in the axons and soma of dopaminergic neurons in mice (18).

Protein turnover is defined by the rates of protein synthesis and degradation, and it is previously shown to be dependent on the cell type (19). This underscores a necessity for a reference dataset that focuses on the turnover of the proteins in hDaNs. Dynamic Stable Isotope Labeling with Amino acids in Cell culture (SILAC) has emerged as a powerful tool for investigating protein turnover (20–22). Studies on protein turnover in mice (23, 24) and rats (25–27) have provided crucial insights into the cellular dynamics of dopaminergic neurons, yet further work in human cells is needed to bring forward methods and resources for translational research and preclinical studies.

Axons are elongated subcellular compartments protruding from the cell body (soma). Proper arborization of axons and synapses are essential for neuronal function. Increasing evidence suggests that early primary cilia impairments (affecting

From the [1]Quantitative Proteomics, Department of Biology, Interfaculty Institute of Cell Biology, and [2]Department of Neurodegeneration, Hertie Institute for Clinical Brain Research, University of Tübingen, Tübingen, Germany
‡These authors contributed equally to this work.
*For correspondence: Boris Macek, boris.macek@uni-tuebingen.de; Julia C. Fitzgerald, Julia.Fitzgerald@uni-tuebingen.de.

https://doi.org/10.1016/j.mcpro.2024.100838

neuronal development, axon pathfinding, and migration) contribute to PD etiology (28–30). Axons possess the machinery for protein synthesis, including mRNA, ribosomes, and other necessary factors (31–34). Regulation of the local translation of mRNAs and protein degradation enables spatial and temporal control of the axonal proteome in response to multiple stimuli (35). Local translation in axons is especially important for axonal guidance and synaptic plasticity, due to the considerable distance from the soma, the primary site for protein synthesis in neurons (36). Recent work has also highlighted the importance of local translation in axons to support mitophagy (37), a form of mitochondrial quality control associated with aging and PD (38–40). The study of local protein synthesis using pulsed SILAC in primary neurons derived from *Xenopus* embryos has shown that different guidance cues can induce rapid synthesis of new proteins in the axons within minutes (41). Microfluidic devices have been used to study axonal injury and regeneration, where the authors also demonstrated their utility in providing fluidic isolation between the wells (42). These devices have also been used for targeted studies, for example, to investigate the effect of a mutation in the neurofilament light gene in human iPSC-derived motor neurons (43) or to study the replication of mitochondrial DNA in the axons, operating independently of the soma in primary neurons from mice (44). Furthermore, there is a large body of work demonstrating retrograde transport of murine proteins (Importin β1, Stat3, mTOR, CREB, and ATF4) synthesized in axons in response to injury stimuli (45–49).

In this study, we employ a workflow based on mass spectrometry and stable isotope labeling of neurons, in combination with cell culture in microfluidic devices, to uncover protein composition, turnover dynamics, and spatial regulation of proteins in untreated human iPSC-derived hDaNs from a healthy donor. We cover approximately 9400 proteins and use dynamic SILAC to measure the half-life of more than 4300 proteins. We employ differential dynamic SILAC labeling in combination with microfluidic devices to analyze local protein synthesis and transport between axons and soma. We report novel axonal markers and detect translocation of proteins between axons and the soma. Importantly, we provide evidence for local synthesis of over 150 proteins in the axon and their retrograde transport to the soma.

EXPERIMENTAL PROCEDURES

Experimental Design and Statistical Rationale

All experiments were performed in biological triplicates, all of which presented independent differentiations of iPSC-derived hDaNs. For the turnover dataset, only proteins with detectable label incorporation in at least four out of five times points in at least two out of three replicates were taken into consideration. For the data from microfluidic devices, only proteins with label incorporation in two out of three replicates were taken into consideration. These filtering criteria were chosen as a compromise between statistical stringency and number of data points that remain after filtering. Statistical analysis was performed with two-tailed unpaired *t* test in GraphPad Prism. Significance is indicated by asterisks: $*p \leq 0.05$, $**p \leq 0.01$, $***p < 0.001$. For the pathway enrichment analysis, a Fisher exact test with a false discovery rate (FDR) < 0.05 was performed.

Generation of neural progenitor cells and Differentiation to hDaNs

Human Dopaminergic Neuron Differentiation—An iPSC line derived from a healthy female donor was previously generated and characterized by Schwarz, et.al., 2021 (50). Briefly, iPSCs were used to generate human dopaminergic neurons (hDaNs) *via* neural progenitor cell intermediates using chemical induction as described in Schwarz, *et. al*., 2022 (51) and based on a protocol described by Reinhardt, *et. al*., 2013 (52) with slight modification (13). Experiments were performed at day 18 (mature hDaNs) and the cells were harvested at day 23 for proteomic analysis.

Characterization of hDaNs—The efficiency of differentiation was validated with immunofluorescence data (Supplemental Fig. S5, *A* and *B*) and analysis of the proteomic dataset for dopaminergic markers compared with markers of mature neurons and their subtypes (TH for dopaminergic neurons, TPH for serotonergic neurons, GAD1 for GABAergic neurons, and ChAT for cholinergic neurons) (Supplemental Fig. S5*C*). These data are in line with previous, published characterization of mid-brain–specific dopaminergic neurons differentiated *via* neuronal progenitors using the same protocol and same cells (13, 52).

Culturing hDaNs in Microfluidic Devices—On day 9 post-differentiation start, cells were dissociated using Accumax, Cell Dissociation Solution (#P10-21200, PAN-Biotech) and plated onto XonaChips XC900 (# XC900, Xona Microfluidics) at a density of 70,000 cells per chamber in the proximal or somatodendritic well (140,000 cells in total), according to the manufacturer's protocol. hDaN differentiation was then induced and specific experiments were performed after maturation at day 18 post-differentiation start and harvested at the day 23 post-differentiation.

Imaging

Eighteen days prior to imaging, 140,000 differentiating hDaNs (day 9 post differentiation start) were seeded on Matrigel-coated Xona XC900 Microfluidic chip. For labeling of mitochondria and neutral lipids, hDaNs (day 27 post differentiation start) were stained continuously at 37 °C with 5% CO2 with 100 nM MitoTracker deep red (#M22426, Thermo Fisher Scientific) and 4.77 μM Bodipy (#790389-500 MG, Sigma), respectively. For imaging, the medium was not replaced and a Leica DMi8 Microscope (4 × and 10× objective) with the LASX software was used.

For imaging on microscopy slides, ~30,000 differentiating hDaNs (day 15 post differentiation start) were seeded on matrigel-coated coverslips. On day 18, the cells were fixed using 4% paraformaldehyde solution for 15 min at room temperature. Post fixation, the cells were permeabilized and blocked using a 1% bovine serum albumin (BSA) + 0.3% Triton X-100 solution in PBS for 1 h. The primary antibodies STMN2 (mouse, #sc-135620, SantaCruz), DHX30 (rabbit, ab254660, Abcam), and GAP43 (rabbit, #NB300-143SS, Novus) were added at 1:500 dilution in 1% BSA + 0.1% Triton X-100 solution in PBS overnight at room temperature. The following day, secondary antibodies goat anti-mouse 488 and goat anti-rabbit 488 were added at 1:500 in 1% BSA + 0.1% Triton X-100 solution in PBS for 1 h at room temperature protected from direct light. The cells were washed with PBS three times and incubated with Hoechst stain (#H3569, Molecular Devices) at 1:5000 in PBS for 5 min. The cells were then washed with PBS and mounted with Dako fluorescent mounting medium (#S3023, Agilent) and placed onto microscopy slides, sealed with nail polish, and stored at 4 °C prior to imaging. For

imaging, Zeiss Imager.Z1 equipped with an ApoTome.2 and an AxioCam MRm was used and the images were captured using the 40× and 63× objective. ImageJ2 (Fiji) was used for processing the images.

For fixed cells imaging on microfluidic devices, the same fixation, permeabilization, blocking, and antibody addition protocol was followed as described above. Tyrosine hydroxylase antibody (mouse, #sc-25269, Santa Cruz) was used at 1:500 dilution. The secondary antibodies goat anti-mouse 488 was used at 1:500 dilution. Following antibodies staining, Hoechst stain was added followed by a PBS wash and Dako fluorescent mounting medium was added to the top wells as advised by Xona microfluidic manual for immunofluorescence staining. The images were captured using Leica DMi8 Microscope (4× and 10× objective). The images were processed using ImageJ2 (Fiji).

Treatments

Dulbecco's modified Eagle's medium (DMEM)-SILAC (Sigma-Aldrich) lacking arginine and lysine supplemented with penicillin/streptomycin (100 U/ml, PAN) and stable isotope-encoded arginine and lysine was added to the cells. The 'light' SILAC media was supplemented with L-[$^{12}C_6$,$^{14}N_2$] lysine (Lys0) and L-[$^{12}C_6$,$^{14}N_4$] arginine (Arg0) (Cambridge Isotope Laboratories), whereas L-[$^{2}H_4$] lysine (Lys4) and L-[$^{13}C_6$] arginine (Arg6) were added to the 'medium-heavy' SILAC media and L-[$^{13}C_6$,$^{15}N_2$] lysine (Lys8) and L-[$^{13}C_6$,$^{15}N_4$] arginine (Arg10) to 'heavy' SILAC media.

For the turnover dataset, hDaNs (on day 18) were cultured in DMEM-SILAC heavy/medium-heavy media for 0, 6, 12, 48, 72, and 120 h and were all harvested on day 23. For the 120 h timepoint, hDaNs were cultured in SILAC medium on day 18, while for the 72 h timepoint, hDaNs were cultured in SILAC media on day 20 and similar for the other timepoints. This was done so that the cells were harvested on day 23, all at the same time and to avoid differences that could arise due to the cell's maturation state.

For the experiments in microfluidic devices, after axons protruded through the microgroove barriers, DMEM-SILAC "medium-heavy" medium was added in the somatodendritic enriched well and DMEM-SILAC "heavy" was added in the axonal well for 12, 48, 72, and 120 h. At the somatodendritic (proximal) well, 150 µl media was added, while at the axonal (distal) well, 120 µl media was added to create hydrostatic pressure and ensure fluidic isolation between the two wells. The cells were harvested on day 23 for all timepoints.

To prevent protein translation, 100 µM cycloheximide (CHX) solution (#239765, Calbiochem) was used (33) and added to the somatodendritic well and/or to the axonal side.

Sample Preparation for Mass Spectrometry Analysis

Cell Lysis—For data-independent acquisition (DIA) and turnover dataset, cells pellets were lysed with urea lysis buffer (6 M urea, 2 M thiourea, 60 mM Tris pH 8.0) and kept on ice for 20 min. DNA and RNA were removed from the cell lysate using benzonase (1 U/ml, Merck Millipore) for 10 min at room temperature (RT) and samples centrifuged for 10 min at 13,000 rpm and 4 °C.

Protein quantification was performed with Bradford reagent, using a standard curve with known concentrations of BSA, and the absorbance was measured at 595 nm.

Extraction from Microfluidic Devices—The cells were washed with PBS (#D8537, Sigma-Aldrich) followed by the addition of 30 µl of urea lysis buffer (6 M urea, 2 M thiourea, 60 mM Tris pH 8.0) into each well. A 10 µl pipette tip was used to scrape the surface of the device and the lysates were collected and stored at −80 °C until further analysis.

Protein In-Solution Digestion—Proteins were reduced with 10 mM of DTT for 1 hour, alkylated with 55 mM iodoacetamide for 1 hour, and digested with Lys-C (Lysyl Endopeptidase, Wako Chemicals) for 3 hours at RT. Afterwards, four volumes of 10 mM ammonium bicarbonate were added and proteins were digested with trypsin (Promega Corporation) overnight. To stop the digestion, 1% TFA was added.

High pH Reverse-Phase Chromatography—For the DIA and turnover datasets, samples were fractionated with the Pierce High pH Reversed-Phase Peptide Fractionation Kit (Thermo Fisher Scientific, Kit #84868). First, the samples were purified by solid phase extraction on Sep-Pak C18 cartridges (Waters). Hundred micrograms of peptides were loaded in the conditioned spin columns and separated into nine fractions according to the hydrophobicity. Elution was done with a steep gradient of acetonitrile and ammonia (5%-50% acetonitrile in 10 mM NH_4OH). Finally, fractions were acidified to pH to <2.7 with TFA, dried by vacuum centrifugation, and purified on C18 StageTips prior LC-MS/MS measurements.

LC–MS Measurement

Peptide samples were measured on an Exploris 480 mass spectrometer (Thermo Fisher Scientific) online-coupled to an Easy-nLC 1200 UHPLC (Thermo Fisher Scientific). Peptides were separated using a 20-cm-long, 75-µm-inner diameter analytical HPLC column (ID PicoTip fused silica emitter; New Objective) packed in-house with ReproSil-Pur C18-AQ 1.9-µm silica beads (Dr Maisch GmbH).

For DIA analysis, samples were measured using 90 min LC gradient which was optimized for each HpH fraction. The full scan range was set to 400 to 1000 m/z at a resolution of 120k. Fragment ions were analyzed in 40 DIA windows, with an isolation window of 15 Th (1 Th overlap), at a resolution of 30,000.

In the turnover experiment, samples were measured using 90 min gradient optimized for each HpH fraction. Automatic gain control was set to "standard" and the mass spectrometer was operated in the positive ion mode. Full MS scans were acquired in a range of 300 to 1750 m/z at resolution of 60,000. Twenty most intense multiply charged ions were selected for HCD fragmentation with a dynamic exclusion period of 30 s and tandem MS (MS/MS) spectra were acquired at resolution of 30.000.

For all measurements of samples from microfluidic devices, peptides were eluted using a 60-min segmented gradient from to 10-33 to 50 to 90% of solvents A (0.1% formic acid) and B (80% acetonitrile in 0.1% formic acid) at a constant flow rate of 200 nl/min. The mass spectrometer was operated in the positive ion mode. Full MS scans were acquired in a range of 300 to 1750 m/z at resolution of 120,000. 20 most intense multiple-charged ions were selected for HCD fragmentation with a dynamic exclusion period of 30 s and MS/MS spectra were acquired at resolution of 15,000. Automatic gain control set to "custom".

The column temperature was maintained at 40 °C using an integrated Sonation column oven. Peptides were ionized using nanospray ionization; the source temperature was set to 275 °C.

MS Data Processing

The LC-MS/MS acquired DDA raw data was processed using the MaxQuant software package (version 2.2.0.0.). Spectra were searched against Uniprot *Homo sapiens* database (103,830 entries, downloaded 2022/12/16) and 286 commonly observed laboratory contaminants. The SILAC labels were defined as follows: Lys0 and Arg0 as the "light," Lys4 and Arg6 as the "medium-heavy," and Lys8 and Arg10 as the "heavy" channel. Carbamidomethylation on cysteine was set as a fixed modification, while N-terminal acetylation and methionine oxidation were selected as variable modifications. For MS and MS/MS, the peptide mass tolerance was set at 4.5 ppm and 20 ppm, respectively. Only two missed cleavages were allowed for the tryptic digestion. FDR was set to 1% at both peptide and protein level. Intensity-based absolute quantification (iBAQ) was enabled. For the turnover dataset, the "requantification" option was enabled.

For the DIA dataset, the MaxDIA version 2.4.2.0. was used in discovery mode, and the default parameters were used unless otherwise stated. Label-free quantification was enabled. In silico–predicted library for all human peptides with up to one missed cleavage was downloaded on 30.05.2023 from http://annotations.perseus-framework.org. The spectral libraries of peptides were uploaded to the MaxQuant software in the form of 'evidence' and 'msms' files. Carbamidomethylation on cysteine was set as a fixed modification, while N-terminal acetylation and methionine oxidation were selected as variable modifications. For MS and MS/MS, the peptide mass tolerance was set at 4.5 ppm and 20 ppm, respectively. Only two missed cleavages were allowed for the tryptic digestion. FDR was set to 1% at both peptide and protein level. Label-free quantification and iBAQ were enabled.

MS Data Analysis and Statistical Analysis

Downstream analysis of the 'proteinGroups.txt' output table was performed in Perseus (version 1.6.15.0). Contaminants, "reversed" protein hits and proteins only identified by one site were filtered out. Proteins were functionally annotated with Gene Ontology (GO) Biological Processes, GO Cellular Compartment, GO Molecular Functions, and Kyoto Encyclopedia of Genes and Genomes, as well as MitoCarta3.0.

The fisher exact test (FDR ≤0.5) was used to assess the over-represented categories. It was performed with the PANTHER Classification System software (Version 18.0 released 2023-08-01), available online at https://www.pantherdb.org (53).

For the turnover experiment, normalized protein H/L ratios from proteinGroups.txt were used for protein quantification. Only proteins with ratios in four out of five time points in two out of three replicates were considered.

Label incorporation was calculated with the following formula:

$$\frac{\textit{Heavy label intensity}}{\sum \textit{label intensity}} \textit{ or } \frac{\textit{Medium label intensity}}{\sum \textit{label intensity}} \quad (1)$$

Protein turnover rate (k) was determined using a described formula (54) independent of the growth rate (Equation 2), by linear regression of the natural logarithm of protein SILAC H/L ratio over time, where m is the number of time points (ti) and rti is protein H/L ratio measured in a time point ti. To determine the half-life of a protein ($T1/2$), the turnover rate k was divided by the natural logarithm (Equation 3).

$$k = \frac{\sum_{i=1}^{m} \log_e(r_{t_i} + 1)t_i}{\sum_{i=1}^{m} t_i^2} \quad (2)$$

$$T_{1/2} = \frac{2}{k} \quad (3)$$

Protein turnover rates are reported in the Supplemental Table S2.

For the microfluidic experiment, label incorporation was calculated following Equation 1 from the intensities found in proteinGroups.txt.

For generation of Venn diagrams, the online tool https://www.stefanjol.nl/venny and https://bioinfogp.cnb.csic.es/tools/venny/index.html were used. Box plot analysis of label incorporation was prepared in the online tool: http://shiny.chemgrid.org/boxplotr/. Additional graphical visualization was performed in the R environment (version 4.1.1) and in GraphPad (version 8.0.1.). Statistical analysis was performed with two-tailed unpaired t test in GraphPad Prism. Significance is indicated by asterisks: $^{*}p \leq 0.05$, $^{**}p \leq 0.01$, $^{***}p < 0.001$.

RESULTS

To perform a comprehensive analysis of proteome dynamics of hDaNs, we used three distinct workflows (Fig. 1). In order to maximize the proteome coverage, we first performed in-depth identification of proteins in hDaN cultures by high-pH fractionation followed by MS measurement using DIA. We next focused on the investigation of protein turnover using dynamic SILAC labeling of hDaNs under standard cell culture conditions. Finally, we analyzed differential expression, local synthesis, and trafficking of proteins between the axon and the soma by combining dynamic SILAC with culturing of neurons in microfluidic devices that featured physical separation of axons and soma. The hDaNs were differentiated from healthy human iPSCs using a previously described protocol (52) and characterization (13, 50–52, 55). Characterization of the markers of mature neuronal subtypes by microscopy (Supplemental Fig. S5, *A* and *B*) and mass spectrometry (Supplemental Fig. S5*C*) confirmed the dopaminergic lineage.

The Proteome of iPSC-Derived hDaNs to a Depth of 9409 Proteins

Healthy hDaNs were bulk-harvested at day 23 from three independent hDaN differentiations. After trypsin digestion, peptides were fractionated using high pH reversed-phase chromatography and measured by DIA on an Orbitrap Exploris 480 instrument. This resulted in the identification of 9409 protein groups. Based on the coverage of annotated mitochondrial proteins (913 or 80.6%) and mitochondrial outer membrane proteins (91 or 81.3%), we estimate similar coverage of the cellular proteome (Supplemental Fig. S1, *A* and *B* and Supplemental Table S1-1). Identified proteins were stratified according to their intensity into five bins (Supplemental Fig. S1*C*); the Fisher exact test (FDR< 0.05) was performed to determine which molecular pathways, according to Panther (53, 56), were enriched in each intensity bin (Supplemental Fig. S1*D* and Supplemental Table S1-2). Within the bin with the highest DIA intensity, we detected a significant over-representation of proteins involved in Huntington's disease, Parkinson's disease, and Cytoskeletal regulation by Rho GTPase and glycolysis. They were followed by proteins from central metabolic pathways such as TCA cycle, pyruvate metabolism, pentose phosphate pathway, and glycolysis in the bin with the second-highest DIA intensity. Interestingly, physiological processes of dopaminergic neurons including those related to PD such as the ubiquitin-proteasome pathway, synaptic vesicle trafficking, Hedgehog signaling, dopamine receptor signaling, and axon guidance were also enriched in this bin (Supplemental Fig. S1*D*).

Dynamic SILAC Enables Measurement of Protein Turnover for over 4300 Proteins

In order to generate a reference protein turnover dataset, we pulsed differentiated dopaminergic neurons with "heavy"

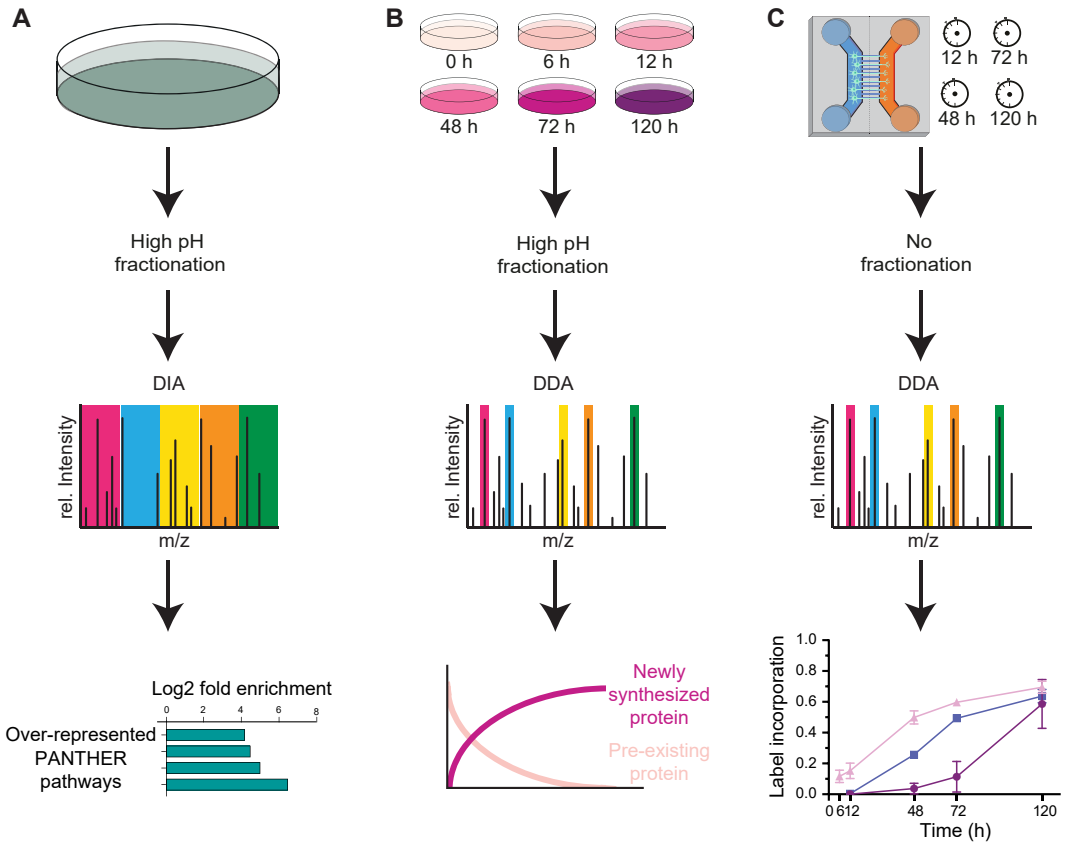

FIG. 1. **Schematic representation of the methodologies employed for protein detection in hDANs.** The workflows delineate distinct procedures for protein quantification, turnover analysis, and investigation of local protein synthesis and trafficking. *A*, depiction of the first method, used to get a comprehensive coverage of the proteome of healthy hDaN cultures (day 23). *B*, schematic illustration showing an investigation of protein turnover dynamics using SILAC. Following cell differentiation and maturation (day 18), the culture medium is replaced with DMEM containing heavy (H) amino acids for varying durations (0 h, 6 h, 12 h, 48 h, 72 h, or 120 h) prior to protein harvesting at day 23 (n = 3 for each time point). *C*, schematic illustration of the dynamic SILAC approach applied to study local synthesis and trafficking of proteins in dopaminergic neurons. Following cell differentiation, cells are seeded in microfluidic devices, allowing axonal growth for 10 days. Subsequently, the culture medium is changed, with the soma well receiving DMEM containing medium-heavy (M) amino acids and the axonal well DMEM with heavy (H) amino acids for varying durations (12 h, 48 h, 72 h, or 120 h) prior to LC-MS analysis (n = 3 for each time point).

stable isotope-labeled Arg and Lys amino acids and harvested the cells after five time points (6, 12, 48, 72, and 120 h). Following high-pH reversed-phase fractionation and MS measurement, about 6000 protein groups were quantified in each time point (Supplemental Table S2-1). The average label incorporation after 120 h was approximately 50% (Fig. 2*A* and Supplemental Table S2-2). We next used the previously described approach to calculate protein half-lives (54), taking into consideration only proteins with detectable label incorporation in at least four out of five time points in at least two out of three replicates. This led to determination of the protein half-life for 4397 proteins (Supplemental Table S2-3), out of which 554 were annotated as mitochondrial and 59 as mitochondrial outer membrane proteins. The measured half-lives ranged from 1 day to more than 20 days (Supplemental Fig. S2*B*), with a median of 97 h (Fig. 2*C*).

We then examined the relationship between protein half-life and its cellular location and/or function. As depicted in Figure 2*B*, most proteins exhibited a diverse range of half-lives that were not significantly different from the population average. However, in agreement with previous reports, both mitochondrial and ribosomal proteins deviated from the population average and exhibited significantly longer half-lives than other groups. Synaptic proteins, on the other hand, had significantly shorter half-lives than the median of all proteins. We next stratified proteins according to their half-life into seven bins (Supplemental Fig. S2*C*), subjected each bin to a Fisher's exact test (FDR< 0.05), and generated over-represented pathways according to the Panther database (Supplemental Fig. S2*D* and Supplemental Table S2-4). Among the most short-lived proteins (less than 3 days), synaptic vesicle trafficking, Wnt signaling, and Alzheimer's disease-amyloid and -presenilin pathways were over-represented. Multiple signaling pathways, such as purine synthesis, pyruvate metabolism, TCA cycle, cholesterol metabolism, and glycolysis, were highly enriched in a group

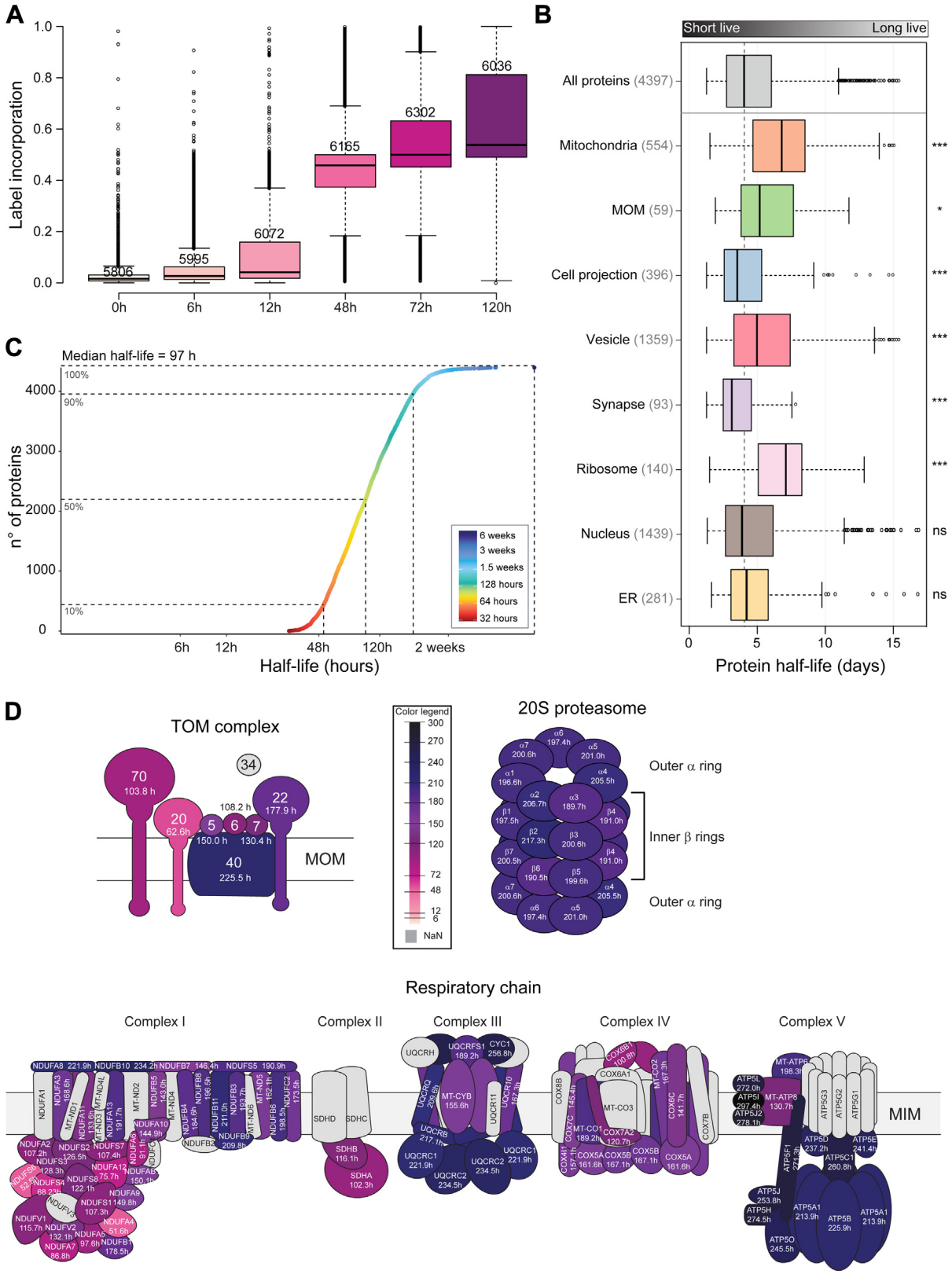

FIG. 2. **Protein turnover of hDANs.** *A*, SILAC label incorporation across all time points calculated as H/(L + H). Only proteins with ratio in two out of three replicates were considered. Number of proteins depicted are n = 5806, 5995, 6072, 6165, 6302, 6036 for their corresponding time points. *B*, distribution of total proteins with measured half-lives (4397) organized in eight different cellular compartments according to their

with longer half-lives (between seven and 11 days). Among the proteins with average half-lives (between 3 and 7 days), dopamine receptor-mediated pathways, DNA replication, hormone signaling, and PDGF signaling were enriched (Supplemental Fig. S2*D*). We next focused on protein complexes and pathways. Whereas conserved complexes and protein classes, such as the proteasome subunits, E3-ligases, and Rab proteins, had relatively uniform half-lives, we observed several interesting outliers. In agreement with previous reports, the components TOM20 and TOM70 of the TOM complex had shorter half-lives than other TOM components (Fig. 2*D* and Supplemental Fig. S3*A*). Interestingly, the peptidyl-prolyl cis-trans isomerase FKBP8, a putative chaperone that plays a role in mitophagy and apoptosis, had a significantly shorter half-life than other members of these pathways, making it an interesting subject for further investigations (Supplemental Fig. S3*C*). Also interesting were the proteins from the cytosolic (80S) ribosome, which had significantly different half-lives between large and small ribosomal subunit (Supplemental Fig. S3, *A* and *B*). This was not the case for the proteins of the mitochondrial (70S) ribosome, which overall had shorter and more uniform half-lives than the 80S-proteins (Supplemental Fig. S3, *A* and *B*). We then investigated the turnover rates of respiratory chain complexes due to their association with mitochondrial dysfunction in Parkinson's disease. There is a large range of turnover across complexes and subunits, especially within complex I (Fig. 2*D*), which contains the most subunits (44 in total, including seven encoded by the mitochondrial DNA). Complex V is a large complex and contains subunits that have the longest half-lives (notably, none of the alpha subunits of complex V were detected), while the peripheral arm of complex I has the shortest half-lives (Fig. 2*D*). We compared the respiratory complex turnover rates from dopaminergic neurons used in this study (post-mitotic), with published data from cancer cells, which are proliferative (57), and found that overall respiratory chain complex turnover is slower in dopaminergic neurons than cancer cells (Supplemental Table S2-6). Interestingly, slower turnover of respiratory complex subunits in dopaminergic neurons as compared to cancer cells was not observed for those subunits encoded by the mitochondrial genome (Supplemental Table S2-6).

Microfluidic Devices Enable Differential Analysis of Somatodendritic and Axonal Proteins

In order to study proteome dynamics in axons, we used two-well microfluidic devices (Xona Microfluidics), which feature fluidic isolation between the wells. In such devices, differentiating neurons seeded in one well (termed proximal or somatodendritic well) elongate their axons across the 900 μm-long microgroove barrier into the adjacent well (termed distal or axonal well). This allows for a spatial differential analysis of the somatodendritic and axonal proteome and selective usage of the SILAC label in the somatodendritic or in the axonal well.

To validate the absence of fluidic diffusion between the wells, we first seeded neurons (day 9 post-differentiation start) in the proximal well, and 24 h after seeding, added the heavy SILAC medium into the empty distal well. This timeframe was long enough to allow cell attachment but too short for axons to protrude through the microgroove barrier (Supplemental Fig. S4*A*). After 48 h of SILAC incubation, only 0.02% of the proteins in the proximal well were detected with the heavy label, which was below the FDR threshold of 1%. As a negative control, we also searched the database for medium-heavy labeled proteins, which were not present in the sample. As expected, the number of identified medium-heavy labeled proteins was below the 1% FDR threshold (Fig. 3, *A–C*), validating the dataset. This experiment confirmed the absence of detectable fluidic diffusion of heavy amino acids between the wells. We also performed live imaging of the microfluidic devices over a 24 h period where we followed mitochondria stained in the axonal side only by using MitoTracker deep red and neutral lipids stained in the soma side only by using BODIPY-green (Supplemental Fig. S5, *D–F*). This experiment confirmed only intracellular transport of stained mitochondria or lipids at the microgroove barrier.

To independently investigate the proteome dynamics of somatodendritic and axonal proteins, we seeded the differentiating hDaNs into the proximal (somatodendritic) well and allowed for axonal elongation across the microgroove barrier into the distal (axonal) well (Supplemental Fig. S4*B*). After 10 days, we added different SILAC amino acids into each well: medium-heavy (Lys4/Arg6) in the somatodendritic well and heavy (Lys8/Arg10) in the axonal well (Fig. 3*D*). The employed combination of labeled amino acids allowed us to determine the origin of each detected protein and therefore address local protein synthesis and transport between axons and the soma. Samples from both wells were harvested at 12, 48, 72, and 120 h after SILAC labeling and measured separately by LC-MS. This led to quantification of up to 3400 protein groups in the somatodendritic well and about 500 proteins in the axonal well across all timepoints (Fig. 3, *E* and *F* and Supplemental Table S3-1).

GOCC annotation. Number of protein groups assigned to each compartment is given in brackets. Significant $^{*}p \leq 0.05$, $^{**}p \leq 0.01$, and $^{***}p \leq 0.001$, *t* test. For the boxplots, center lines show the medians; box limits indicate the 25th and 75th percentiles as determined by R software; whiskers extend 1.5 times the interquartile range from the 25th and 75th percentiles, outliers are represented by dots. *C*, range of $\log_2$ scale half-lives of hDANs proteins, with a median of 97 h. *D*, schematic illustration of the TOM complex (*upper left* panel), the 20S proteasome (*upper right* panel), and the respiratory chain (*lower* panel) showing half-lives for individual components of each complex. Proteins are color coded as a gradient from *light pink* (shortest half-life) to *dark blue-black* (longest half-life).

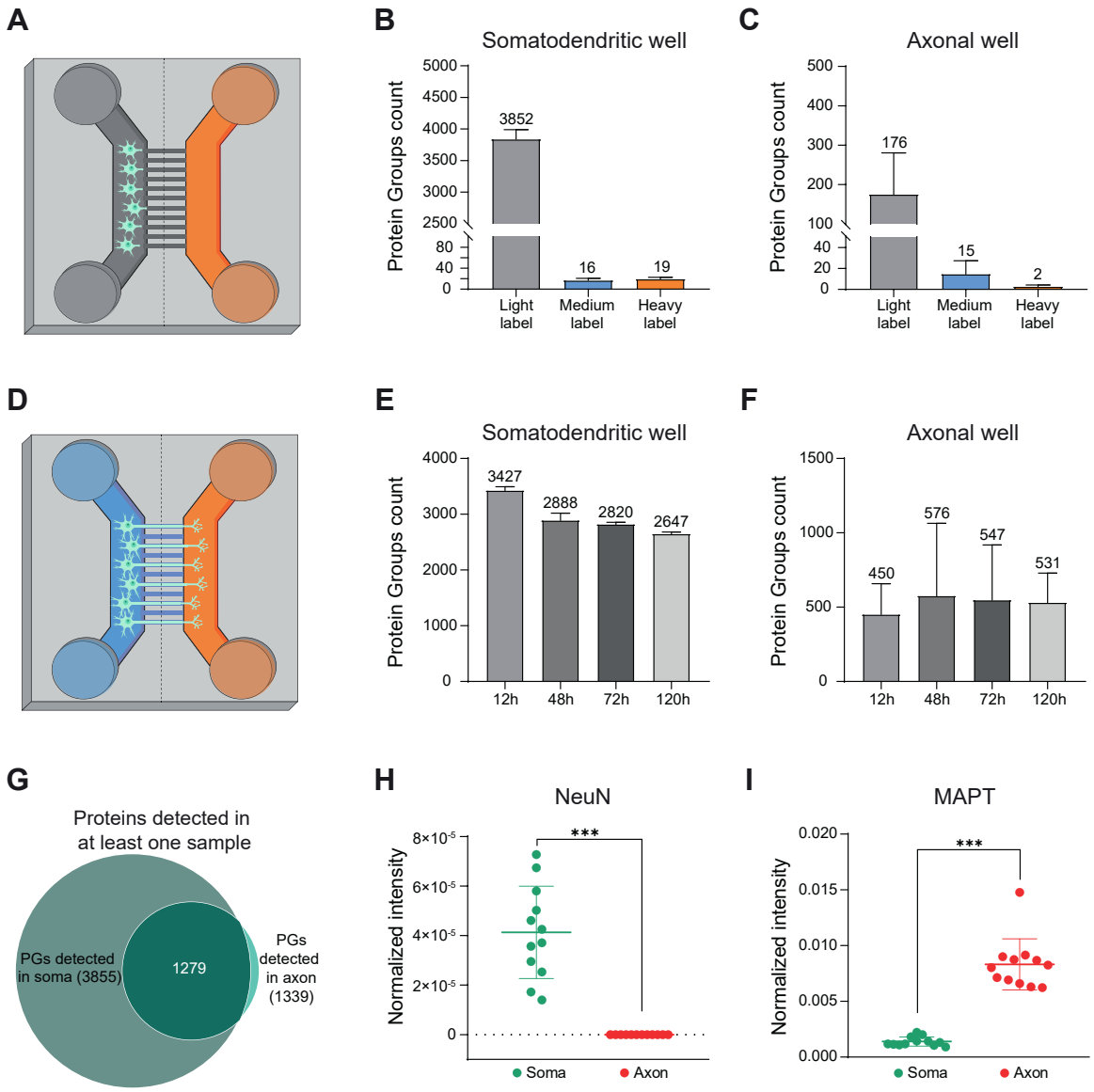

FIG. 3. **Qualitative proteome analysis of hDANs cultured in microfluidic devices.** *A*, schematic illustration of the experimental set up of diffusion experiment. hDANs were seeded in the proximal well (*gray* color) and heavy SILAC medium was added into the empty distal well (*orange* color) after 24 h. *B*, number of PGs with each label identified in the soma sample in diffusion experiment after incubation for 48 h. *C*, number of PGs identified with each label in the axon sample in diffusion experiment after incubation for 48 h. *D*, schematic illustration of the experimental set up and identifications in time course experiment. hDaNs were seeded into the somatodendritic well (*blue* color) and allowed for axonal elongation into the axonal well (*orange*). After 10 days, the medium-heavy and heavy label were added into the somatodendritic well and the axonal well, respectively. *E*, number of PGs identified in each time point in the somatodendritic well. *F*, number of PGs identified in each time point in the axonal well. All the bar graphs represent mean with error bars (SEM) from three biological replicates. *G*, Venn diagram of identified PGs in at least one sample in the soma side (3855 in total) and in the axon side (1339 in total). *H*, normalized intensity of NeuN, a known soma marker, from all time points and replicates from somatodendritic well (*green*) and the axonal well (*red*) are shown. *I*, normalized intensity of MAPT, a known axonal marker, from all times points and replicates from somatodendritic well (*green*) and the axonal well (*red*) are shown. ***$p \leq 0.001$, *t* test. PG, protein group.

We next assessed the overlap of proteins identified in the somatodendritic and axonal well. Of a total of 3915 proteins, 1279 were detected in both wells, with 60 exclusively detected in the axonal well and 2576 in the somatodendritic well (Fig. 3*G*). Principal component analysis performed between the somatodendritic and axonal proteins revealed two separate, nonintersecting clusters (Supplemental Fig. S4*C*). To assess the purity of each well, we compared normalized intensities of several marker proteins. Neuronal nuclear protein NeuN, present exclusively in the nucleus (soma), was

significantly enriched in samples from the somatodendritic well (Fig. 3*H* and Supplemental Table S3-3), whereas proteins MAPT and MAP1B, known structural and axonal markers, were enriched in samples from the axonal well (Fig. 3*I* and Supplemental Fig. S4*D* and Supplemental Table S3-3).

We further investigated the 60 proteins exclusively detected in the axonal well, as well as those with four-fold higher relative abundance in the axonal well than the somatodendritic well (total of 67 proteins) (Supplemental Fig. S4*E*). This combined dataset of 127 proteins included 22 proteins classified as axonal according to GO, among which were the known axonal markers MAPT and MAP1B. The remaining 105 proteins have a likely axonal localization but have not yet been annotated as axonal proteins (Supplemental Fig. S4*F* and Supplemental Table S3-4). We validated the axonal location of two of these proteins using immunofluorescence microscopy, namely GAP43 and STMN2 which had a high fluorescence intensity in the axons (Supplemental Fig. S5, *G* and *H*). We next subjected the list of proteins exclusively detected in the axonal well and those enriched in axons to a Fisher exact test (FDR< 0.05). Cell-cell contact zones, synaptic vesicle membrane, synaptic vesicle, SNARE complex, and exocytic vesicles were highly enriched among other Panther terms, further pointing to axonal specificity (Supplemental Fig. S5*G* and Supplemental Table S3-5).

Differential SILAC Labeling Reveals Local Protein Synthesis and Transport Between the Soma and Axons

We next analyzed the SILAC label incorporation in each well. Incorporation of the medium-heavy SILAC label in proteins detected in the somatodendritic well (Fig. 4*A* and Supplemental Table S3-2) followed a pattern very similar to that of whole neurons (Fig. 2*A*). This was expected, as the cells in this well are very similar to the neuronal cell (not all axons generated by the neurons in the somatodendritic well cross the microgroove barrier). Importantly, 141 proteins detected in the axonal well contained the medium-heavy SILAC label, pointing to their synthesis in the soma and anterograde transport into the axons. Conversely, 154 proteins detected in the somatodendritic well contained the heavy SILAC label, pointing to their synthesis in the axon and retrograde transport into the soma. Of note, 107 out of these 154 proteins were also detected in the unlabeled axonal proteome (Fig. 3*G*). In total, differential SILAC labeling revealed 269 proteins that were trafficking between the soma and the axon during the time window of our analysis (26 of them in both directions).

To validate local protein synthesis, we inhibited translation by adding CHX together with the SILAC labels for 72 h in each well separately. As expected, the CHX treatment in the somatodendritic well almost completely abolished incorporation of the medium-heavy SILAC label, pointing to a block in protein synthesis. Interestingly, CHX treatment in the somatodendritic well also decreased incorporation of the heavy SILAC label in the axonal well. CHX treatment in the axonal well did not lead to any detectable effect, likely due to the low amount of proteins detected in the axonal well (Fig. 4*B*, Supplemental Tables S3-7, and S3-8). Combined, these results confirmed that dynamic SILAC applied to microfluidic devices can measure protein synthesis independently in the soma and the axon.

We next focused on the protein transport between the soma and the axon. To this end, we analyzed temporal SILAC incorporation profiles of proteins known to be trafficking between the two cellular components. We focused on the Kinesin Family Member 5C (KIF5C), a motor protein essential for intracellular transport, primarily involved in anterograde transport, moving cargo from the neuron cell body (soma) towards the synaptic terminals in the axon (58). In our dataset, KIF5C was labeled with medium-heavy SILAC and detected both in the soma sample and in the axonal well (Fig. 5*A*). Importantly, the patterns of the SILAC label incorporation were markedly different in the soma and in the axon: the pattern in the soma was similar to that measured in the whole neuronal cell, where 50% of the protein was labeled after 72 h. However, in the axon, only 10% of the protein was labeled in that time frame. Interestingly, after 120 h, the label incorporation was identical in both soma and axon, pointing to the time frame needed for the pool of newly synthesized KIF5C molecules to equilibrate within the cell. Upon CHX treatment in the soma, the protein was no longer synthesized (Supplemental Fig. S6*A*).

Kinesin Light Chain 1 (KLC1) is an integral part of the kinesin-1 motor complex, since this complex is typically formed by two kinesin heavy chains (KIF5s) and two KLCs (59). Similar to KIF5C, the curve of medium-heavy label incorporation in the soma and in the axon were different. In this case, after 72 h, 55% of KIF5C was labeled in the soma, but only 15% was labeled in the axon (Fig. 5*B*). Upon CHX treatment in the soma, the protein was no longer newly synthesized (Supplemental Fig. S6*B*).

Interestingly, several proteins that are involved in RNA biology were detected as synthesized in the axon and transported into the soma. These included adenosine deaminase ADAR1 (double-stranded RNA-specific adenosine deaminase) (60) and RNA helicase DHX30 (ATP-dependent RNA helicase DHX30), involved in the assembly of mitochondrial ribosomes (61). Both proteins were labeled with medium-heavy SILAC and with heavy SILAC and detected in the soma sample. The heavy labeled DHX30 increased in the soma at a faster rate than the medium-heavy labeled, which highlights the importance of the synthesis of this protein in the axon and its retrograde transport (Fig. 5*C*). Overall, the majority of the DHX30 protein copies in the soma were synthesized in the axon. On the other hand, ADAR1 is also synthesized in the axons and later on transported towards the soma, but at a

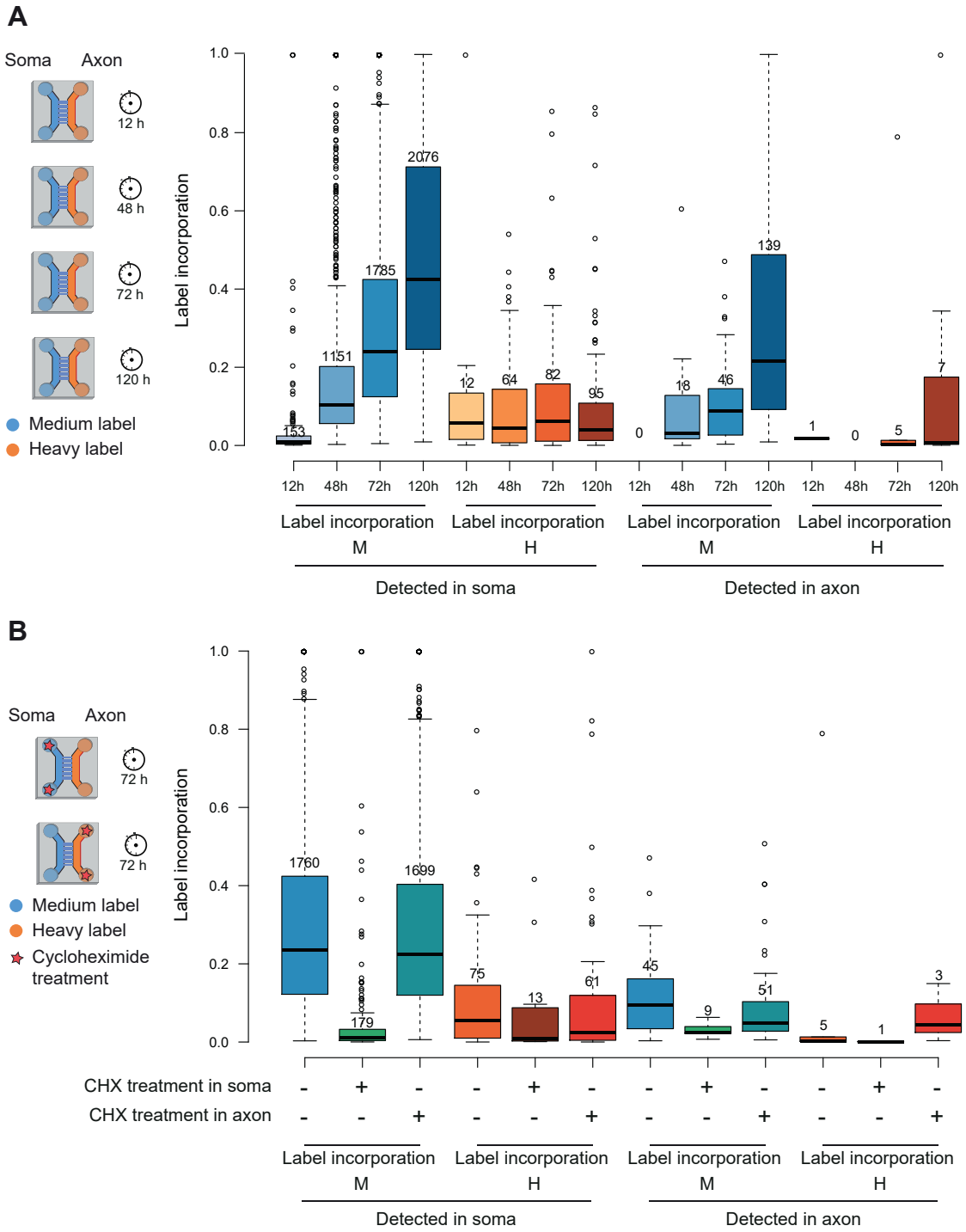

FIG. 4. **Quantitative proteome analysis of hDANs cultured in microfluidic devices**. *A*, schematic illustration of the experimental set up (*right* label) for time course experiment. Boxplots depicting SILAC label incorporation (*left* panel) across all time points in the soma well and the axon well calculated as H/(L +M+ H) and M/(L +M+ H). Only those proteins with label incorporation in two out of three replicates were considered. Color coding: *blue* for label in the soma side and *orange* for label in the axon side, with increasing darkness for longer time points. *B*, schematic illustration of the experimental set up (*right* label) for protein synthesis inhibition by CHX experiment. Boxplots depicting label incorporation (*left* panel) across all samples in the soma side and the axon side calculated as H/(L +M+ H) and M/(L +M+ H). Only those proteins with label incorporation in two out of three replicates were considered. Color coding: *blue* tone for soma side label, *orange* tone for the axon side label. For the boxplots, center lines show the medians; box limits indicate the 25th and 75th percentiles as determined by R software; whiskers extend 1.5 times the interquartile range from the 25th and 75th percentiles; outliers are represented by dots.

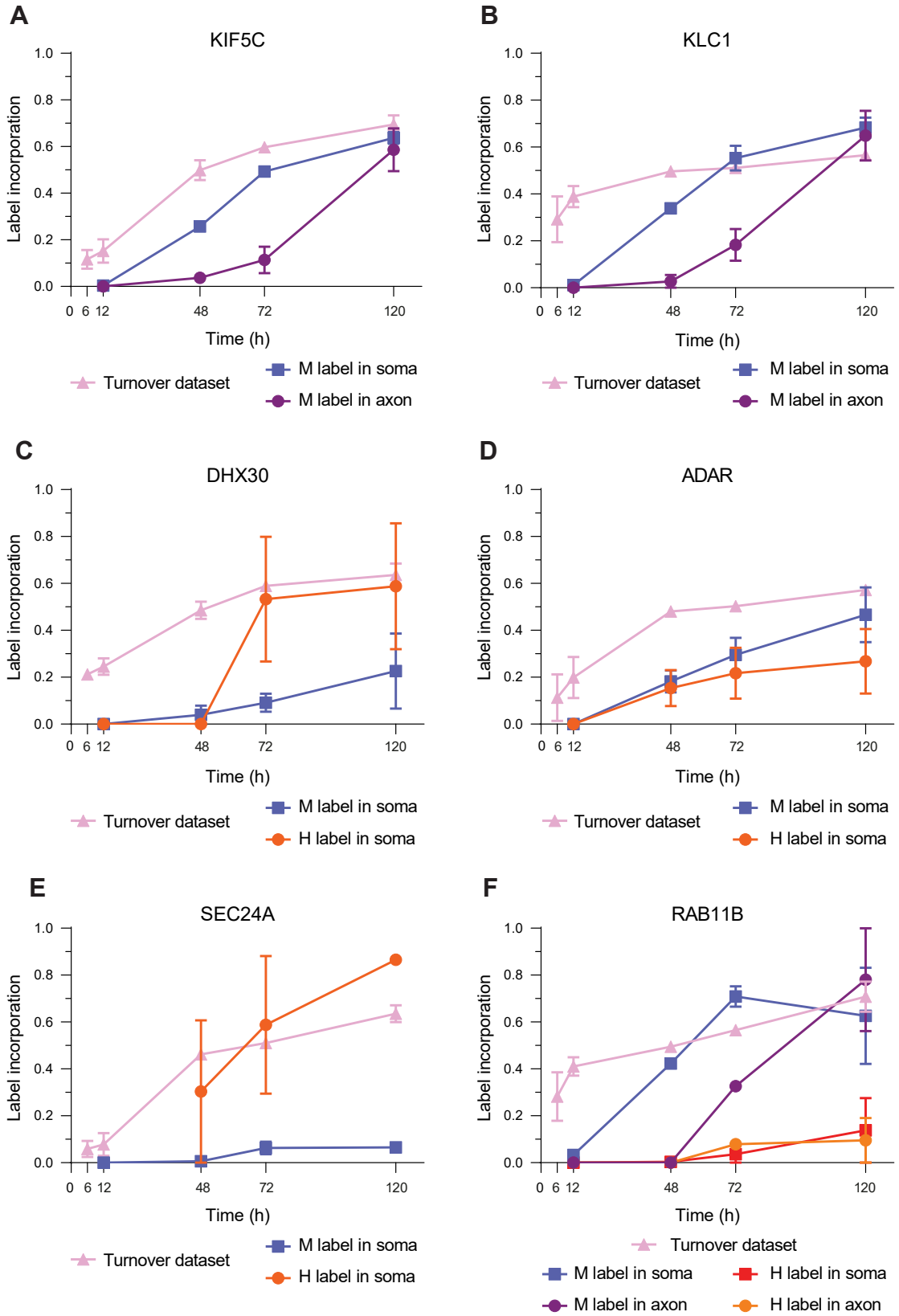

FIG. 5. **Examples of proteins trafficked between soma and axon.** *A*, SILAC label incorporation curves of the medium-heavy label of KIF5C in the soma side and in the axon side and the label incorporation curve of KIF5C in the turnover dataset. *B*, label incorporation curves of the

slower rate (Fig. 5*D*). We validated the localization of DHX30 using fluorescence microscopy, which was mainly localized in the axons (Supplemental Fig. S5*I*).

Another group of interesting trafficked proteins are those involved in vesicle transport such as SEC24A (Protein transport protein Sec24A) and RAB11B (Ras-related protein Rab-11B). SEC24A is a component of the coat protein complex II, which plays a crucial role in the formation of transport vesicles from the endoplasmic reticulum (ER). It was labeled with medium-heavy SILAC and with heavy SILAC. Similar to DHX30, the amount of heavy label SEC24A was higher than the medium-heavy label, which suggests that the majority of the protein in the soma was synthesized in axon and retrogradely transported (Fig. 5*E*). RAB11B belongs to the Ras superfamily of small GTPases, which are key regulators of intracellular membrane trafficking, from the formation of transport vesicles to their fusion with membranes (62). RAB11B was labeled with medium-heavy SILAC and detected both in the soma sample and in the axonal sample and was also labeled with heavy SILAC and detected both in the soma sample and in the axonal sample. The label incorporation indicated that the majority of the protein was synthesized in the soma and transported to the axonal side. However, some of the RAB11B was also synthesized in the axon and transported to the soma (Fig. 5*F*).

DISCUSSION

Using previously characterized iPSC-derived hDaNs, we report the proteome, protein turnover and the first spatial proteome datasets for this cell type and model system. Our study provides a workflow and resource for future applications of quantitative proteomics to cultured human neurons in general.

We first confirmed the dopaminergic differentiation of neurons using immunofluorescence-based and proteomic-based characterization of mature neuronal markers (Supplemental Fig. S5, *A* and *B*). We detected serotonergic marker TPH2 as the second most abundant mature neuronal marker (Supplemental Fig. S5*C*), indicating that our cultures contained serotonergic neurons. We did not detect significant markers of glutaminergic or GABAergic neurons (Supplemental Fig. S5*C*). This is in line with previously published characterization of the differentiation method (13, 51, 55).

We next employed extensive fractionation and DIA to achieve high proteome coverage. We identified over 9400 proteins from bulk extraction of iPSC-derived hDaNs. The coverage of the mitochondrial and mitochondrial outer membrane proteomes was >80% based on MitoCarta 3.0, one of the best annotated reference proteomes available to date (63). Mitochondrial proteins and their dynamics have a pivotal role in dopaminergic neurons and in neuronal health, linking them to energy metabolism and the pathophysiology of neurodegenerative disorders (64–66). Previous studies have relied on prior enrichment of mitochondria to achieve 65% coverage using DIA for iPSC-derived hDaNs (13) and in mapping more than 1100 mitochondrial proteins in mammalian cells (57). Since we report the first axonal proteome for human iPSC-derived dopaminergic neurons, we compared our data to two existing axonal transcriptomes from human iPSC-derived spinal motor neurons and mouse primary neurons. The first study with spinal motor neurons used the same devices (67) and we found an overlap of nine gene/protein groups. In the other study, we found an overlap of 37 gene/protein groups where another microfluidic system utilizing mouse neurons was used (68). The relatively low overlap may be attributed to different cell types and technological platform (transcriptomics) used in these studies.

Our study also provides the first protein turnover dataset for iPSC-derived hDaNs. Most of the studies that addressed proteome turnover data to date have employed tissue or primary neuronal cultures from rodents (24, 26) or mRNA data from human brain tissue (69), nonmammalian cells (70), or human midbrain-like organoids (71). These studies led to the discovery of cell type specificity and influence of glia and other non-neuronal subtypes on the neuronal proteome. Pathway analysis based on our protein turnover data showed that the longest-lived proteins associated with central metabolism; pyruvate metabolism and *de novo* purine and cholesterol biosynthesis, biosynthesis of nucleotides, and the ubiquitin proteasome pathway. We also detected serotonergic pathways such as 5-HT degradation together with PDGF, EGF, and VEGF signaling, confirming the presence of serotonergic neurons and possibly oligodendroglia and neuroepithelial cells.

Depiction of the half-lives of individual subunits of the proteasome highlights the relatively long lived, uniform, synchronous turnover of the proteasome in hDaNs. In contrast, a study using mouse embryonic neurons reported shorter half-lives of those that we observe (19). Previous studies have reported an inverse correlation between organismal life-span and protein turnover (72, 73). This may explain why mouse embryonic neurons have shorter protein half-lives than human neurons.

medium-heavy label of KLC1 in the soma side and in the axon side and the label incorporation curve of KLC1 in the turnover dataset. *C*, label incorporation curves of the heavy and medium-heavy label of DHX30 in the soma side and the label incorporation curve of DHX30 in the turnover dataset. *D*, label incorporation curves of the heavy and medium-heavy label of ADAR in the soma and the label incorporation curve of ADAR in the turnover dataset. *E*, label incorporation curves of the heavy and medium-heavy label of SEC24A in the soma side and the label incorporation curve of SEC24A in the turnover dataset. *F*, label incorporation curves of the heavy and medium-heavy label of RAB11B in the soma side and in the axon side and the label incorporation curve of RAB11B in the turnover dataset.

In our study, long-lived processes included cytoskeletal regulation by Rho GTPases, which include a large number of proteins involved in cytoskeletal processes crucial for neuronal function such as the filopodia, lamellipodia, and vesicle transport. The mitochondrial Rho proteins regulate several aspects of mitochondria homeostasis and transport. One of the encoded proteins, a Rho GTPase known as Miro1, was detected in two protein groups and had a half-life of 99.8 h for isoforms 1/4 and 126.9 h for isoforms 3/5/7 in hDaNs. Miro1 regulates mitophagy and calcium handling and is currently a biomarker and drug development target for PD (74, 75). We also looked in more detail at mitophagy and the TOM complex. Component subunits of the TOM complex have non-uniform half-lives, in agreement with a previous report (57). The detailed organization and binding activities of the TOM complex are particularly relevant in PD, since the interaction of PD protein PINK1 with the TOM complex is intensely studied due to its relevance for activation of the kinase (76–79). Similar to previous studies in rat primary neuron cultures, we show that synaptic proteins tend to be short-lived, while mitochondrial proteins tend to be long-lived (25, 26). We further looked into the half-lives of ribosomal proteins. Our analysis revealed distinctions in the stability of proteins associated with the large and small subunits of the ribosome (Supplemental Fig. S3, *A* and *B*). Interestingly, the 55S mitochondrial ribosome proteins had significantly shorter half-lives than their 80S human counterparts, with no discernible variations in protein half-lives between its two subunits (Supplemental Fig. S3, *A* and *B*). The mitochondrial ribosomes are subjected to substantial oxidative damage, particularly in neurons, which could explain the need for a faster turnover. To our knowledge, this was never reported so far. However, it should be mentioned that the coverage of the cytosolic (80S) ribosome proteins in our dataset was 94%, while the coverage of the mitochondrial (70S) ribosome was 70%, so there is a chance that some proteins with lower turnover were not detected.

Most axonal proteins in neurons are delivered from their site of synthesis in the soma to the axon *via* anterograde vesicular transport and undergo retrograde transport for redistribution and/or lysosomal degradation (80). After synthesis in the cell body, proteins are transported down the axon as various kinds of membrane organelles or protein complexes (81). Furthermore, active transport is the primary mechanism by which organelles, proteins, nucleic acids, and lipids are delivered to relatively distant regions of a growing neuron (82). To address local protein synthesis and transport between axon and soma, we developed and optimized hDaN spatial proteomics using microfluidic devices. This is particularly challenging, due to the very small amount of starting material that can be harvested from the chambers for mass spectrometry. Other groups have successfully performed axon *versus* soma analysis from mouse brain slices with apex (18) and the nascent proteome in retinal axons from *Xenopus laevis* using dynamic SILAC (41). Here we provide the first evidence of local protein synthesis of 154 proteins in the axon and their retrograde transport to the soma of hDaN. In addition, we provide a database for proteome dynamics (axons *versus* soma) in hDaNs over a 120 h period. We did not identify retrograde transport of proteins previously shown to be synthesized in mouse axons and transported to the soma such as Importin, Stat3, mTOR, CREB, or ATF4 following injury (45–49). These protein examples are not ideal controls because in our study, we do not induce axonal injury. Instead, we chose six other proteins as examples to demonstrate and discuss the method: KIF5C, KLC1, DHX30, ADAR, SEC24A, and RAB11B.

There are three isoforms of Kinesin Family Member 5 (KIF5), the ubiquitous KIF5A, KIF5B, and KIF5C, which are isoforms found specifically in neurons (83). Interestingly, KIF5C was the only isoform of KIF5 detected to be newly synthesized and transported within the 120 h time period. It was also the most abundant of all three forms, while KIF5A was not detected at all time points (Supplemental Fig. S7*B*). The half-life of KIF5B was 116 h, while of KIF5C is 68 h, which could also explain the lack of observed label incorporation seen for KIF5B in the time course of our study (Supplemental Fig. S7*A*). Interestingly, KIF5 motors bind Miro1 to facilitate mitochondrial trafficking and importantly, mitochondrial stopping (84), a prerequisite for mitophagy.

KLC1 had similar dynamics to KIF5C. Transcriptome analysis in mice revealed that KLC1 splicing could modify amyloid beta accumulation (85) and therefore could contribute to AD. Later studies showed that KIF and KLC1 implicated axoplasmic transport is disrupted in AD and axonal transport in general is significantly associated with neurodegenerative diseases (86). Another protein of the transport machinery, DYNC1H1 (Dynein, cytoplasmic 1, heavy chain 1), is a component of the cytoplasmic dynein complex, primarily known for its role in retrograde transport, moving cargoes from the axon terminal back to the soma (59). We observed it to be newly synthesized in the soma but could not detect it with medium-heavy label in the axon. Notably, it was also detected as heavy-labeled in the soma, which indicated that it is also synthesized in the axon (Supplemental Fig. S7*C*) and CHX treatment abolished its synthesis in the soma (Supplemental Fig. S7*D*).

Since the length of the microgroove barrier is known (900 μm), as are the axonal velocity rates of kinesin and dynein (0.5–1.0 μm/sec) (87), it is tempting to analyze our data in the context of transport rates. However, these rates will be difficult to estimate, as we measure the bulk protein population in numerous cells and our approach requires extra time to accumulate enough protein molecules to detect the signal on each side of the barrier.

An increasing number of studies has highlighted the crucial role of local protein synthesis in axons. In particular, the role of local synthesis of mitochondrial proteins in axons to maintain

the health of neurons and meet energy demands (88, 89). Interestingly, the mRNA population only partially predicts the local protein population in neurons and this relationship significantly varies between different gene groups (90). Our method could assist in better dissection of RNA transport and local protein synthesis in iPSC-derived neurons. Of 154 proteins that incorporated the heavy SILAC label and were therefore synthesized in the axon, we discuss only those with the highest label incorporation.

DHX30 is an RNA helicase that is part of the DExD/H-box protein family, which is involved in various aspects of RNA metabolism. It has been shown to be a RNA granule protein and has an important role in the assembly of mitochondrial ribosomes (61). In our study, this protein was synthesized locally in the axons and transported in a retrograde manner into the soma. Another interesting protein in terms of dynamics was ADAR, which catalyzes the hydrolytic deamination of adenosine to inosine in dsRNA, which is referred to as A-to-I RNA editing (60). In our dataset, we refer to ADAR1, which is an essential player in the regulation of cellular immune responses, transcriptomic diversity, and cell senescence (91). Of a small number of conserved mammalian ADAR editing sites, they tend to be located in genes encoding neurotransmitter receptors or other synapse-related proteins (92). Indeed, this protein is reported to have an important role in metazoan nervous system, where it modifies pre-mRNAs of proteins involved in electrical and chemical neurotransmission, such as pre-synaptic release complexes and voltage- and ligand-gated ion channels (93). So far, it was reported to be localized mainly in the soma (nucleus) (93). The proteomics data points to the importance of the synthesis of this protein in the axon and its retrograde transport into the soma. Finally, we focused on the protein transport protein SEC24A, a component of the coat protein complex II and RAB11B, a Rab family GTPase involved in the transport of vesicles and endocytic recycling important for synaptic function. SEC24A regulates the control of the formation of transport vesicles from the ER and Ca^{2+} flux between the ER and mitochondria (94). In our dataset, the majority of SEC24A was synthesized in the axons and retrogradely transported to the soma after 48 h. Rab proteins have been associated with PD following discovery of Rab8A, Rab10, Rab8A, Rab8B, and Rab13 as substrates of the PD kinases LRRK2 (95) and PINK1 (96). In our study, we detected Rab11B, which is highly expressed in the brain and involved in recycling *via* the recycling endosome (97) and implicated in several neurodegenerative diseases (98). Rab11 is particularly interesting in the context of mitochondrial dysfunction in PD since many Rab proteins are essential in regulating autophagy and Rab11 was shown to regulate mitophagy downstream of PINK1 and parkin (99) and upstream of alpha synuclein (100). In hDaNs, Rab11B was synthesized in both soma and axons and transported bidirectionally.

Limitations of the Study

Studying global protein turnover and transport in cultured iPSC-derived hDaNs is challenging, and our study is not free of experimental bias. Dynamic SILAC is a powerful method to study protein turnover, but its application over a relatively short experimental time frame leads to low label incorporation in proteins with low turnover, which in turn leads to high variability of the measured SILAC ratios. Conversely, high turnover proteins may already have been completely labeled by the time the first sample was taken for analysis (6 h). It is therefore important to note that half-lives of proteins with high or low turnover are either missing or are prone to high measurement error due to the employed experimental design. Furthermore, recycling of unlabeled amino acids released from the degradation of pre-existing proteins may cause a dilution of the labeled amino acid pool and result in apparently lower turnover rates, as described before (101). These values can be corrected using a recycling factor that can be calculated by measuring label incorporation in partially labeled missed cleaved peptides (102). Although these issues may influence the overall sensitivity and accurate estimation of individual protein turnover rates, we do not expect that they lead to a false detection of the newly synthesized proteins in our dataset.

Culturing of neurons in Xona microfluidic devices, as done in this and other studies (103), provides a robust way of separating axons and soma. However, the relatively small well size enables seeding of only up to 140,000 cells in the proximal (somatodendritic well), which leads to a very low amount of proteins extracted from the distal (axonal) well. Indeed, based on the median of the total iBAQ intensity in all samples, we estimate that the biomass in the distal well was about 33 times lower than in the proximal well. The low number and low intensity of identified proteins in the axonal well pose a significant challenge for quantitation, due to the dynamic range needed to measure low SILAC incorporation. For this reason, heavy-labeled proteins (synthesized in axon) were mainly detected in the somatodendritic well, where the protein amount and signal intensity were higher. Given that the amount of cell seeding is limited by the employed microfluidic devices, increasing cell seeding would lead to the clogging of the microgroove barrier; therefore, application of higher capacity microfluidic devices and improvements in MS sensitivity will be crucial for better coverage of the axonal translatome. Diffusion of small molecules (*e.g.* amino acids) between the wells is another critical aspect in the application of dynamic SILAC to microfluidic devices. We experimentally confirmed that diffusion does not take place in three ways: addition of heavy SILAC amino acids into an empty distal well did not lead to any significant detection of SILAC incorporation in the cells cultured in the proximal well, even after prolonged incubation time (Fig. 3, *A–C*). In theory, diffusion can also take place intracellularly, after a small molecule enters the

cytosol. This was addressed in the experiment where CHX was used to inhibit the protein synthesis (Fig. 4*B*). Addition of CHX to the distal (axonal) well did not have an influence on the protein synthesis in the proximal well, confirming that no measurable intracellular diffusion took place in the time course of analysis. The use of differential dynamic SILAC labeling to study protein transport between cell compartments is complicated by the fact that two processes, protein synthesis and protein transport, are being simultaneously measured. Therefore, the transport of even abundant but low turnover proteins could not be detected in our experimental setup and only limited information on transport rates can be inferred from our data. Finally, we used commercially available dyes that are taken up by cells to stain mitochondria (MitoTracker Deep Red) and neutral lipids (Bodipy) on only one side of the microfluidic devices. We tracked the stained organelles and lipids on either side and could observe only intracellular diffusion/transport in the axons traversing the microgroove (Supplemental Fig. S5, *D–F*).

DATA AVAILABILITY

The mass spectrometry proteomics data have been deposited to the ProteomeXchange Consortium *via* the PRIDE (104) partner repository with the dataset identifier: PXD050991 (DIA dataset), PXD051015 (turnover dataset), and PXD051016 (microfluidic devices). The annotated spectra were deposited in MS viewer (105) with the search keys gq4asqc8vd (dataset 2) and gmtoiiyuod (dataset 3.3).

Supplemental data—This article contains supplemental data.

Acknowledgments—We thank Payal Nashier for the discussions and critical evaluation of the manuscript and Ignacio Garcia Ribelles for his bioinformatic technical support. The authors also wish to thank Bianca Lemke for her assistance with part of cell culture and Polina Volos, a student at the Graduate Training Centre of Neuroscience, University of Tübingen for assisting with some of the immunofluorescence work. Also, Nicolas Casadei, head of the next generation sequencing core facility cATG, Institute of Human Genetics and Applied Genomics, University of Tübingen for helping in bioinformatics comparing existing transcriptomic data with the proteomic datasets.

Funding and additional information—This research was funded by the German Research Foundation (DFG) through GRK2364. B. M. and C. C.-R. acknowledge support by the High Performance and Cloud Computing Group at the Center for Data Processing of the University of Tübingen, the state of Baden-Wuerttemberg through bwHPC. We acknowledge support from the Open Access Publication Fund of the University of Tübingen.

Author contributions—C. C.-R. writing–original draft; C. C.-R. and K. S. methodology; C. C.-R. and K. S. investigation; C. C.-R. formal analysis; C. C.-R. data curation; C. C.-R., K. S., J. C. F., and B. M. conceptualization; K. S., J. C. F., and B. M. writing–review and editing; J. C. F. and B. M. supervision; J. C. F. and B. M. resources; J. C. F. and B. M. project administration; J. C. F. and B. M. funding acquisition.

Conflicts of interest—The authors declare no competing interests.

Abbreviations—The abbreviations used are: AD, Alzheimer's disease; BSA, bovine serum albumin; CHX, cycloheximide; DMEM, Dulbecco's modified Eagle's medium; DIA, data-independent acquisition; ER, endoplasmic reticulum; FDR, false discovery rate; GO, gene ontology; hDaN, human dopaminergic neuron; iBAQ, intensity-based absolute quantification; iPSC, induced pluripotent stem cell; KIF5, Kinesin Family Member 5; KIF5C, Kinesin Family Member 5C; KLC1, Kinesin Light Chain 1; MS/MS, tandem MS; PD, Parkinson's disease; SILAC, Stable Isotope Labeling with Amino acids in Cell culture; SN, *Substantia nigra*.

Received March 28, 2024, and in revised form, August 18, 2024
Published, MCPRO Papers in Press, September 7, 2024, https://doi.org/10.1016/j.mcpro.2024.100838

REFERENCES

1. Iversen, S. D., and Iversen, L. L. (2007) Dopamine: 50 years in perspective. *Trends Neurosci.* **30**, 188–193
2. Liss, B., and Roeper, J. (2008) Individual dopamine midbrain neurons: functional diversity and flexibility in health and disease. *Brain Res. Rev.* **58**, 314–321
3. Wise, R. A. (2004) Dopamine, learning and motivation. *Nat. Rev. Neurosci.* **5**, 483–494
4. Bjorklund, A., and Dunnett, S. B. (2007) Dopamine neuron systems in the brain: an update. *Trends Neurosci.* **30**, 194–202
5. Surmeier, D. J., Obeso, J. A., and Halliday, G. M. (2017) Selective neuronal vulnerability in Parkinson disease. *Nat. Rev. Neurosci.* **18**, 101–113
6. Jang, Y., Pletnikova, O., Troncoso, J. C., Pantelyat, A. Y., Dawson, T. M., Rosenthal, L. S., *et al*. (2023) Mass spectrometry-based proteomics analysis of human substantia nigra from Parkinson's disease patients identifies multiple pathways potentially involved in the disease. *Mol. Cell Proteomics* **22**, 100452
7. Fingleton, E., Li, Y., and Roche, K. W. (2021) Advances in proteomics allow insights into neuronal proteomes. *Front. Mol. Neurosci.* **14**, 647451
8. Focking, M., Lopez, L. M., English, J. A., Dicker, P., Wolff, A., Brindley, E., *et al*. (2015) Proteomic and genomic evidence implicates the postsynaptic density in schizophrenia. *Mol. Psychiatry* **20**, 424–432
9. Rosato, M., Stringer, S., Gebuis, T., Paliukhovich, I., Li, K. W., Posthuma, D., *et al*. (2021) Combined cellomics and proteomics analysis reveals shared neuronal morphology and molecular pathway phenotypes for multiple schizophrenia risk genes. *Mol. Psychiatry* **26**, 784–799
10. Tshilenge, K. T., Aguirre, C. G., Bons, J., Gerencser, A. A., Basisty, N., Song, S., *et al*. (2023) Proteomic analysis of huntington's disease medium spiny neurons identifies alterations in lipid droplets. *Mol. Cell Proteomics* **22**, 100534
11. Bogetofte, H., Ryan, B. J., Jensen, P., Schmidt, S. I., Vergoossen, D. L. E., Barnkob, M. B., *et al*. (2023) Post-translational proteomics platform identifies neurite outgrowth impairments in Parkinson's disease GBA-N370S dopamine neurons. *Cell Rep.* **42**, 112180
12. Antoniou, N., Prodromidou, K., Kouroupi, G., Boumpoureka, I., Samiotaki, M., Panayotou, G., *et al*. (2022) High content screening and proteomic

analysis identify a kinase inhibitor that rescues pathological phenotypes in a patient-derived model of Parkinson's disease. *NPJ Parkinsons Dis.* **8**, 15
13. Bus, C., Zizmare, L., Feldkaemper, M., Geisler, S., Zarani, M., Schaedler, A., *et al*. (2020) Human dopaminergic neurons lacking PINK1 exhibit disrupted dopamine metabolism related to vitamin B6 Co-factors. *iScience* **23**, 101797
14. Connor-Robson, N., Booth, H., Martin, J. G., Gao, B., Li, K., Doig, N., *et al*. (2019) An integrated transcriptomics and proteomics analysis reveals functional endocytic dysregulation caused by mutations in LRRK2. *Neurobiol. Dis.* **127**, 512–526
15. Novak, G., Kyriakis, D., Grzyb, K., Bernini, M., Rodius, S., Dittmar, G., *et al*. (2022) Single-cell transcriptomics of human iPSC differentiation dynamics reveal a core molecular network of Parkinson's disease. *Commun. Biol.* **5**, 49
16. Schmidt, S., Stautner, C., Vu, D. T., Heinz, A., Regensburger, M., Karayel, O., *et al*. (2023) A reversible state of hypometabolism in a human cellular model of sporadic Parkinson's disease. *Nat. Commun.* **14**, 7674
17. van Oostrum, M., Blok, T. M., Giandomenico, S. L., Tom Dieck, S., Tushev, G., Furst, N., *et al*. (2023) The proteomic landscape of synaptic diversity across brain regions and cell types. *Cell* **186**, 5411–5427.e23
18. Hobson, B. D., Choi, S. J., Mosharov, E. V., Soni, R. K., Sulzer, D., and Sims, P. A. (2022) Subcellular proteomics of dopamine neurons in the mouse brain. *Elife* **11**, e70921
19. Mathieson, T., Franken, H., Kosinski, J., Kurzawa, N., Zinn, N., Sweetman, G., *et al*. (2018) Systematic analysis of protein turnover in primary cells. *Nat. Commun.* **9**, 689
20. Doherty, M. K., Hammond, D. E., Clague, M. J., Gaskell, S. J., and Beynon, R. J. (2009) Turnover of the human proteome: determination of protein intracellular stability by dynamic SILAC. *J. Proteome Res.* **8**, 104–112
21. Ross, A. B., Langer, J. D., and Jovanovic, M. (2021) Proteome turnover in the spotlight: approaches, applications, and perspectives. *Mol. Cell Proteomics* **20**, 100016
22. Schwanhausser, B., Gossen, M., Dittmar, G., and Selbach, M. (2009) Global analysis of cellular protein translation by pulsed SILAC. *Proteomics* **9**, 205–209
23. Bulovaite, E., Qiu, Z., Kratschke, M., Zgraj, A., Fricker, D. G., Tuck, E. J., *et al*. (2022) A brain atlas of synapse protein lifetime across the mouse lifespan. *Neuron* **110**, 4057–40573.e8
24. Fornasiero, E. F., Mandad, S., Wildhagen, H., Alevra, M., Rammner, B., Keihani, S., *et al*. (2018) Precisely measured protein lifetimes in the mouse brain reveal differences across tissues and subcellular fractions. *Nat. Commun.* **9**, 4230
25. Cohen, L. D., Zuchman, R., Sorokina, O., Muller, A., Dieterich, D. C., Armstrong, J. D., *et al*. (2013) Metabolic turnover of synaptic proteins: kinetics, interdependencies and implications for synaptic maintenance. *PLoS One* **8**, e63191
26. Dorrbaum, A. R., Kochen, L., Langer, J. D., and Schuman, E. M. (2018) Local and global influences on protein turnover in neurons and glia. *Elife* **7**, e34202
27. Glock, C., Biever, A., Tushev, G., Nassim-Assir, B., Kao, A., Bartnik, I., *et al*. (2021) The translatome of neuronal cell bodies, dendrites, and axons. *Proc. Natl. Acad. Sci. U. S. A.* **118**, e2113929118
28. Iqbal, A., Baldrighi, M., Murdoch, J. N., Fleming, A., and Wilkinson, C. J. (2020) Alpha-synuclein aggresomes inhibit ciliogenesis and multiple functions of the centrosome. *Biol Open* **9**, bio054338
29. Schmidt, S., Luecken, M. D., Trumbach, D., Hembach, S., Niedermeier, K. M., Wenck, N., *et al*. (2022) Primary cilia and SHH signaling impairments in human and mouse models of Parkinson's disease. *Nat. Commun.* **13**, 4819
30. Steger, M., Diez, F., Dhekne, H. S., Lis, P., Nirujogi, R. S., Karayel, O., *et al*. (2017) Systematic proteomic analysis of LRRK2-mediated Rab GTPase phosphorylation establishes a connection to ciliogenesis. *Elife* **6**, e31012
31. Merianda, T. T., Lin, A. C., Lam, J. S., Vuppalanchi, D., Willis, D. E., Karin, N., *et al*. (2009) A functional equivalent of endoplasmic reticulum and Golgi in axons for secretion of locally synthesized proteins. *Mol. Cell Neurosci.* **40**, 128–142
32. Spillane, M., Ketschek, A., Merianda, T. T., Twiss, J. L., and Gallo, G. (2013) Mitochondria coordinate sites of axon branching through localized intra-axonal protein synthesis. *Cell Rep.* **5**, 1564–1575
33. Verma, P., Chierzi, S., Codd, A. M., Campbell, D. S., Meyer, R. L., Holt, C. E., *et al*. (2005) Axonal protein synthesis and degradation are necessary for efficient growth cone regeneration. *J. Neurosci.* **25**, 331–342
34. Bassell, G. J., Zhang, H., Byrd, A. L., Femino, A. M., Singer, R. H., Taneja, K. L., *et al*. (1998) Sorting of beta-actin mRNA and protein to neurites and growth cones in culture. *J. Neurosci.* **18**, 251–265
35. Turner-Bridger, B., Caterino, C., and Cioni, J. M. (2020) Molecular mechanisms behind mRNA localization in axons. *Open Biol.* **10**, 200177
36. Spaulding, E. L., and Burgess, R. W. (2017) Accumulating evidence for axonal translation in neuronal homeostasis. *Front. Neurosci.* **11**, 312
37. Harbauer, A. B., Hees, J. T., Wanderoy, S., Segura, I., Gibbs, W., Cheng, Y., *et al*. (2022) Neuronal mitochondria transport Pink1 mRNA *via* synaptojanin 2 to support local mitophagy. *Neuron* **110**, 1516–15131.e9
38. Hou, X., Fiesel, F. C., Truban, D., Castanedes Casey, M., Lin, W. L., Soto, A. I., *et al*. (2018) Age- and disease-dependent increase of the mitophagy marker phospho-ubiquitin in normal aging and Lewy body disease. *Autophagy* **14**, 1404–1418
39. Narendra, D. P., Jin, S. M., Tanaka, A., Suen, D. F., Gautier, C. A., Shen, J., *et al*. (2010) PINK1 is selectively stabilized on impaired mitochondria to activate Parkin. *PLoS Biol.* **8**, e1000298
40. Geisler, S., Holmstrom, K. M., Skujat, D., Fiesel, F. C., Rothfuss, O. C., Kahle, P. J., *et al*. (2010) PINK1/Parkin-mediated mitophagy is dependent on VDAC1 and p62/SQSTM1. *Nat. Cell Biol.* **12**, 119–131
41. Cagnetta, R., Frese, C. K., Shigeoka, T., Krijgsveld, J., and Holt, C. E. (2018) Rapid cue-specific remodeling of the nascent axonal proteome. *Neuron* **99**, 29–46.e4
42. Taylor, A. M., Blurton-Jones, M., Rhee, S. W., Cribbs, D. H., Cotman, C. W., and Jeon, N. L. (2005) A microfluidic culture platform for CNS axonal injury, regeneration and transport. *Nat. Methods* **2**, 599–605
43. Sainio, M. T., Rasila, T., Molchanova, S. M., Jarvilehto, J., Torregrosa-Munumer, R., Harjuhaahto, S., *et al*. (2021) Neurofilament light regulates axon caliber, synaptic activity, and organelle trafficking in cultured human motor neurons. *Front. Cell Dev. Biol.* **9**, 820105
44. Van Laar, V. S., Arnold, B., Howlett, E. H., Calderon, M. J., St Croix, C. M., Greenamyre, J. T., *et al*. (2018) Evidence for compartmentalized axonal mitochondrial biogenesis: mitochondrial DNA replication increases in distal axons as an early response to Parkinson's disease-relevant stress. *J. Neurosci.* **38**, 7505–7515
45. Baleriola, J., Walker, C. A., Jean, Y. Y., Crary, J. F., Troy, C. M., Nagy, P. L., *et al*. (2014) Axonally synthesized ATF4 transmits a neurodegenerative signal across brain regions. *Cell* **158**, 1159–1172
46. Cox, L. J., Hengst, U., Gurskaya, N. G., Lukyanov, K. A., and Jaffrey, S. R. (2008) Intra-axonal translation and retrograde trafficking of CREB promotes neuronal survival. *Nat. Cell Biol.* **10**, 149–159
47. Terenzio, M., Koley, S., Samra, N., Rishal, I., Zhao, Q., Sahoo, P. K., *et al*. (2018) Locally translated mTOR controls axonal local translation in nerve injury. *Science* **359**, 1416–1421
48. Hanz, S., and Fainzilber, M. (2006) Retrograde signaling in injured nerve–the axon reaction revisited. *J. Neurochem.* **99**, 13–19
49. Perry, R. B., Doron-Mandel, E., Iavnilovitch, E., Rishal, I., Dagan, S. Y., Tsoory, M., *et al*. (2012) Subcellular knockout of importin beta1 perturbs axonal retrograde signaling. *Neuron* **75**, 294–305
50. Schwarz, L., Casadei, N., and Fitzgerald, J. C. (2021) Generation of R272Q, S156A and K572R RHOT1/Miro1 point mutations in iPSCs from a healthy individual using FACS-assisted CRISPR/Cas9 genome editing. *Stem Cell Res.* **55**, 102469
51. Schwarz, L., and Fitzgerald, J. C. (2022) Steady-state levels of Miro1 linked to phosphorylation at serine 156 and mitochondrial respiration in dopaminergic neurons. *Cells* **11**, 1269
52. Reinhardt, P., Glatza, M., Hemmer, K., Tsytsyura, Y., Thiel, C. S., Hoing, S., *et al*. (2013) Derivation and expansion using only small molecules of human neural progenitors for neurodegenerative disease modeling. *PLoS One* **8**, e59252
53. Thomas, P. D., Ebert, D., Muruganujan, A., Mushayahama, T., Albou, L. P., and Mi, H. (2022) PANTHER: making genome-scale phylogenetics accessible to all. *Protein Sci.* **31**, 8–22
54. Schwanhausser, B., Busse, D., Li, N., Dittmar, G., Schuchhardt, J., Wolf, J., *et al*. (2011) Global quantification of mammalian gene expression control. *Nature* **473**, 337–342
55. Schwarz, L., Sharma, K., Dodi, L. D., Rieder, L. S., Fallier-Becker, P., Casadei, N., *et al*. (2022) Miro1 R272Q disrupts mitochondrial calcium

handling and neurotransmitter uptake in dopaminergic neurons. *Front. Mol. Neurosci.* **15**, 966209
56. Mi, H., and Thomas, P. (2009) PANTHER pathway: an ontology-based pathway database coupled with data analysis tools. *Methods Mol. Biol.* **563**, 123–140
57. Morgenstern, M., Peikert, C. D., Lubbert, P., Suppanz, I., Klemm, C., Alka, O., *et al*. (2021) Quantitative high-confidence human mitochondrial proteome and its dynamics in cellular context. *Cell Metab.* **33**, 2464–2483.e18
58. Chua, J. J., Jahn, R., and Klopfenstein, D. R. (2013) Managing intracellular transport. *Worm* **2**, e21564
59. Cason, S. E., and Holzbaur, E. L. F. (2022) Selective motor activation in organelle transport along axons. *Nat. Rev. Mol. Cell Biol.* **23**, 699–714
60. Barraud, P., and Allain, F. H.-T. (2011) ADAR proteins: double-stranded RNA and Z-DNA binding domains. *Curr. Top Microbiol. Immunol.* **353**, 35–60
61. Antonicka, H., and Shoubridge, E. A. (2015) Mitochondrial RNA granules are centers for posttranscriptional RNA processing and ribosome biogenesis. *Cell Rep.* **10**, 920–932
62. Mignogna, M. L., and D'Adamo, P. (2018) Critical importance of RAB proteins for synaptic function. *Small GTPases* **9**, 145–157
63. Rath, S., Sharma, R., Gupta, R., Ast, T., Chan, C., Durham, T. J., *et al*. (2021) MitoCarta3.0: an updated mitochondrial proteome now with sub-organelle localization and pathway annotations. *Nucleic Acids Res.* **49**, D1541–D1547
64. Gonzalez-Rodriguez, P., Zampese, E., Stout, K. A., Guzman, J. N., Ilijic, E., Yang, B., *et al*. (2021) Disruption of mitochondrial complex I induces progressive parkinsonism. *Nature* **599**, 650–656
65. Pacelli, C., Giguere, N., Bourque, M. J., Levesque, M., Slack, R. S., and Trudeau, L. E. (2015) Elevated mitochondrial bioenergetics and axonal arborization size are key contributors to the vulnerability of dopamine neurons. *Curr. Biol.* **25**, 2349–2360
66. Zampese, E., Wokosin, D. L., Gonzalez-Rodriguez, P., Guzman, J. N., Tkatch, T., Kondapalli, J., *et al*. (2022) Ca(2+) channels couple spiking to mitochondrial metabolism in substantia nigra dopaminergic neurons. *Sci. Adv.* **8**, eabp8701
67. Nijssen, J., Aguila, J., Hoogstraaten, R., Kee, N., and Hedlund, E. (2018) Axon-seq decodes the motor axon transcriptome and its modulation in response to ALS. *Stem Cell Rep.* **11**, 1565–1578
68. Yang, Z., Yu, J., Zhang, J., Song, H., Ye, H., Liu, J., *et al*. (2023) Facilitation of axonal transcriptome analysis with quantitative microfluidic devices. *Lab Chip* **23**, 2217–2227
69. Cahoy, J. D., Emery, B., Kaushal, A., Foo, L. C., Zamanian, J. L., Christopherson, K. S., *et al*. (2008) A transcriptome database for astrocytes, neurons, and oligodendrocytes: a new resource for understanding brain development and function. *J. Neurosci.* **28**, 264–278
70. Munchel, S. E., Shultzaberger, R. K., Takizawa, N., and Weis, K. (2011) Dynamic profiling of mRNA turnover reveals gene-specific and system-wide regulation of mRNA decay. *Mol. Biol. Cell* **22**, 2787–2795
71. Dong, J., Duchesne, A., Bayne, A. N., Mohamed, N. V., Yi, W., Mathur, M., *et al*. (2022) An approach to measuring protein turnover in human induced pluripotent stem cell organoids by mass spectrometry. *Methods* **203**, 17–27
72. Swovick, K., Firsanov, D., Welle, K. A., Hryhorenko, J. R., Wise, J. P., Sr, *et al*. (2021) Interspecies differences in proteome turnover kinetics are correlated with life spans and energetic demands. *Mol. Cell Proteomics* **20**, 100041
73. Swovick, K., Welle, K. A., Hryhorenko, J. R., Seluanov, A., Gorbunova, V., and Ghaemmaghami, S. (2018) Cross-species comparison of proteome turnover kinetics. *Mol. Cell Proteomics* **17**, 580–591
74. Bharat, V., Durairaj, A. S., Vanhauwaert, R., Li, L., Muir, C. M., Chandra, S., *et al*. (2023) A mitochondrial inside-out iron-calcium signal reveals drug targets for Parkinson's disease. *Cell Rep.* **42**, 113544
75. Hsieh, C. H., Li, L., Vanhauwaert, R., Nguyen, K. T., Davis, M. D., Bu, G., *et al*. (2019) Miro1 marks Parkinson's disease subset and Miro1 reducer rescues neuron loss in Parkinson's models. *Cell Metab.* **30**, 1131–11340.e7
76. [preprint] Chin, R. M., Rakhit, R., Ditsworth, D., Wang, C., Bartholomeus, J., Liu, S., *et al*. (2023) Pharmacological PINK1 activation ameliorates Pathology in Parkinson's Disease models. *bioRxiv*. https://doi.org/10.1101/2023.02.14.528378
77. Kakade, P., Ojha, H., Raimi, O. G., Shaw, A., Waddell, A. D., Ault, J. R., *et al*. (2022) Mapping of a N-terminal alpha-helix domain required for human PINK1 stabilization, Serine228 autophosphorylation and activation in cells. *Open Biol.* **12**, 210264
78. Maruszczak, K. K., Jung, M., Rasool, S., Trempe, J. F., and Rapaport, D. (2022) The role of the individual TOM subunits in the association of PINK1 with depolarized mitochondria. *J. Mol. Med. (Berl)* **100**, 747–762
79. Rasool, S., Veyron, S., Soya, N., Eldeeb, M. A., Lukacs, G. L., Fon, E. A., *et al*. (2022) Mechanism of PINK1 activation by autophosphorylation and insights into assembly on the TOM complex. *Mol. Cell* **82**, 44–59.e6
80. Bekku, Y., and Salzer, J. L. (2021) Dual color, live imaging of vesicular transport in axons of cultured sensory neurons. *Bio Protoc.* **11**, e4067
81. Terada, S., Kinjo, M., Aihara, M., Takei, Y., and Hirokawa, N. (2010) Kinesin-1/Hsc70-dependent mechanism of slow axonal transport and its relation to fast axonal transport. *EMBO J.* **29**, 843–854
82. Bauer, C. T., Shtridelman, Y., Lema Tome, C. M., Grim, J. Q., Turner, C. P., Tytell, M., *et al*. (2008) Intraneuronal vesicular organelle transport changes with cell population density *in vitro*. *Neurosci. Lett.* **441**, 173–177
83. Kanai, Y., Okada, Y., Tanaka, Y., Harada, A., Terada, S., and Hirokawa, N. (2000) KIF5C, a novel neuronal kinesin enriched in motor neurons. *J. Neurosci.* **20**, 6374–6384
84. Wang, X., Winter, D., Ashrafi, G., Schlehe, J., Wong, Y. L., Selkoe, D., *et al*. (2011) PINK1 and Parkin target Miro for phosphorylation and degradation to arrest mitochondrial motility. *Cell* **147**, 893–906
85. Morihara, T., Hayashi, N., Yokokoji, M., Akatsu, H., Silverman, M. A., Kimura, N., *et al*. (2014) Transcriptome analysis of distinct mouse strains reveals kinesin light chain-1 splicing as an amyloid-beta accumulation modifier. *Proc. Natl. Acad. Sci. U. S. A.* **111**, 2638–2643
86. Berth, S. H., and Lloyd, T. E. (2023) Disruption of axonal transport in neurodegeneration. *J. Clin. Invest.* **133**, e168554
87. Maday, S., Twelvetrees, A. E., Moughamian, A. J., and Holzbaur, E. L. (2014) Axonal transport: cargo-specific mechanisms of motility and regulation. *Neuron* **84**, 292–309
88. Harbauer, A. B. (2017) Mitochondrial health maintenance in axons. *Biochem. Soc. Trans.* **45**, 1045–1052
89. Hees, J. T., and Harbauer, A. B. (2022) Metabolic regulation of mitochondrial protein biogenesis from a neuronal perspective. *Biomolecules* **12**, 1595
90. Perez, J. D., Fusco, C. M., and Schuman, E. M. (2021) A functional dissection of the mRNA and locally synthesized protein population in neuronal dendrites and axons. *Annu. Rev. Genet.* **55**, 183–207
91. Eisenberg, E., and Levanon, E. Y. (2018) A-to-I RNA editing - immune protector and transcriptome diversifier. *Nat. Rev. Genet.* **19**, 473–490
92. Pinto, Y., Cohen, H. Y., and Levanon, E. Y. (2014) Mammalian conserved ADAR targets comprise only a small fragment of the human editosome. *Genome Biol.* **15**, R5
93. Savva, Y. A., Rieder, L. E., and Reenan, R. A. (2012) The ADAR protein family. *Genome Biol.* **13**, 252
94. Chidawanyika, T., Chakrabarti, R., Beauchemin, K. S., Higgs, H. N., and Supattapone, S. (2021) SEC24A facilitates colocalization and Ca2+ flux between the endoplasmic reticulum and mitochondria. *J. Cell Sci.* **134**, jcs249276
95. Steger, M., Tonelli, F., Ito, G., Davies, P., Trost, M., Vetter, M., *et al*. (2016) Phosphoproteomics reveals that Parkinson's disease kinase LRRK2 regulates a subset of Rab GTPases. *Elife* **5**, e12813
96. Lai, Y. C., Kondapalli, C., Lehneck, R., Procter, J. B., Dill, B. D., Woodroof, H. I., *et al*. (2015) Phosphoproteomic screening identifies Rab GTP ases as novel downstream targets of PINK 1. *EMBO J.* **34**, 2840–2861
97. Ullrich, O., Reinsch, S., Urbe, S., Zerial, M., and Parton, R. G. (1996) Rab11 regulates recycling through the pericentriolar recycling endosome. *J. Cell Biol.* **135**, 913–924
98. Sultana, P., and Novotny, J. (2022) Rab11 and its role in neurodegenerative diseases. *ASN Neuro* **14**. https://doi.org/10.1177/17590914221142360
99. Rai, P., and Roy, J. K. (2022) Rab11 regulates mitophagy signaling pathway of Parkin and Pink1 in the Drosophila model of Parkinson's disease. *Biochem. Biophys. Res. Commun.* **626**, 175–186
100. Breda, C., Nugent, M. L., Estranero, J. G., Kyriacou, C. P., Outeiro, T. F., Steinert, J. R., *et al*. (2015) Rab11 modulates alpha-synuclein-mediated defects in synaptic transmission and behaviour. *Hum. Mol. Genet.* **24**, 1077–1091

101. Semanjski, M., Gratani, F. L., Englert, T., Nashier, P., Beke, V., Nalpas, N., *et al*. (2021) Proteome dynamics during antibiotic persistence and resuscitation. *mSystems* **6**, e0054921
102. Schwanhausser, B., Busse, D., Li, N., Dittmar, G., Schuchhardt, J., Wolf, J., *et al*. (2013) Corrigendum: global quantification of mammalian gene expression control. *Nature* **495**, 126–127
103. Salehi, S., Zare, A., Prezza, G., Bader, J., Schneider, C., Fischer, U., *et al*. (2023) Cytosolic Ptbp2 modulates axon growth in motoneurons through axonal localization and translation of Hnrnpr. *Nat. Commun.* **14**, 4158
104. Perez-Riverol, Y., Csordas, A., Bai, J., Bernal-Llinares, M., Hewapathirana, S., Kundu, D. J., *et al*. (2019) The PRIDE database and related tools and resources in 2019: improving support for quantification data. *Nucleic Acids Res.* **47**, D442–D450
105. Baker, P. R., and Chalkley, R. J. (2014) MS-viewer: a web-based spectral viewer for proteomics results. *Mol. Cell Proteomics* **13**, 1392–1396

PINK1 regulates cholesterol homeostasis via SCAP phosphorylation in human dopaminergic neurons

Karan Sharma[1], Claudia Cavarischia-Rega[2], Dina Ivaniuk[1], Christine Fröhlich[1], Jos F. Brouwers[3], Gerard J.M. Martens[4], Philip Seibler[5], Javier Jarazo[6], Thomas Gasser[1,7], Daniela M. Vogt Weisenhorn[8,9], Boris Macek[2] and Julia C. Fitzgerald[1*]

Abstract

Cholesterol is a key lipid enriched in neuronal membranes and essential for signaling and synaptic transmission. An imbalance in cholesterol levels may affect synaptic plasticity and contribute to neurodegeneration. Here, we identify in human dopaminergic neurons a mechanism linking loss of function of the Parkinson's disease (PD) gene *PINK1* to altered cholesterol homeostasis. Loss of functional PINK1 impaired SCAP phosphorylation at Ser822 and Ser838, stabilizing SCAP and driving excess cholesterol biosynthesis. Cholesterol accumulated at the plasma membrane and in flotillin-rich lipid rafts, causing reduced neurotransmitter uptake and altering the distribution of dopamine transporter (DAT). Restoring PINK1 expression normalized cholesterol biosynthesis and levels. Moreover, the cholesterol-lowering drugs simvastatin and β-cyclodextrin rescued DAT distribution and neurotransmitter uptake defects. These findings demonstrate that PINK1 influences cholesterol homeostasis through SCAP phosphorylation at Ser822 and Ser838 and that restoring cholesterol levels mitigates phenotypes observed in PINK1 PD neurons. These findings further highlight the cross-talk between mitochondria and lipid homeostasis in PD models, underscoring the relevance of cholesterol levels to dopaminergic functions.

Keywords: PINK1, Cholesterol, Parkinson's disease, SCAP, Phosphorylation

Author affiliations:

1 Department of Neurodegeneration, Hertie Institute for Clinical Brain Research, Centre for Neurology, Faculty of Medicine, University of Tübingen, 72076 Tübingen, Germany.

2 Quantitative Proteomics Group, Department of Biology, Interfaculty Institute of Cell Biology, University of Tübingen, 72076 Tübingen, Germany.

3 Research Group Analysis Techniques in the Life Sciences, Centre of Expertise Perspective in Health, Avans University of Applied Science, 4818 AJ Breda, The Netherlands.

4 Department of Molecular Animal Physiology, Donders Centre for Neuroscience (DCN), Radboud University, Heyendaalseweg 135, 6525 AJ Nijmegen, The Netherlands.

5 Institute of Neurogenetics, University of Lübeck, Lübeck, Germany.

6 OrganoTherapeutics SARL, 29 Henri Koch, 4354 Esch-sur-Alzette, Luxembourg.

7 DZNE - German Center for Neurodegenerative Diseases, Tübingen, 72076 Tübingen, Germany.

8 Institute of Developmental Genetics, Helmholtz Zentrum München, Ingolstädter Landstraße 1, 85764, Neuherberg, Germany.

9 Chair of Developmental Genetics, Munich School of Life Sciences Weihenstephan, Technical University of Munich, Alte Akademie 8, 85354, Freising, Germany.

***Correspondence:**

Julia C. Fitzgerald. Department of Neurodegeneration, Hertie Institute for Clinical Brain Research, Otfried Müller Strasse 27, Tübingen 72076, Germany. julia.fitzgerald@uni-tuebingen.de

Running title: PINK1 regulates cholesterol homeostasis via SCAP phosphorylation.

Introduction

Mutations in phosphatase and tensin homolog-induced kinase 1 (*PINK1*) typically cause autosomal recessive Parkinson's disease (PD)[1]. Clinically, PINK1-PD presents early (median age at 32 years) with tremor, bradykinesia and rigidity and responds well to levodopa treatment[2]. PINK1-associated neuropathology involves the selective degeneration of dopaminergic neurons (DaNs) in the *substantia nigra*, while Lewy body pathology is inconsistently observed[3 4].

The canonical function of PINK1 is mitochondrial quality control. Upon mitochondrial depolarization, PINK1 accumulates at the outer mitochondrial membrane, where it phosphorylates ubiquitin and Parkin, initiating an outside-in PINK1/Parkin-dependent mitophagy to remove damaged mitochondria[5-20]. Beyond mitochondria, PINK1 has been implicated in maintaining endoplasmic reticulum (ER) homeostasis by promoting selective clearance of the organelle[21], regulating ER calcium release mediated by IP_3R[22] and modulating the ER unfolded protein response (UPR)[23 24]. PINK1 loss of function (LOF) also disrupts ER-mitochondria contacts and calcium buffering, suggesting broader roles at ER-mitochondria interfaces [25].

Cholesterol, synthesized in the ER, is an essential structural and functional component of neuronal membranes. At the plasma membrane cholesterol supports neuronal signaling, vesicle trafficking and synaptic neurotransmission[26]. Cholesterol is synthesized *de novo* in the brain as cholesterol does not cross the blood brain barrier (BBB)[27]. Young and developing neurons make their own cholesterol, while adult neurons rely mainly on cholesterol imported from neighbouring astrocytes[28 29].

Cholesterol biosynthesis is tightly regulated by the sterol regulatory element-binding protein (SREBP) pathway, with sterol regulatory element-binding protein cleavage-activating protein (SCAP) as a key regulator[30]. During synthesis, insulin-induced gene (INSIG) proteins are dissociated from the SCAP-SREBP2 complex at the ER membrane[30-33]. The SREBP2-SCAP complex then leaves the ER and translocate to the Golgi, where SREBP2 is cleaved by site 1 and site 2 proteases (S1P and S2P, respectively). Cleaved SREBP2 then goes to the nucleus and binds to the sterol regulatory element (SRE) to transcribe SREBP2 target genes i.e., 3-hydroxy-3-methylglutaryl-CoA reductase (HMGCR) and squalene monooxygenase (SQLE) that are the rate-limiting enzymes for cholesterol biosynthesis[30 34]. The activity of SCAP is

negatively regulated by five sterol-sensing transmembrane (TM) helices (TM domains 2-6) and by phosphorylation involving the atypical protein kinase C λ/ι (PKCλ/ι) that phosphorylates multiple serine residues of SCAP at the C-terminus[35].

Alteration of key proteins involved in cholesterol regulation, levels in blood and cellular distribution have been implicated in neurodegenerative diseases. In PD, the role of cholesterol in disease progression is unclear as there are conflicting reports about the association between serum cholesterol levels and PD risk[36-41]. However, the levels of cholesterol and their cellular impact in PD neurons remain unexplored.

Here, we investigated cholesterol regulation in PINK1 LOF DaNs. An unbiased phosphoproteomics screen revealed reduced phosphorylation of SCAP at Ser822 and Ser838 in PINK1 knockout (KO) and PINK1-Q456X PD neurons. Reduced regulation by phosphorylation, stabilized SCAP, enhanced cholesterol biosynthesis, and led to cholesterol accumulation at plasma membrane and in Flotillin 1 (FLOT1) rich lipid rafts. Elevated cholesterol disrupted dopamine transporter (DAT) distribution and impaired neurotransmitter uptake. Notably, both genetic restoration of wildtype (WT) PINK1 and pharmacological cholesterol lowering with simvastatin or β-cyclodextrin (βCD) rescued these phenotypes. Our findings identify regulation of cholesterol homeostasis as a previously unrecognized role of PINK1, mediated through SCAP phosphorylation, and suggest that targeting cholesterol metabolism may improve neuronal function in PINK1-linked PD.

Materials and methods

Ethics statement

The study was approved by the ethics committee (Institutional Review Board) of the Medical Faculty of the University of Tübingen and the University Clinic Tübingen (146/2009BO1 and 102/2005). A general consent form of the Hertie Institute for Clinical Brain Research Neurobiobank and a project-specific consent form including an information sheet about the study were used. All participants gave written, informed consent. All research adheres to the current, updated version of the Helsinki declaration.

Cell culture

DaN differentiation

PINK1 wildtype (WT) and knockout (KO) iPSCs were previously generated and characterized in Bus et al.[42], PINK1 Q456X and gene corrected (GC) iPSCs from PD patients #1 and #2 were previously generated and characterized in Jarazo et al.[43]. The PINK1 Q126P patient line was previously described in Prestel et al.[44] and gene corrected by our group. These iPSC lines were differentiated by chemical induction using small molecules based on the protocol from Reinhardt, et al,[45] with slight modifications[42]. The experiments were performed on day 21 post-differentiation start.

HeLa cell culture

WT and PINK1 W437X HeLa cells, characterized in Wettengel et al.[46] were maintained in Dulbecco's Modified Eagles Medium: 4.5 g/L glucose (D6429; Sigma-Aldrich) and supplemented with 10% fetal bovine serum and 1% penicillin/streptomycin.

Generation of PINK1 Q126P Gene Corrected iPSCs

The homozygous PINK1 Q126P iPSCs were cultured in mTeSR1 Plus medium (Stem Cell Technologies) on Matrigel (Corning). Endogenous expression of Cas9 was established by introducing a doxycycline-inducible Cas9 construct (Addgene 12551,[47]) within safe-harbour AAVS1 locus using plasmid-mediated HDR and Crispr-Cas9 in homozygous PINK1 Q126P iPSCs. A detailed description is given in the Supplementary methods.

PINK1 KO mice

PINK1 KO mice, previously described in Glasl et al. [48], were used at 4 months (young) and 16 months (old) of age and bred in accordance with the regulations from the government of Upper Bavaria. The mice were kept on a C57BL/6J background and on an inverse 12-h light/12-h dark cycle (lights off at 18:00). Mice were provided with ad libitum access to standard chow and water. Mice were killed by cervical dislocation and the brains immediately removed. Thereafter, single-brain regions were dissected and the tissue shock frozen in liquid nitrogen.

Cell Treatments

***Cycloheximide treatment*:** To check for protein stability, cells were treated with 100 µM cycloheximide solution (CHX; 239765; Calbiochem, Merck Chemicals GmbH, an

affiliate of Merck KGaA, Darmstadt, Germany) with an equal volume of DMSO used as a vehicle.

***Mitophagy induction*:** Mitochondria were depolarized using 100 µM Antimycin A (#A8674-50MG Merck). Equal volumes of 95% ethanol were added as vehicle.

***Simvastatin*:** Simvastatin was used at 10 µM concentration. The powder (#S1792, Selleckchem) was resuspended in ethanol and stored at -80ºC. For each experiment, 200 µL of this solution was added to 300 µL 0.1N NaOH solution and heated for 2h at 50 ºC. Then the pH was adjusted to 7 with HCl and the total volume was adjusted to 1.431 mL. This final solution was freshly prepared before each experiment and kept in the media for 16 hours.

***β-cyclodextrin (βCD)*:** A 1 mM concentration of (2-Hydroxypropyl)-β-cyclodextrin (#H107-5G, Sigma-Aldrich) was freshly made with culture media and added to the cells for 16 hours.

***Cholesterol*:** 100 µM cholesterol (#C3045, Sigma) freshly resuspended in culture media was used to treat the cells and kept for 16 hours.

***DAT inhibitor*:** 10 µM of DAT inhibitor (GBR 12935 dihydrochloride, #0514, Tocris) was resuspended in DMSO and added to cells for 16 hours.

Measurement of Free Cholesterol

The Total Cholesterol Assay Kit (Fluorometric) (STA-390, Cell Biolabs Inc) was used to measure free cholesterol (non esterified) according to manufacturer's instructions. Absolute cholesterol levels were measured using cholesterol standards and normalized to protein input in the lipid extraction. For the mouse brain tissues, free cholesterol levels were normalized to the tissue mass used.

Mass-Spectrometry-Based Phosphoproteomics

For each phosphoproteomics experiment, 1 mg total protein per sample was used. Proteins were reduced with 1 mM dithiothreitol (DTT), which was incubated for one hour at room temperature (RT) while shaking. To stabilize the reduction, 5.5 mM iodoacetamide (IAA) was added and incubated for one hour at RT while shaking in the dark. Samples were pre-digested with Lysyl Endopeptidase (LysC, Wako Chemicals) for 3 hours at RT. Next, four volumes of water were added and proteins were digested

with trypsin (Promega Corporation) overnight. The reaction was stopped the following morning by acidifying the samples using around 0.1% v/v of trifluoroacetic acid. The peptides for proteome and phosphoproteome analysis were desalted and purified using C18 StageTips (Empore). Samples were measured on an Exploris 480 mass spectrometer (Thermo Fisher Scientific) online-coupled to a VanquishNeo UHPLC (Thermo Fisher Scientific). Chromatographic separation was performed on a 20 cm long, 75 µm inner diameter analytical HPLC column (ID PicoTip fused silica emitter; New Objective), packed in-house with ReproSil-Pur C18-AQ 1.9-µm silica beads (Dr Maisch GmbH). The raw data were processed using the MaxQuant program (version 2.2.0.0). The raw spectra were searched against the UniProt Homo sapiens database (104556 entries, downloaded 30.01.2024). The downstream analysis of MaxQuant output data was performed in Perseus (version 2.0.10.0). Contaminants, reversed hits and proteins identified only by site were filtered out. Scatter plots were prepared to assess reproducibility between replicates and Pearson's correlation was calculated. For the proteome, Label-Free Quantification intensity was used to conduct a t-test and the results were displayed in a volcano plot. This was also done for the unnormalized phosphoproteome. To normalize the phosphosites, the t-test difference of the phospho was subtracted from the t-test difference of the proteome. Sites with a difference of 1 or -1 were considered significantly upregulated or downregulated, respectively. The intensity of the phosphorylation (p)-sites from WT and KO was summed, as depicted in a scatter plot. Regulated p-sites underwent a Fisher's exact test based on KEGG. Additional graphical visualization was performed in the R environment (version 4.1.1) and GraphPad (version 8.0.1), while figures were edited using Adobe Illustrator. A detailed description can be found in Supplementary methods.

The mass spectrometry proteomics data have been deposited to the ProteomeXchange Consortium via the PRIDE[49] partner repository with the dataset identifier PXD067740 and 10.6019/PXD067740

Immunofluorescence

Neurons, plated onto coverslips, were fixed using 4% paraformaldehyde solution, washed and blocked for 1 hour at RT. Primary antibodies were added in 0.1% Triton X-100 and 1% bovine serum albumin overnight at 4°. Finally, the coverslips were washed and mounted to slides using Dako fluorescent mounting medium (S3023,

Agilent). Fixed cells were imaged using a standard inverted laser scanning Olympus FV 3000 confocal microscope. Representative images of the cells are shown in the figures with equal and optimal adjustment of brightness and contrast for better visualization.

Primary antibodies include SREBP2 (#28212-1-AP, Proteintech) at 1:500, FLOT1 (#18634, Cell Signaling) at 1:500, DAT (#22524-1-AP, Proteintech) at 1:500 and TOM20 (#sc11415, SantaCruz Biotechnology) at 1:200. Recombinant Clostridium perfringens Perfringolysin O (PFO) tagged with 6xHis (#CSB-EP314820CMB, Hölzel Diagnostika Handels GmbH) and resuspended in 1:1 ratio of water:glycerol to make a 1 mg/mL stock concentration and stored at -20^{o}C. PFO was used at 2.5 µg/mL final concentration onto coverslips. The NR12A dye, a kind gift from Dr. Andrey Klymchenko (University of Strasbourg, France) was used at 40 nM and incubated for 7 minutes. Following the incubation, the media was changed to phenol red free and live-cell imaging was performed using a Leica DMi8 epifluorescence microscope and images were captured using the LASX software. A detailed description can be found in Supplementary methods.

Immunoblotting

SDS-PAGE gel and protein transfer was followed by blot incubation with primary antibodies – HMGCR (NBP2-66888, Novus Biologicals) at 1:500, SQLE (12544-1-AP, Proteintech) at 1:500, INSIG2 (24766-1-AP, Proteintech) at 1:500, SCAP (PA5-28982, Invitrogen) at 1:500, Miro1 (NBP1-89011, Novus Biologicals) at 1:500, MFN2 (H00009927-M01, Abnova) at 1:500, β3-tubulin (801202, Biolegend) at 1:5000, Vinculin (V9131, Sigma) at 1:2000, GAPDH (CB1001, Sigma) at 1:5000, PKCλ/ι (610208, Biolegend) at 1:500 and PINK1 (846202, Biolegend) at 1:500. Bands were detected with Odyssey CLx (LI-COR) using Image Studio software (LICOR). The band intensities were normalized to a total protein stain – ponceau S solution (#A2935, PanReac AppliChem ITW Reagents) unless otherwise mentioned in the quantification as housekeeping genes – GAPDH and Vinculin were also used for some blots. Image Studio Lite Ver 5.2 (Licor) was used for the quantification of the intensity of bands. A detailed description can be found in Supplementary methods.

Neurotransmitter Uptake Assay

Neurotransmitter transporter activity in DaNs was measured using the Neurotransmitter Transporter Uptake Assay Kit (#R8174, Molecular Devices) according to the manufacturer's instructions. Mature DaNs were seeded in Matrigel-coated black, clear bottom 96 well plates prior to the assay at a density of 60,000 cells/well. DaNs were treated with the specific DAT inhibitor GBR 12935 dihydrochloride. Uptake fluorescence was measured using the SpectraMax M2e microplate reader in kinetic mode (Molecular Devices) measuring every 30 s. After the assay, the DaNs were washed and fixed in 4% (v/v) performic acid containing Hoechst to account for cell number in each well.

Lipidomics.

Lipidomics of whole DaNs from independent differentiations (n=3) were performed according to the exact method described in Xicoy et al.[50]

Mitochondrial Respiration

For the basic mitochondrial stress test, Oxygen Consumption Rate (OCR) and Extracellular Acidification Rate (ECAR)were measured in DaNs using a Seahorse™ XF96 Extracellular Flux Analyzer. Cells were seeded in Matrigel-coated Seahorse cell plates 24-48 h prior to the experiment. A detailed description can be found in Supplementary methods.

Immunoprecipitation (IP)

A non-denaturing lysis buffer was used containing 20 mM Tris HCl at pH 8, 137 mM NaCl, 10% glycerol, 1% NP-40 and 2 mM EDTA solution. cOmplete protease inhibitor (#11873580001; Sigma) and PhosStop phosphatase inhibitor (#4906837001; Sigma) were added before use. Lysed cells were centrifuged at 15000g for 20 minutes at 4 ^{o}C and the supernatant was collected. 1 µg of SCAP polyclonal antibody (PA5-28982, Invitrogen) was added to 1000 µg of total protein and incubated under constant agitation overnight at 4 ^{o}C. The next day, 50 µL of Protein A Sepharose beads was added to the solution and incubated under constant agitation for 4 h at 4 ^{o}C. A detailed description can be found in Supplementary methods.

Lipid Order Measurement

NR12A dye, described in Danylchuk et al. [51], a kind gift from Dr. Andrey Klymchenko (University of Strasbourg, France) was used at 40 nM and incubated for 7 minutes. Fluorescence was measured using SpectraMax M2e microplate reader with 10 flashes per well in an endpoint reading mode. The excitation wavelength was set at 520 nm and emissions at 560 nm and 630 nm.

Statistics

For statistical analyses, GraphPad Prism version 8.4.0 was used. The data is presented as mean +/- standard error of mean (SEM) (*$P < 0.05$; **$P < 0.005$; ***$P < 0.0005$; ****$P < 0.0001$; nsP > 0.05, where ns represents non-significant). Statistical comparisons between more than two conditions were analyzed using an ordinary one-way ANOVA with Tukey's multiple comparisons tests. Statistical significance between two conditions were determined using unpaired t-test, two-tailed.

Results

PINK1 LOF DaNs have reduced SCAP phosphorylation at S822 and S838

To uncover molecular alterations caused by PINK1 LOF, we performed mass spectrometry–based phosphoproteomics in human DaNs carrying either a PINK1 knockout (KO) or the PD patient-derived PINK1 Q456X mutation, each compared to its isogenic control (Fig. 1A-C, Fig. S1A–D). Across all conditions, we consistently quantified around 2000 proteins, with no significant changes (Fig S1A; Supplementary Table 1). A total of 13000 p-sites with a localization probability above 75% were identified, with around 6500 p-sites per condition (Fig S1B; Supplementary Table 1). Among these, SCAP was identified in both PINK1 LOF DaNs having reduced phosphorylation at Ser822 and Ser838 (Supplementary Table 1). Manual inspection of the corresponding annotated MS/MS spectra confirmed the presence and precise localization of these p-sites (Fig S2). Of note, the modified serine residues were assigned as Ser429 and Ser445 in Supplementary Table 1. Mapping of the peptide sequence to UniProt canonical SCAP sequence (Q12770-1) revealed that this residue corresponds to Ser822 and Ser838 respectively having a localization probability > 0.95. We therefore refer to this site as SCAP Ser822 and Ser838 throughout the manuscript. Since no phosphorylation was identified at SCAP Ser 822 and S838 in PINK1 LOF DaNs, it was not possible to include these sites in Fig 1B-C.

Some of the other differentially phosphorylated proteins identified in PINK1 LOF DaNs included CLASP1 (S598), CLASP2 (S455), MAP1B (S23), and KLC4 (S163), which are associated with microtubule regulation; PAK2 (T169) and DAB2IP (S728), which participate in dendrite development; TBC1D5 (S539) and WDR44 (T94), which function in the endo-lysosomal system; PPME1 (S25) and PPP1R37 (S560), which contribute to protein dephosphorylation and SLC4A7 (S1109) which is involved in the regulation of de novo purine and pyrimidine synthesis downstream of mTORC1 signaling (Supplementary Table 1, Fig 1B-C).

PINK1 LOF DaNs have increased cholesterol biosynthesis due to increased SCAP stability

Since C-terminal SCAP phosphorylation regulates its stability and interaction with SREBP2[30], we examined SREBP2 localization. In PINK1 KO DaNs, SREBP2 puncta accumulated in the nucleus compared to the cytosol (Fig. 1D–E), consistent with activation of cholesterol biosynthesis. Immunoblotting revealed upregulation of SQLE and downregulation of INSIG2, whereas HMGCR levels remained unchanged (Fig. 1F–I). As a control we treated DaNs with βCD, a chemical that hydrolyses cholesterol and induces cholesterol biosynthesis.

To show that cholesterol biosynthesis is regulated by PINK1 and not due to clonal artefacts, we expressed WT PINK1 and 3x-kinase-dead (3xKD) mutant PINK1 in PINK1 KO neurons using lentivirus and blotted for HMGCR, SQLE and INSIG2 (Fig S3A-E). Expression of WT PINK1, but not a kinase-dead mutant, normalized SQLE and partially restored INSIG2. However, similar to our observation with βCD treatment, protein levels of HMGCR were unaffected by the expression of WT or 3xKD PINK1.

Reduced phosphorylation in the C-terminus of SCAP in the absence of kinase PKCλ/ι has been previously associated with increased cholesterol biosynthesis due to reduced SCAP degradation[35]. Cycloheximide pulse–chase experiments demonstrated increased SCAP stability in PINK1 KO neurons (Fig. 1J–K), while total SCAP and PKCλ/ι levels were unaffected (Fig. S4A–C). PINK1 did not co-immunoprecipitate with SCAP, suggesting regulation is indirect (Fig. S4D). Together, these results identify impaired SCAP phosphorylation and enhanced cholesterol biosynthesis as downstream consequences of PINK1 loss of function.

PINK1 LOF increases neuronal cholesterol that is enriched at the plasma membrane and in flotillin-rich lipid rafts

PINK1 has multiple domains including a mitochondrial targeting sequence (MTS), and the TM, the N-terminal (NT), the kinases lobes and the C-terminal region (CTR) (Fig 2A). To gain insights into the pathomechanism, we measured cholesterol content across multiple PINK1 mutations (affecting multiple domains) and LOF models. Free cholesterol was elevated in PINK1 KO and PINK1 Q456X DaNs but not in PINK1 Q126P DaNs (mutation in the N-terminal domain) or in HeLa cells harboring endogenous PINK1 W437X (Fig. 2B–F), suggesting a kinase-domain and neuron-specific phenotype. In PINK1 KO mice, increased striatal cholesterol was observed in young mice but not in the old/adult mice (Fig 2G), consistent with developmental-stage neuronal cholesterol synthesis. In accordance with PD pathology, the ventral midbrain region did not have altered cholesterol both in young and old mice (Fig 2H).

Whole cell lipidomics in PINK1 WT and KO DaNs covering other major lipid classes - phosphatidylglycerol (PG), bis(monoacylglycerol)phosphate (BMP), phosphatidylinositol (PI), phosphatidylethanolamine (PE), phosphatidylserine (PS), phosphatidylcholine (PC), sphingomyelin (SM), lysophosphatidylethanolamine (LPE), cardiolipin (CL), ceramide (Cer) -, revealed no significant alterations (Fig S5).

We next sought to find where in the neurons the level of cholesterol is increased. As the majority of cholesterol is found in the plasma membrane, we used a dye (NR12A) that specifically stains the plasma membrane in live cells. We found that PINK1 KO neurons have increased NR12A binding at the plasma membrane compared to WT neurons (Fig 2I). We also determined the lipid order ratio, using NR12A quantification with a plate reader assay, and found a significant increase in lipid order ratio in PINK1 KO neurons (Fig 2J). Cholesterol was added to the media as a positive control. Additionally, the cholesterol-lowering agents simvastatin and βCD rescued the lipid order ratio.

To visualize if excess cholesterol is also present within the subcellular compartments, we co-stained the neurons with PFO, a toxin that binds to cholesterol[52], and FLOT1 (a marker for lipid rafts) (Fig 2K). This revealed increased PFO puncta in PINK1 KO neurons that colocalized to FLOT1. Additionally, the signal intensity of FLOT1 is also higher in PINK1 KO neurons suggesting internalization of lipid rafts. By contrast, PFO

did not colocalize with mitochondria (Fig. S6), consistent with their normally low cholesterol content. Thus, PINK1 loss specifically drives plasma membrane and FLOT1-rich lipid raft cholesterol accumulation.

Cholesterol accumulation is independent of mitophagy and does not affect mitochondrial respiration

Since PINK1 regulates mitophagy, we tested whether altered cholesterol levels were linked to this pathway. Antimycin A–induced mitochondrial depolarization failed to trigger degradation of the canonical mitophagy markers Miro1 and MFN2 in PINK1 KO DaNs (Fig. 3A–C), confirming impaired mitophagy.

The upregulation of cholesterol has been previously shown to inhibit mitophagy[53 54]. However, the levels of cholesterol during mitophagy initiation and whether impaired mitophagy has any effect on cholesterol levels have not been previously studied. Hence, we assessed free cholesterol levels upon mitophagy induction using Antimycin A. However, free cholesterol levels remained unchanged during mitophagy induction (Fig. 3D).

We then assessed whether cholesterol modulates mitochondrial respiration. Seahorse analysis revealed reduced maximal respiration and spare respiratory capacity in PINK1 KO DaNs, while basal and non-mitochondrial respiration were unaffected (Fig. 3E–J). This would suggest that mitochondria are unable to reach their full capacity in the absence of PINK1 as spare respiratory capacity and maximal respiration depends on multiple parameters including the integrity of electron transport chain complexes, the ability of mitochondria to oxidize energetic substrates and mitochondrial health in general[55]. Neither cholesterol depletion nor supplementation altered respiratory parameters. These findings indicate that cholesterol dysregulation in PINK1 neurons occurs independently of mitophagy and does not directly impair basal mitochondrial respiration.

Excess cholesterol disrupts DAT distribution and neurotransmitter uptake

Cholesterol-rich lipid rafts regulate trafficking of DAT, which contains a cholesterol-binding domain and is internalized through FLOT1-positive microdomains. In PINK1 KO DaNs, DAT redistributed from the plasma membrane to perinuclear regions, partially overlapping with PFO-positive cholesterol puncta (Fig. 4A). Cholesterol depletion with simvastatin or βCD restored normal DAT localization.

Due to altered DAT distribution and increased cholesterol at the plasma membranes, we performed a neurotransmitter uptake assay (Fig 4B) and found it to be significantly reduced in PINK1 KO DaNs (Fig 4C). This defect was rescued by cholesterol-lowering treatments and was largely DAT dependent, as shown by pharmacological inhibition (Fig 4C). These results demonstrate that cholesterol accumulation in PINK1 LOF neurons disrupts DAT trafficking and impairs dopaminergic function.

Discussion

By integrating phosphoproteomics and functional assays in multiple PINK1 models, we identify reduced phosphorylation of SCAP at Ser822 and Ser838 as an early event in PINK1-deficient neurons. This reduction stabilizes SCAP, enhances cholesterol biosynthesis, and drives cholesterol accumulation in plasma membrane and FLOT1-rich lipid rafts, with downstream disruption of DAT distribution and neurotransmitter uptake.

SCAP stability is normally controlled by C-terminal phosphorylation, which promotes its ubiquitination and degradation via the proteasome[32]. We observed reduced phosphorylation of SCAP, increased SREBP2 in the nucleus, and reduced INSIG2 and increased SQLE protein levels in PINK1 LOF neurons, consistent with enhanced cholesterol biosynthesis. Basal SCAP and PKCλ/ι levels were unaffected, raising the possibility that additional kinases or altered post-translational regulation underlie the defect in SCAP phosphorylation.

The physical and biochemical communication between mitochondria and ER at mitochondria-ER contacts sites have been shown to regulate calcium homeostasis[22], mitochondria dynamics and energetics[56], apoptosis[57], and cholesterol metabolism[58], among others[59]. Identifying the molecular composition and phosphorylation-dependent regulation of these contacts could clarify how PINK1 LOF perturbs cholesterol metabolism in neurons.

A-kinase anchor protein 11 (AKAP11) was another candidate that had reduced phosphorylation at Thr1100 in PINK1 LOF DaNs. It has been reported that astrocytes lacking AKAP11 have upregulated lipid metabolism and an accumulation of esterified cholesterol[60]. While it is not known how phosphorylation of AKAP11 at Thr1100 affects its activity, it has been predicted that PKA and AKAP11 phosphorylates large ribosomal protein 34 (RPL34) at Ser12[61]. Since we also observe a significant downregulation of RPL34 phosphorylation at Ser12 in both PINK1 LOF DaNs, we hypothesize that AKAP11 Thr1100 could impair its activity and may also play a role in cholesterol regulation in PINK1 LOF DaNs.

No differences in cholesterol levels were detected in PINK1 Q126P DaNs. Unlike the Q456X mutation, which resides in the kinase domain, Q126P affects the NT domain of PINK1. This mutation has been reported to disrupt NT–CTR interactions, thereby preventing PINK1 autophosphorylation and stabilization at the outer mitochondrial membrane[62]. Another mutation in the TM region, R98W, alters protein positioning or processing and, in contrast, increases mitophagy through PINK1 accumulation at the outer mitochondrial membrane[63]. Since Q126P does not directly affect the kinase domain, it remains unclear whether its substrate phosphorylation activity is impaired. This underscores the need for further studies to dissect the specific consequences of Q126P and other NT/TM PINK1 mutations.

Cholesterol accumulation has been shown to impair PINK1-Parkin-dependent mitophagy by reducing optineurin recruitment and lysosomal clearance, a phenotype observed in Alzheimer's disease across several model systems and in *post mortem* brain tissue despite elevated PINK1/Parkin signaling[53 54]. A genome-wide RNAi screen further identified SREBP1 and SREBP2 as key regulators of mitophagy induction, acting by stabilizing PINK1 and promoting Parkin translocation to the mitochondria[64]. These findings suggest that, by disrupting lysosomal clearance, excess cholesterol may impose an additional burden on mitophagy in PINK1 LOF neurons. Moreover, PINK1/Parkin-independent mechanisms for mitochondrial clearance could also be compromised under conditions of cholesterol accumulation.

DAT has six Cholesterol Recognition Amino acid Consensus (CRAC) motifs[65] through which it can interact with plasma membrane cholesterol/cholesterol-rich lipid rafts. Our study has identified functional consequences of cholesterol accumulation in the

plasma membrane. DAT mislocalization to perinuclear regions and its possible partial sequestration into cholesterol-rich rafts impaired neurotransmitter uptake. Restoring the cholesterol balance with simvastatin or βCD corrected these defects, supporting a causal role for cholesterol accumulation. Using super-resolution microscopy, a similar DAT distribution has also been observed in neurons following cholesterol depletion[66]. Interestingly, βCD has also previously been shown to improve differentiation efficiency, bioenergetic profiles and neuronal firing in PINK1 neuronal and midbrain organoid PD models[43]. Our findings align with clinical and preclinical observations that DAT dysregulation precedes neurodegeneration and highlight the contribution of cholesterol homeostasis to dopaminergic vulnerability[67].

Cholesterol-rich lipid rafts organize signaling and trafficking in neurons[68]. Our observation that FLOT1-positive rafts are increased in PINK1 LOF neurons parallels prior links between lipid rafts and PD-related proteins including α-synuclein, LRRK2, DJ-1, Parkin, and PINK1 itself[69-73]. Notably, loss of Parkin also promotes cholesterol-dependent raft internalization[74], suggesting convergent lipid regulatory mechanisms across genetic forms of PD.

In summary, we identify reduced SCAP phosphorylation at Ser822 and Ser838 and consequent cholesterol accumulation as early pathogenic features of PINK1 LOF neurons. By linking cholesterol homeostasis to dopaminergic dysfunction, this work expands the biological repertoire of PINK1 beyond mitochondrial quality control and suggests that targeting cholesterol metabolism could modify disease onset or progression in PINK1-related PD.

Implications and limitations

iPSC-derived DaN model system mimics early stages of neurogenesis, differentiation and maturation, and do not recapitulate aging. We show that these young PINK1 LOF DaNs have increased cholesterol biosynthesis and levels. However, adult neurons do not synthesize their own cholesterol, instead they take in cholesterol predominantly from astrocytes. It is possible that PINK1 astrocytes also exhibit impaired cholesterol homeostasis and future work in astrocytes could be helpful to understand the relevance of cholesterol in PINK1 LOF.

Nonetheless, we observed increased cholesterol levels in the striatum only in the young PINK1 KO mice but not in older mice. This would suggest that this impaired cholesterol homeostasis phenotype could only be present early in the brain when the onset of PD might not be evident. Direct transdifferentiation to human DaNs and/or astrocytes will be useful to understand the relevance of age and cholesterol homeostasis in PINK1 PD.

Acknowledgements

We thank the study participants, spouses and PD patients who have donated samples to the Hertie Institute for Clinical Brain Research NeuroBiobank. Without their participation, basic research into neuronal mechanisms of disease would not be possible. We thank Nicolas Snaidero, University of Tübingen for providing support with Olympus FV3000 confocal microscopy. We thank the HIH-CIN Imaging Cluster of Microscopy, Core Facility of the Medical Faculty at the University of Tübingen for providing support (especially Olga Oleksiuk) and instrumentation with Leica Dmi8 epifluorescence microscopy. We thank Andrey Klymchenko, University of Strasbourg, France for sharing NR12A dye. We thank Ulrich Rothbauer, University of Tübingen for sharing pLenti6/V5-DEST plasmid with us. pLenti6-DEST PINK1-V5 WT and pLenti6-DEST PINK1-V5 KD were a gift from Mark Cookson, National Institute of Aging, NIH, Bethesda. We thank Jens Schwamborn, Luxembourg Centre for Systems Biomedicine, Luxembourg and Christine Klein, Institute of Neurogenetics, University of Lübeck, Germany for kindly sharing PINK1 Q456X patient and isogenic gene control cell lines with us.

Author Contributions

Karan Sharma: conceptualization, methodology, validation, formal analysis, investigation, writing—original draft, writing—review and editing, and visualization. Claudia Cavarischia Rega: Methodology, formal analysis, investigation, writing—review and editing, and visualization. Dina Ivanuik – Methodology. Christine Fröhlich (née Bus): Methodology, formal analysis and investigation. Jos F. Brouwers: Methodology and formal analysis. Gerard Martens: Methodology and formal analysis. Philipp Seibler: Resources, writing-review and editing. Javier Jarazo: Resources,

writing-review and editing. Thomas Gasser: Resources, writing-review and editing. Daniela M. Vogt Weisenhorn: Resources, writing-review and editing. Boris Macek: Resources, project administration, supervision, writing-review and editing. Julia C. Fitzgerald: conceptualization, methodology, resources, validation, formal analysis, investigation, writing-original draft, writing-review and editing, project administration, supervision, and funding acquisition.

Funding

The work was supported by the DFG, German Research Council, Research Training Group (MOMbrane 654651/GRK2364).

Competing interests

The authors declare no conflict of interest.

Supplementary material

This article contains supplemental data.

References

1. Valente EM, Abou-Sleiman PM, Caputo V, et al. Hereditary early-onset Parkinson's disease caused by mutations in PINK1. *Science* 2004;304(5674):1158-60. doi: 10.1126/science.1096284 [published Online First: 20040415]
2. Schneider SA, Klein C. PINK1 Type of Young-Onset Parkinson Disease. In: Adam MP, Mirzaa GM, Pagon RA, et al., eds. GeneReviews((R)). Seattle (WA)1993.
3. Samaranch L, Lorenzo-Betancor O, Arbelo JM, et al. PINK1-linked parkinsonism is associated with Lewy body pathology. *Brain* 2010;133(Pt 4):1128-42. doi: 10.1093/brain/awq051 [published Online First: 20100330]
4. Takanashi M, Li Y, Hattori N. Absence of Lewy pathology associated with PINK1 homozygous mutation. *Neurology* 2016;86(23):2212-3. doi: 10.1212/WNL.0000000000002744 [published Online First: 20160504]
5. Geisler S, Holmstrom KM, Skujat D, et al. PINK1/Parkin-mediated mitophagy is dependent on VDAC1 and p62/SQSTM1. *Nat Cell Biol* 2010;12(2):119-U70. doi: 10.1038/ncb2012
6. Kane LA, Lazarou M, Fogel AI, et al. PINK1 phosphorylates ubiquitin to activate Parkin E3 ubiquitin ligase activity. *J Cell Biol* 2014;205(2):143-53. doi: 10.1083/jcb.201402104
7. Kazlauskaite A, Kondapalli C, Gourlay R, et al. Parkin is activated by PINK1-dependent phosphorylation of ubiquitin at Ser65. *Biochem J* 2014;460(1):127-39. doi: 10.1042/BJ20140334

8. Kondapalli C, Kazlauskaite A, Zhang N, et al. PINK1 is activated by mitochondrial membrane potential depolarization and stimulates Parkin E3 ligase activity by phosphorylating Serine 65. *Open Biol* 2012;2 doi: ARTN 120080

10.1098/rsob.120080
9. Koyano F, Okatsu K, Kosako H, et al. Ubiquitin is phosphorylated by PINK1 to activate parkin. *Nature* 2014;510(7503):162-+. doi: 10.1038/nature13392
10. Lazarou M, Jin SM, Kane LA, et al. Role of PINK1 binding to the TOM complex and alternate intracellular membranes in recruitment and activation of the E3 ligase Parkin. *Dev Cell* 2012;22(2):320-33. doi: 10.1016/j.devcel.2011.12.014 [published Online First: 20120125]
11. Okatsu K, Oka T, Iguchi M, et al. PINK1 autophosphorylation upon membrane potential dissipation is essential for Parkin recruitment to damaged mitochondria. *Nat Commun* 2012;3 doi: ARTN 1016

10.1038/ncomms2016
12. Ordureau A, Sarraf SA, Duda DM, et al. Quantitative Proteomics Reveal a Feedforward Mechanism for Mitochondrial PARKIN Translocation and Ubiquitin Chain Synthesis. *Mol Cell* 2014;56(3):360-75. doi: 10.1016/j.molcel.2014.09.007
13. Rasool S, Veyron S, Soya N, et al. Mechanism of PINK1 activation by autophosphorylation and insights into assembly on the TOM complex. *Mol Cell* 2022;82(1):44-+. doi: 10.1016/j.molcel.2021.11.012
14. Shiba-Fukushima K, Imai Y, Yoshida S, et al. PINK1-mediated phosphorylation of the Parkin ubiquitin-like domain primes mitochondrial translocation of Parkin and regulates mitophagy. *Sci Rep-Uk* 2012;2 doi: ARTN 1002

10.1038/srep01002
15. Trempe JF, Gehring K. Structural Mechanisms of Mitochondrial Quality Control Mediated by PINK1 and Parkin. *J Mol Biol* 2023:168090. doi: 10.1016/j.jmb.2023.168090 [published Online First: 20230412]
16. Wang X, Winter D, Ashrafi G, et al. PINK1 and Parkin target Miro for phosphorylation and degradation to arrest mitochondrial motility. *Cell* 2011;147(4):893-906. doi: 10.1016/j.cell.2011.10.018
17. Wauer T, Simicek M, Schubert A, et al. Mechanism of phospho-ubiquitin-induced PARKIN activation. *Nature* 2015;524(7565):370-+. doi: 10.1038/nature14879
18. Youle RJ, Narendra DP. Mechanisms of mitophagy. *Nat Rev Mol Cell Biol* 2011;12(1):9-14. doi: 10.1038/nrm3028
19. Lechado-Terradas A, Schepers S, Zittlau KI, et al. Parkin-dependent mitophagy occurs via proteasome-dependent steps sequentially targeting separate mitochondrial sub-compartments for autophagy. *Autophagy Reports* 2022;1(1):576-602. doi: 10.1080/27694127.2022.2143214
20. Zittlau KI, Lechado-Terradas A, Nalpas N, et al. Temporal Analysis of Protein Ubiquitylation and Phosphorylation During Parkin-Dependent Mitophagy. *Mol Cell Proteomics* 2022;21(2):100191. doi: 10.1016/j.mcpro.2021.100191 [published Online First: 20211230]
21. Wang R, Fortier TM, Chai F, et al. PINK1, Keap1, and Rtnl1 regulate selective clearance of endoplasmic reticulum during development. *Cell* 2023;186(19):4172-88 e18. doi: 10.1016/j.cell.2023.08.008 [published Online First: 20230825]

22. Ham SJ, Yoo H, Woo D, et al. PINK1 and Parkin regulate IP(3)R-mediated ER calcium release. *Nat Commun* 2023;14(1):5202. doi: 10.1038/s41467-023-40929-z [published Online First: 20230825]
23. Celardo I, Costa AC, Lehmann S, et al. Mitofusin-mediated ER stress triggers neurodegeneration in pink1/parkin models of Parkinson's disease. *Cell Death Dis* 2016;7(6):e2271. doi: 10.1038/cddis.2016.173 [published Online First: 20160623]
24. Cui Y, Wen X, Nan Y, et al. Overexpressed PERK suppresses the neurodegenerative phenotypes in PINK1(B9) flies by enhancing mitochondrial function. *Neurochem Int* 2020;140:104825. doi: 10.1016/j.neuint.2020.104825 [published Online First: 20200906]
25. Grossmann D, Malburg N, Glass H, et al. Mitochondria-Endoplasmic Reticulum Contact Sites Dynamics and Calcium Homeostasis Are Differentially Disrupted in PINK1-PD or PRKN-PD Neurons. *Mov Disord* 2023;38(10):1822-36. doi: 10.1002/mds.29525 [published Online First: 20230714]
26. Shin KC, Ali Moussa HY, Park Y. Cholesterol imbalance and neurotransmission defects in neurodegeneration. *Exp Mol Med* 2024;56(8):1685-90. doi: 10.1038/s12276-024-01273-4 [published Online First: 20240801]
27. Zhang J, Liu Q. Cholesterol metabolism and homeostasis in the brain. *Protein Cell* 2015;6(4):254-64. doi: 10.1007/s13238-014-0131-3 [published Online First: 20150215]
28. Genaro-Mattos TC, Anderson A, Allen LB, et al. Cholesterol Biosynthesis and Uptake in Developing Neurons. *ACS Chem Neurosci* 2019;10(8):3671-81. doi: 10.1021/acschemneuro.9b00248 [published Online First: 20190619]
29. Funfschilling U, Jockusch WJ, Sivakumar N, et al. Critical time window of neuronal cholesterol synthesis during neurite outgrowth. *J Neurosci* 2012;32(22):7632-45. doi: 10.1523/JNEUROSCI.1352-11.2012
30. Brown MS, Radhakrishnan A, Goldstein JL. Retrospective on Cholesterol Homeostasis: The Central Role of Scap. *Annu Rev Biochem* 2018;87:783-807. doi: 10.1146/annurev-biochem-062917-011852 [published Online First: 20170825]
31. Song BL, Javitt NB, DeBose-Boyd RA. Insig-mediated degradation of HMG CoA reductase stimulated by lanosterol, an intermediate in the synthesis of cholesterol. *Cell Metab* 2005;1(3):179-89. doi: 10.1016/j.cmet.2005.01.001
32. Sever N, Yang T, Brown MS, et al. Accelerated degradation of HMG CoA reductase mediated by binding of insig-1 to its sterol-sensing domain. *Mol Cell* 2003;11(1):25-33. doi: 10.1016/s1097-2765(02)00822-5
33. Yan RH, Cao PP, Song WQ, et al. A structure of human Scap bound to Insig-2 suggests how their interaction is regulated by sterols. *Science* 2021;371(6533):1012-+. doi: ARTN eabb2224

10.1126/science.abb2224
34. Luo J, Yang H, Song BL. Mechanisms and regulation of cholesterol homeostasis. *Nat Rev Mol Cell Biol* 2020;21(4):225-45. doi: 10.1038/s41580-019-0190-7 [published Online First: 20191217]
35. Muta Y, Linares JF, Martinez-Ordonez A, et al. Enhanced SREBP2-driven cholesterol biosynthesis by PKClambda/iota deficiency in intestinal epithelial cells promotes aggressive serrated tumorigenesis. *Nat Commun* 2023;14(1):8075. doi: 10.1038/s41467-023-43690-5 [published Online First: 20231213]

36. Al-Kuraishy HM, Al-Gareeb AI, Alexiou A, et al. Pros and cons for statins use and risk of Parkinson's disease: An updated perspective. *Pharmacol Res Perspect* 2023;11(2):e01063. doi: 10.1002/prp2.1063
37. Alrouji M, Al-Kuraishy HM, Al-Mahammadawy AAA, et al. The potential role of cholesterol in Parkinson's disease neuropathology: perpetrator or victim. *Neurol Sci* 2023;44(11):3781-94. doi: 10.1007/s10072-023-06926-2 [published Online First: 20230710]
38. Gao X, Simon KC, Schwarzschild MA, et al. Prospective study of statin use and risk of Parkinson disease. *Arch Neurol* 2012;69(3):380-4. doi: 10.1001/archneurol.2011.1060
39. Hu G. Total cholesterol and the risk of Parkinson's disease: a review for some new findings. *Parkinsons Dis* 2010;2010:836962. doi: 10.4061/2010/836962 [published Online First: 20091110]
40. Jeong SH, Chung SJ, Yoo HS, et al. Differential effects of cholesterol levels on cognition according to body mass index in Parkinson's disease. *Alzheimers Res Ther* 2024;16(1):24. doi: 10.1186/s13195-023-01326-2 [published Online First: 20240131]
41. Correction to "Pros and cons for statins use and risk of Parkinson's disease: An updated perspective". *Pharmacol Res Perspect* 2024;12(3):e1221. doi: 10.1002/prp2.1221
42. Bus C, Zizmare L, Feldkaemper M, et al. Human Dopaminergic Neurons Lacking PINK1 Exhibit Disrupted Dopamine Metabolism Related to Vitamin B6 Co-Factors. *iScience* 2020;23(12):101797. doi: 10.1016/j.isci.2020.101797 [published Online First: 20201113]
43. Jarazo J, Barmpa K, Modamio J, et al. Parkinson's Disease Phenotypes in Patient Neuronal Cultures and Brain Organoids Improved by 2-Hydroxypropyl-beta-Cyclodextrin Treatment. *Mov Disord* 2022;37(1):80-94. doi: 10.1002/mds.28810 [published Online First: 20211012]
44. Prestel J, Gempel K, Hauser TK, et al. Clinical and molecular characterisation of a Parkinson family with a novel PINK1 mutation. *J Neurol* 2008;255(5):643-48. doi: 10.1007/s00415-008-0763-4
45. Reinhardt P, Glatza M, Hemmer K, et al. Derivation and expansion using only small molecules of human neural progenitors for neurodegenerative disease modeling. *PLoS One* 2013;8(3):e59252. doi: 10.1371/journal.pone.0059252 [published Online First: 20130322]
46. Wettengel J, Reautschnig P, Geisler S, et al. Harnessing human ADAR2 for RNA repair - Recoding a PINK1 mutation rescues mitophagy. *Nucleic Acids Res* 2017;45(5):2797-808. doi: 10.1093/nar/gkw911
47. Mair B, Tomic J, Masud SN, et al. Essential Gene Profiles for Human Pluripotent Stem Cells Identify Uncharacterized Genes and Substrate Dependencies. *Cell Rep* 2019;27(2):599-615 e12. doi: 10.1016/j.celrep.2019.02.041
48. Glasl L, Kloos K, Giesert F, et al. Pink1-deficiency in mice impairs gait, olfaction and serotonergic innervation of the olfactory bulb. *Exp Neurol* 2012;235(1):214-27. doi: 10.1016/j.expneurol.2012.01.002
49. Perez-Riverol Y, Bandla C, Kundu DJ, et al. The PRIDE database at 20 years: 2025 update. *Nucleic Acids Res* 2025;53(D1):D543-D53. doi: 10.1093/nar/gkae1011
50. Xicoy H, Brouwers JF, Kalnytska O, et al. Lipid Analysis of the 6-Hydroxydopamine-Treated SH-SY5Y Cell Model for Parkinson's Disease. *Mol*

Neurobiol 2020;57(2):848-59. doi: 10.1007/s12035-019-01733-3 [published Online First: 20190906]
51. Danylchuk DI, Moon S, Xu K, et al. Switchable Solvatochromic Probes for Live-Cell Super-resolution Imaging of Plasma Membrane Organization. *Angew Chem Int Edit* 2019;58(42):14920-24. doi: 10.1002/anie.201907690
52. Waheed AA, Shimada Y, Heijnen HF, et al. Selective binding of perfringolysin O derivative to cholesterol-rich membrane microdomains (rafts). *Proc Natl Acad Sci U S A* 2001;98(9):4926-31. doi: 10.1073/pnas.091090798 [published Online First: 20010417]
53. Roca-Agujetas V, Barbero-Camps E, de Dios C, et al. Cholesterol alters mitophagy by impairing optineurin recruitment and lysosomal clearance in Alzheimer's disease. *Mol Neurodegener* 2021;16(1):15. doi: 10.1186/s13024-021-00435-6 [published Online First: 20210308]
54. Roca-Agujetas V, de Dios C, Abadin X, et al. Upregulation of brain cholesterol levels inhibits mitophagy in Alzheimer disease. *Autophagy* 2021;17(6):1555-57. doi: 10.1080/15548627.2021.1920814 [published Online First: 20210504]
55. Desler C, Hansen TL, Frederiksen JB, et al. Is There a Link between Mitochondrial Reserve Respiratory Capacity and Aging? *J Aging Res* 2012;2012:192503. doi: 10.1155/2012/192503 [published Online First: 20120605]
56. Völgyi K, Juhász G, Kovács Z, et al. Dysfunction of Endoplasmic Reticulum (ER) and Mitochondria (MT) in Alzheimer's Disease: The Role of the ER-MT Cross-Talk. *Curr Alzheimer Res* 2015;12(7):655-72. doi: Doi 10.2174/1567205012666150710095035
57. Gelmetti V, De Rosa P, Torosantucci L, et al. PINK1 and BECN1 relocalize at mitochondria-associated membranes during mitophagy and promote ER-mitochondria tethering and autophagosome formation. *Autophagy* 2017;13(4):654-69. doi: 10.1080/15548627.2016.1277309
58. Szabo L, Cummins N, Paganetti P, et al. ER-mitochondria contacts and cholesterol metabolism are disrupted by disease-associated tau protein. *Embo Rep* 2023;24(8) doi: 10.15252/embr.202357499
59. Sammeta SS, Banarase TA, Rahangdale SR, et al. Molecular understanding of ER-MT communication dysfunction during neurodegeneration. *Mitochondrion* 2023;72:59-71. doi: 10.1016/j.mito.2023.07.005
60. Liu X-M, Pribiag H, Misri D, et al. Abnormal Lipid Metabolism and Altered Neuronal Support by Astrocytes Lacking Akap11, a Risk Gene for Schizophrenia and Bipolar Disorder. *bioRxiv* 2025:2025.04.25.650548. doi: 10.1101/2025.04.25.650548
61. Segura-Roman A, Citron YR, Shin M, et al. Autophagosomes anchor an AKAP11-dependent regulatory checkpoint that shapes neuronal PKA signaling. *Embo Journal* 2025;44(11):3150-79. doi: 10.1038/s44318-025-00436-x
62. Kakade P, Ojha H, Raimi OG, et al. Mapping of a N-terminal alpha-helix domain required for human PINK1 stabilization, Serine228 autophosphorylation and activation in cells. *Open Biol* 2022;12(1):210264. doi: 10.1098/rsob.210264 [published Online First: 20220119]
63. Brassard R, Arutyunova E, Takyi E, et al. Transmembrane Parkinson's disease mutation of PINK1 leads to altered mitochondrial anchoring. *Journal of Biological Chemistry* 2025;301(3) doi: ARTN 108253

10.1016/j.jbc.2025.108253

64. Ivatt RM, Sanchez-Martinez A, Godena VK, et al. Genome-wide RNAi screen identifies the Parkinson disease GWAS risk locus

as a regulator of mitophagy. *P Natl Acad Sci USA* 2014;111(23):8494-99. doi: 10.1073/pnas.1321207111
65. Epand RM. Proteins and cholesterol-rich domains. *Bba-Biomembranes* 2008;1778(7-8):1576-82. doi: 10.1016/j.bbamem.2008.03.016
66. Rahbek-Clemmensen T, Lycas MD, Erlendsson S, et al. Super-resolution microscopy reveals functional organization of dopamine transporters into cholesterol and neuronal activity-dependent nanodomains. *Nat Commun* 2017;8 doi: ARTN 740

10.1038/s41467-017-00790-3
67. Harraz MM. Selective dopaminergic vulnerability in Parkinson's disease: new insights into the role of DAT. *Front Neurosci-Switz* 2023;17 doi: ARTN 1219441

10.3389/fnins.2023.1219441
68. Grassi S, Giussani P, Mauri L, et al. Lipid rafts and neurodegeneration: structural and functional roles in physiologic aging and neurodegenerative diseases. *J Lipid Res* 2020;61(5):636-54. doi: 10.1194/jlr.TR119000427
69. Fortin DL, Troyer MD, Nakamura K, et al. Lipid rafts mediate the synaptic localization of α-synuclein. *Journal of Neuroscience* 2004;24(30):6715-23. doi: 10.1523/Jneurosci.1594-04.2004
70. Hatano T, Kubo S, Imai S, et al. Leucine-rich repeat kinase 2 associates with lipid rafts. *Hum Mol Genet* 2007;16(6):678-90. doi: 10.1093/hmg/ddm013
71. Kim KS, Kim JS, Park JY, et al. DJ-1 Associates with lipid rafts by palmitoylation and regulates lipid rafts-dependent endocytosis in astrocytes. *Hum Mol Genet* 2013;22(23):4805-17. doi: 10.1093/hmg/ddt332
72. Fallon L, Moreau F, Croft BG, et al. Parkin and CASK/LIN-2 associate via a PDZ-mediated interaction and are co-localized in lipid rafts and postsynaptic densities in brain. *Journal of Biological Chemistry* 2002;277(1):486-91. doi: 10.1074/jbc.M109806200
73. Silvestri L, Caputo V, Bellacchio E, et al. Mitochondrial import and enzymatic activity of PINK1 mutants associated to recessive parkinsonism. *Hum Mol Genet* 2005;14(22):3477-92. doi: 10.1093/hmg/ddi377
74. Cha SH, Choi YR, Heo CH, et al. Loss of parkin promotes lipid rafts-dependent endocytosis through accumulating caveolin-1: implications for Parkinson's disease. *Mol Neurodegener* 2015;10 doi: ARTN 63

10.1186/s13024-015-0060-5

Graphical Abstract

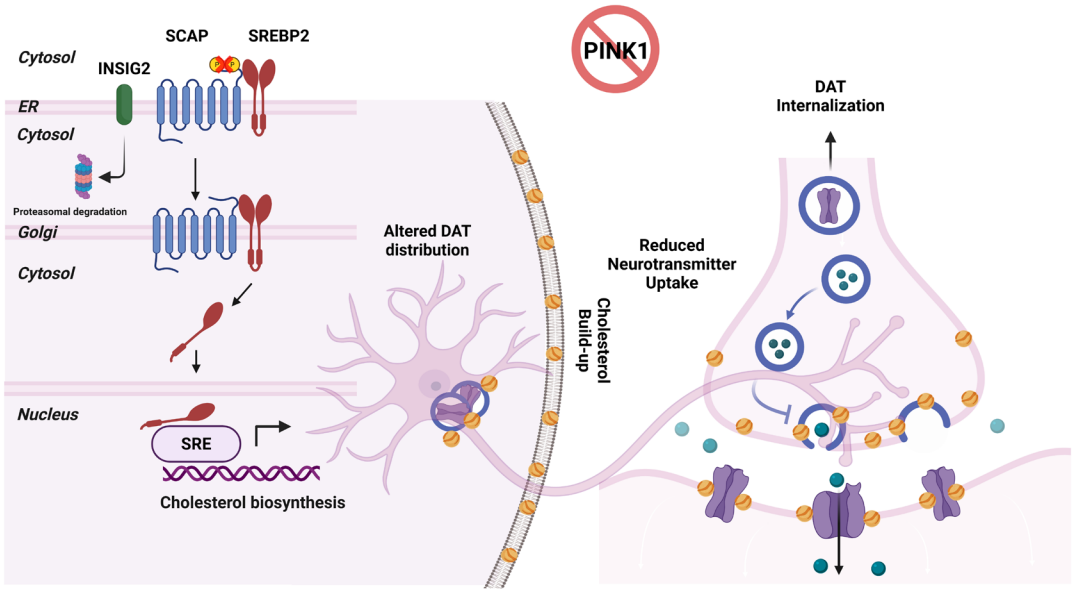

Main Figures

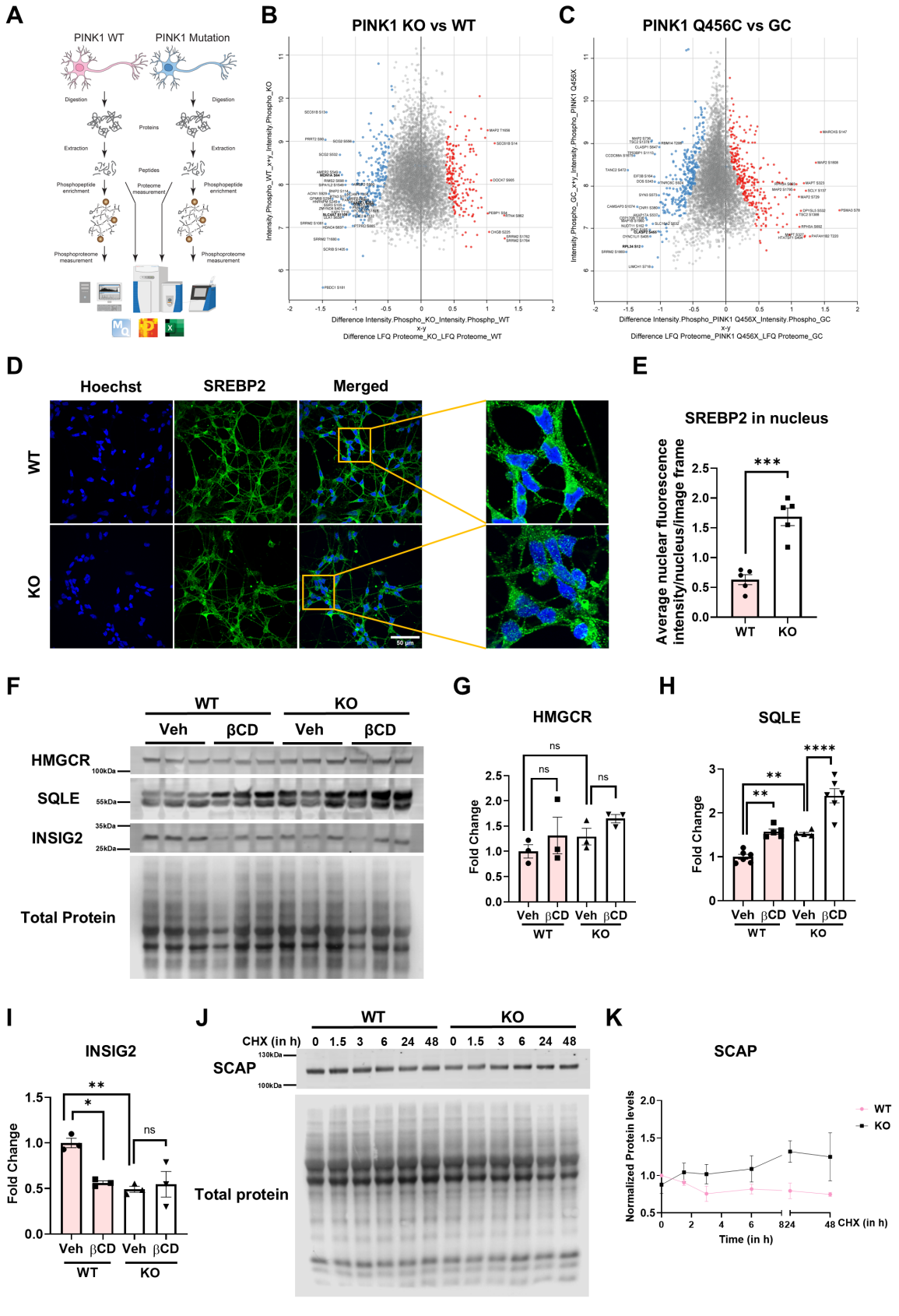

Figure 1: PINK1 LOF dopamine neurons have impaired SCAP phosphorylation at S822 and S838 that increases cholesterol biosynthesis due to increased SCAP stability.

A) A schematic workflow for phosphoproteomics. B) Phosphoproteomic differences in PINK1 wildtype (WT) and knockout (KO) dopamine neurons. C) Phosphoproteomic differences in PINK1 Q456X and gene corrected (GC) dopamine neurons. D) Immunofluorescence images showing neuronal localization of SREBP2 (green) in PINK1 WT and KO neurons. E) Quantification of average nuclear fluorescence intensity of SREBP2 in PINK1 WT and KO neurons (n=5). F) Immunoblot showing basal levels of proteins HMGCR, SQLE and INSIG2 in PINK1 WT and ko neurons. G) Quantification of basal HMGCR protein levels (n=3). H) Quantification of basal SQLE protein levels (n=5-6). I) Quantification of basal INSIG2 protein levels (n=3). J) Immunoblot showing SCAP levels in PINK1 WT and KO neurons following a cycloheximide (CHX) treatment to inhibit protein synthesis with timepoint ranging from 0 – 48 hours. K) Quantification of SCAP levels after CHX treatment (n=3). The error bars show the standard error of mean (SEM). For statistical analysis with more than two samples, an ordinary one-way ANOVA was used with Tukey's multiple comparisons tests. Unpaired t-test (two-tailed) was performed for quantification of the immunofluorescence intensities in (E).

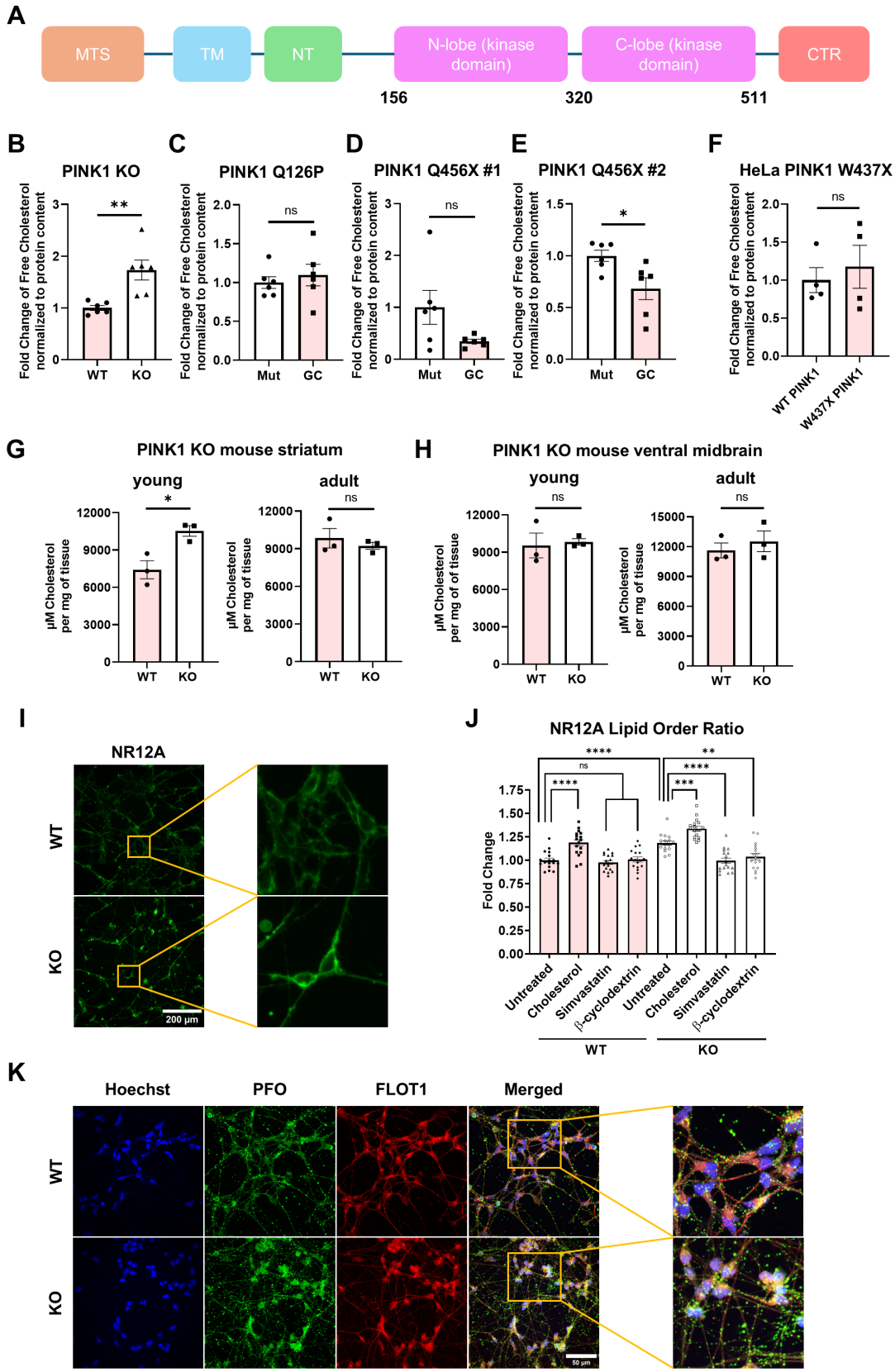
A
MTS
TM
NT
N-lobe (kinase domain)
C-lobe (kinase domain)
CTR
156
320
511
B
PINK1 KO
C
PINK1 Q126P
D
PINK1 Q456X #1
E
PINK1 Q456X #2
F
HeLa PINK1 W437X
Fold Change of Free Cholesterol normalized to protein content
WT
KO
Mut
GC
WT PINK1
W437X PINK1
ns
G
PINK1 KO mouse striatum
H
PINK1 KO mouse ventral midbrain
young
adult
µM Cholesterol per mg of tissue
I
NR12A
200 µm
J
NR12A Lipid Order Ratio
Fold Change
Untreated
Cholesterol
Simvastatin
β-cyclodextrin
K
Hoechst
PFO
FLOT1
Merged
50 µm

Figure 2: PINK1 LOF human dopamine neurons and young mice striatum exhibit increased free cholesterol which is enriched at the plasma membrane and in FLOT1-rich lipid rafts.

A) Schematic for PINK1 domains showing the mitochondrial targeting sequence (MTS) and the kinase domains. Free cholesterol levels of B) PINK1 wildtype (WT) and knockout (KO), C) PINK1 Q126P and gene corrected (GC), D) PINK1 Q456X and GC patient #1, E) PINK1 Q456X and GC patient #2 dopamine neurons (n=6). F) Free cholesterol levels of HeLa cells having endogenous WT PINK1 and PINK1 W437X (n=4). G) Free cholesterol levels of young and old PINK1 WT and KO mice striatum (n=3). H) Free cholesterol levels of young and old PINK1 WT and KO mice ventral midbrain (n=3). I) Live cell epifluorescence images stained with NR12A dye (green) that stains cholesterol at the plasma membranes of PINK1 WT and KO dopamine neurons. J) Plate reader-based quantification of lipid order ratio stained using NR12A dye in live PINK1 WT and KO dopamine neurons (n=17 from 3 independent biological replicates). K) Immunofluorescence images stained with Perfringolysin-O (PFO) in green and Flotillin 1 (FLOT1) in red showing the localization of cholesterol and FLOT1 rich lipid rafts in PINK1 WT and KO dopamine neurons. The error bars show the standard error of mean (SEM). For statistical analysis in (J), an ordinary one-way ANOVA was used with Tukey's multiple comparisons tests. Unpaired t-test (two-tailed) was performed for quantification of free cholesterol levels in (B-H).

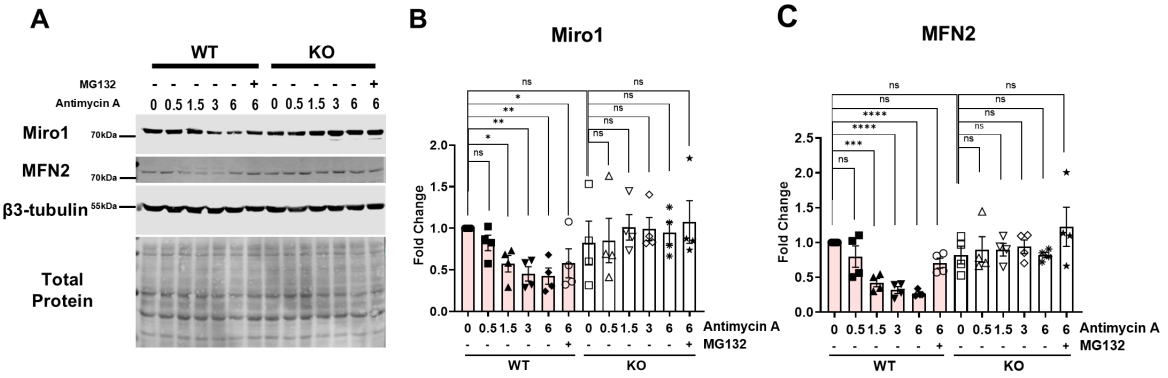
A
WT
KO
MG132
Antimycin A
0 0.5 1.5 3 6 6 0 0.5 1.5 3 6 6
Miro1
70kDa
MFN2
70kDa
β3-tubulin
55kDa
Total Protein
B
Miro1
Fold Change
Antimycin A
MG132
WT
KO
C
MFN2
Fold Change
Antimycin A
MG132
WT
KO

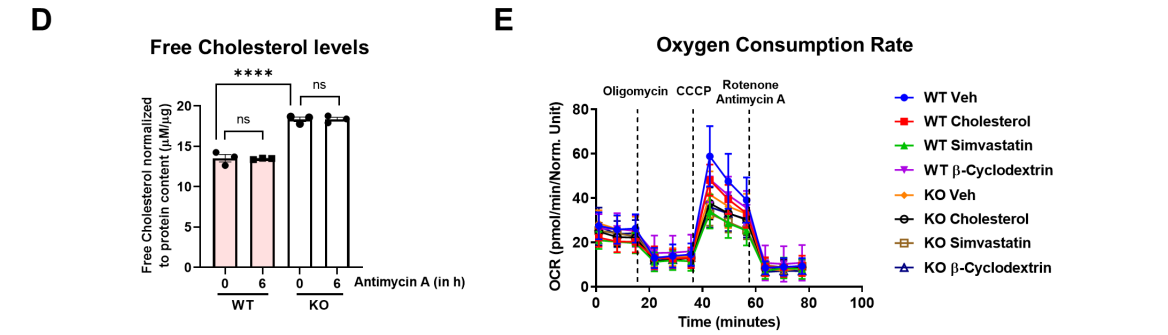
D
Free Cholesterol levels
Free Cholesterol normalized to protein content (μM/μg)
Antimycin A (in h)
WT
KO
E
Oxygen Consumption Rate
Oligomycin
CCCP
Rotenone
Antimycin A
OCR (pmol/min/Norm. Unit)
Time (minutes)
WT Veh
WT Cholesterol
WT Simvastatin
WT β-Cyclodextrin
KO Veh
KO Cholesterol
KO Simvastatin
KO β-Cyclodextrin

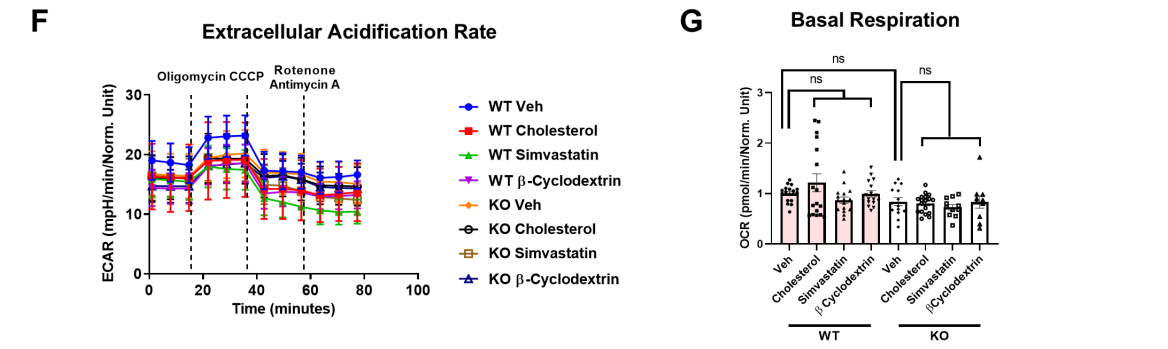
F
Extracellular Acidification Rate
Oligomycin
CCCP
Rotenone
Antimycin A
ECAR (mpH/min/Norm. Unit)
Time (minutes)
WT Veh
WT Cholesterol
WT Simvastatin
WT β-Cyclodextrin
KO Veh
KO Cholesterol
KO Simvastatin
KO β-Cyclodextrin
G
Basal Respiration
OCR (pmol/min/Norm. Unit)
Veh
Cholesterol
Simvastatin
β Cyclodextrin
WT
KO

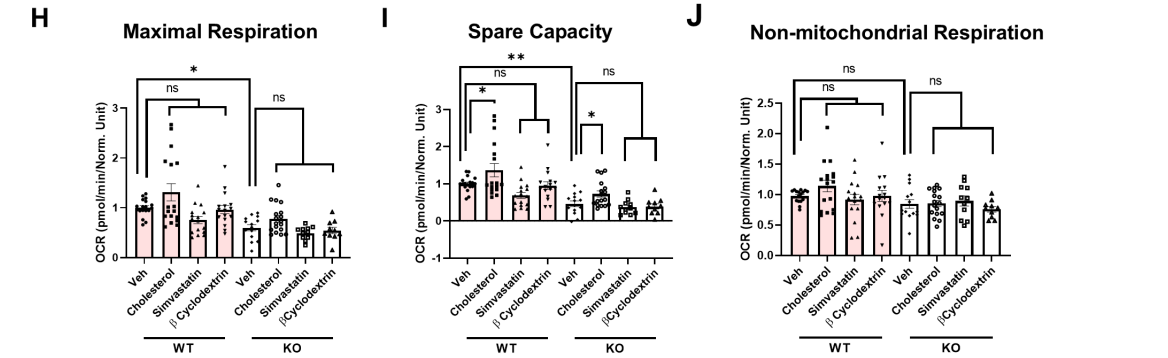
H
Maximal Respiration
OCR (pmol/min/Norm. Unit)
Veh
Cholesterol
Simvastatin
β Cyclodextrin
WT
KO
I
Spare Capacity
OCR (pmol/min/Norm. Unit)
J
Non-mitochondrial Respiration
OCR (pmol/min/Norm. Unit)

Figure 3: Cholesterol accumulation is independent of mitophagy and does not alter mitochondrial respiration.

A) Immunoblot of the mitophagy initiation markers Miro1 and MFN2 in PINK1 wildtype (WT) and knockout (KO) dopamine neurons depolarized using Antimycin A at timepoints ranging 0-6 hours. B) Quantification of Miro1 levels in (A) (n=4). C) Quantification of MFN2 in (A) (n=4). D) Free cholesterol levels measured in PINK1 WT and KO dopamine neurons treated with Antimycin A for 6 hours (n=3). E) Seahorse based mitochondrial stress test to measure Oxygen Consumption Rate (OCR) and F) Extracellular Acidification Rate (ECAR) in PINK WT and KO dopamine neurons treated with cholesterol and cholesterol depleting agents - simvastatin and β-cyclodextrin. G) Quantification of Basal respiration, H) Maximal Respiration, I) Spare capacity and J) Non-mitochondrial respiration in (E) (n=10-18 from 3 independent biological replicates). The error bars show the standard error of mean (SEM). For statistical analysis with more than two samples, an ordinary one-way ANOVA was used with Tukey's multiple comparisons tests.

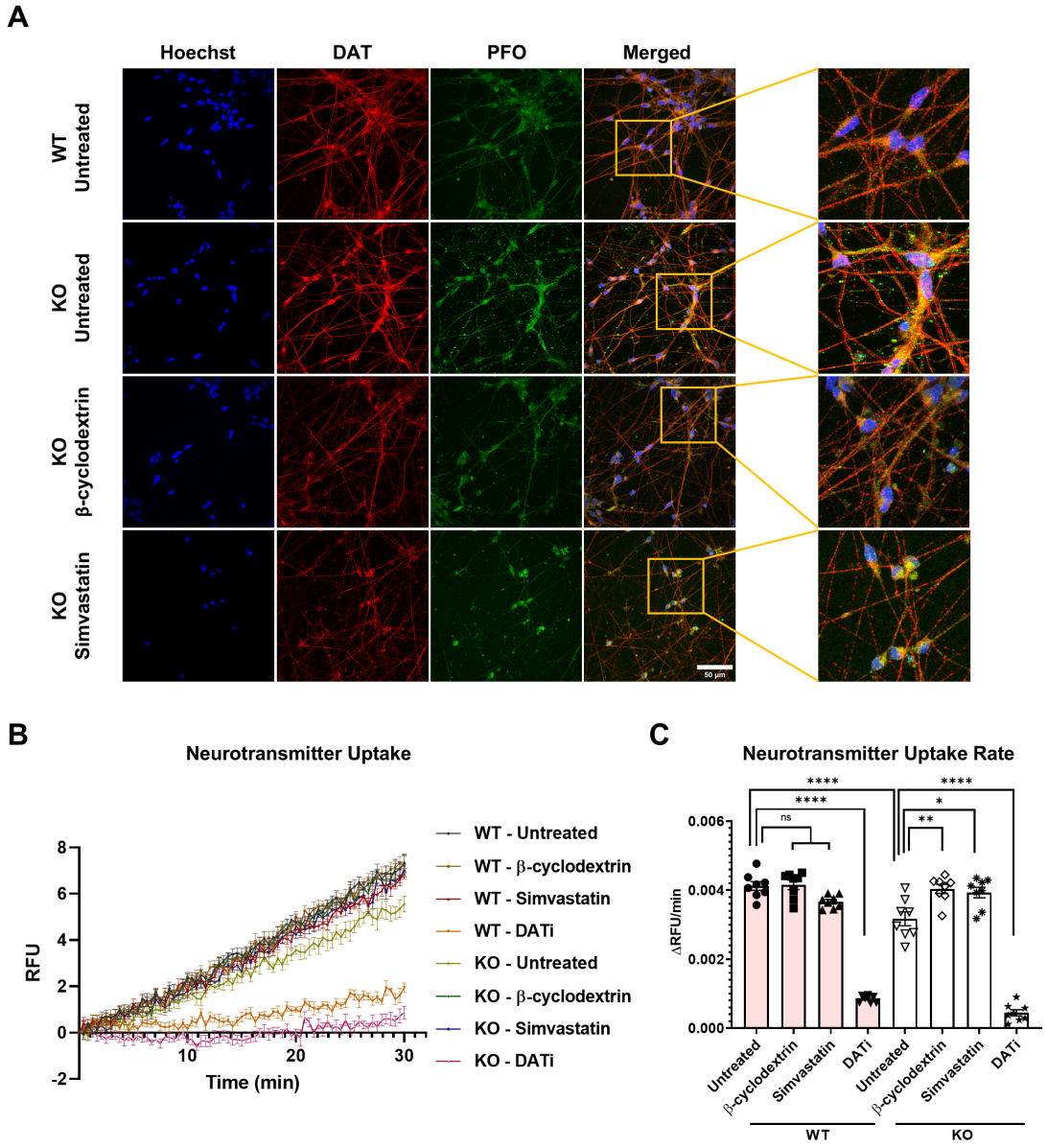
A
Hoechst
DAT
PFO
Merged
WT Untreated
KO Untreated
KO β-cyclodextrin
KO Simvastatin
50 µm
B
Neurotransmitter Uptake
RFU
Time (min)
WT - Untreated
WT - β-cyclodextrin
WT - Simvastatin
WT - DATi
KO - Untreated
KO - β-cyclodextrin
KO - Simvastatin
KO - DATi
C
Neurotransmitter Uptake Rate
ΔRFU/min
ns
Untreated
β-cyclodextrin
Simvastatin
DATi
WT
KO

Figure 4: Excess cholesterol disrupts DAT distribution and neurotransmitter uptake.

A) Immunofluorescence images showing the distribution of dopamine transporter (DAT) in red and Perfringolysin O (PFO) in green in PINK1 wildtype (WT) and knockout (KO) dopamine neurons either untreated or treated with cholesterol depleting agents - simvastatin and β-cyclodextrin. B) Relative Fluorescence Unit (RFU) of neurotransmitter uptake within a time course of 30 minutes in PINK1 WT and KO dopamine neurons either untreated or treated with simvastatin, β-cyclodextrin or dopamine transporter inhibitor (DATi). C) Quantification of neurotransmitter uptake rate in (B) (n=8 from 4 different neuronal differentiations). The error bars show the standard error of mean (SEM). For statistical analysis with more than two samples, an ordinary one-way ANOVA was used with Tukey's multiple comparisons tests.

12. Acknowledgements.

I would like to take this opportunity to thank all the people who made these last years both productive and crazy.

First, a huge thank you to Julia for her supervision over the past four years. Thank you for trusting me with so many exciting projects, for the lively discussions that somehow always ended with more ideas than we started with, and for supporting me through all of it. I also want to thank my TAC members, Boris and Eran, for their encouragement during our meetings. Special thanks to Boris for his extra involvement outside of TAC meetings, which he didn't sign up for. And Philipp, for his CRITICAL but really useful suggestions.

Thanks also to the MOMbrane RTG for creating a genuinely supportive atmosphere, fun collaborations, and biweekly seminars where I always learned something new (and occasionally left more confused, but in a good way). I would also like to thank Petra and Regina for helping with the endless bureaucracy.

To the lab members, past and present: you made science feel less like work and more like teamwork. Julia, Lisa and Lorenzo, thanks for helping me settle in Tü and making my transition to this lab smooth. Dina and Layla, thank you for the chats that kept experiments and me running. Olmo and Judith, thanks for the extra pair of hands and patience during our projects. Nic, thanks for sharing your confocal and Olga for helping with microscopes trainings, without your microscopy support, my pictures would not have been sexy.

Outside the lab, Kasia, Claudia, Bene, Bianca, Zach, and Yannic—thank you for the legendary MOMbrane chill feierabends that kept me sane. And to Orkun, Anna, Berna, Jorge, Nicola, Laura, Shila, Vaibhavi, Ale and Clemens—you made the Neurocampus a place where "breaks" were as memorable as experiments. And to Jai and Tanya, for making being crazy, normal.

And finally, the biggest thank you goes to my family. Thank you for giving me the freedom to chase my dreams without worrying about anything back home. You made it possible for me to fully dive into this PhD adventure, and for that, I'm endlessly grateful.